

THESIS

FLUID INCLUSION STUDY OF THE MESOPROTEROZOIC NONESUCH FORMATION—
BIOGENIC SOURCES AND THERMAL HISTORY OF OIL

Submitted by

Sarah Janette Colbert

Department of Geosciences

In partial fulfillment of the requirements

for the Degree of Master of Science

Colorado State University

Fort Collins, Colorado

Fall 2011

Master's Committee:

Advisor: John Ridley

Sven Egenhoff
Alan Kennan

Copyright by Sarah Janette Colbert 2011

All Rights Reserved

ABSTRACT

FLUID INCLUSION STUDY OF THE MESOPROTEROZOIC NONESUCH FORMATION – BIOGENIC SOURCES AND THERMAL HISTORY

The Nonesuch Formation is part of the Mid-Continent Rift System and is unusual because it contains a relatively high amount of oil that is thought to have formed in situ during the Mesoproterozoic, approximately 1.1 Ga. In this study, primary, pseudosecondary and secondary oil inclusions in samples obtained from Nonesuch Fm outcrop and cores were analyzed using petrography and microthermometry, and one core sample was analyzed by GC-MS. Aqueous inclusions were also studied via petrography and microthermometry. The inclusions studied were hosted in sandstone grains and matrix from parts of the Nonesuch Fm and the upper part of the Copper Harbor Fm, diagenetic calcite nodules from the Marker Bed of the Nonesuch Fm and calcite veins in the Nonesuch and Upper Copper Harbor Fms that formed no later than 30 Ma after deposition. Based on these settings, it can be assumed that all inclusions studied were entrapped during the Mesoproterozoic around the time of deposition of the Nonesuch Fm.

The biomarkers detected by GC-MS have a Proterozoic character and the presence of mid-chain substituted monomethyl alkanes as well as 1,2,5-TMN indicates a cyanobacterial hydrocarbon source. Algal biomarkers have also been found in the oil in previous studies. The ratios calculated from the GC-MS data suggest an early- to peak-oil window maturity for the hydrocarbons, which is consistent with data from previous

studies. The homogenization temperatures obtained by microthermometry are typically used as an estimate of inclusion entrapment temperature; however, in this study, the wide range of homogenization temperatures along with an inconsistency between these and the GC-MS maturity indicators implied that the thermal history of the oil was more complex. The inclusions were likely trapped during diagenesis at temperatures between 100-130°C, which agrees with the evidence from the maturity ratios and previous work on the Nonesuch Fm, and then reheated by hydrothermal activity after entrapment. The microthermometrical evidence implies that the second period of heating raised temperatures to levels exceeding 250°C, and other studies of the Mid-Continent Rift area suggest that this secondary heating occurred either soon after diagenesis or significantly later, around 200-300 Ma.

ACKNOWLEDGEMENTS

First and foremost, thank you to my advisor, Dr. John Ridley, whose mind contains the greatest wealth of geologic knowledge of anyone I've ever met. His guidance and patience when listening to theories and answering questions is endless, and luckily his patience for waiting for papers to be written is slightly less so.

I also thank my committee members, Dr. Sven Egenhoff and Dr. Alan Kennan, for their thoughtful questions and comments. Their input and information was invaluable, and I was fortunate to have the chance to work with them.

I am very grateful to the people at CSIRO Petroleum Lab in Sydney, Australia—Herbert Volk, David Fuentes, Se Gong and most particularly Manzur Ahmed, who spent three weeks explaining and walking me through the process of preparing a sample for GC-MS analysis. I'm sure the preparation would have been quicker and easier without a student to teach, but I am so appreciative for the chance they gave me to learn.

Thank you also to Ted Bornhorst and Michigan Technological University in Houghton, MI, for showing me where to go to find the Nonesuch Fm and for allowing me to take samples from their cores.

I would also like to acknowledge those whose funding made this project possible: the Geological Society of America, the Colorado State University Geosciences Department, both of whom awarded generous grants to this project, and the Australian Research Council, whose grant to Drs Adriana Dutkiewicz (Sydney University) and Simon George (Macquarie University) was used in part to fund the GC-MS work for this study.

Finally, and most importantly, thank you to my family, who are and always have been my biggest supporters. They make me feel smart and capable, and their encouragement leads me to accomplish things I never dreamed I could do.

TABLE OF CONTENTS

Abstract	ii
Acknowledgments	iv
1. Introduction.	1
1.1 Preamble	1
1.2 Biomarkers	3
1.3 Nonesuch Formation	6
2. Methods	13
2.1 Sampling	13
2.2 Petrography and microthermometry	14
2.3 GC-MS	16
3. Results	22
3.1 Petrography results	22
3.1.1 Nonesuch Formation petrography	22
3.1.2 Fluid inclusion petrography	25
3.2 Microthermometry results	28
3.3 GC-MS results	33
3.3.1 General characteristics of inclusion oil.	33
3.3.2 Thermal maturity indicators	36
3.3.3 Biomarkers	37
3.3.4 Comparison with other Nonesuch Formation studies	39
4. Discussion	61
4.1 Biological sources and migration	61
4.2 Thermal history	63
4.3 Interpretation of oil maturation history	69
4.4 Conclusions	71
4.5 Further work on oil inclusions	72
5. References Cited	78
6. Appendices	84
6.1 Appendix A: Samples collected	84
6.2 Appendix B: Microthermometry data	88
6.3 Appendix C: GC-MS data.	91

Chapter 1: Introduction

1.1 Preamble

It is difficult to picture what life was like in the middle Proterozoic, over 1000 million years ago. There was no North America or Asia; the continents were fused together, arranged in a supercontinent: Rodinia. Life was simple—primitive, unicellular algae flourished in the ocean and were beginning to make their way into the continental bodies of water. Eukaryotes had been developing for nearly 1400 million years (Dutkiewicz et al., 2006) and were beginning to photosynthesize (Javaux and Marshal, 2006), though at 1100 million years they were just beginning to form multiple cells and were not nearly as prolific or diverse compared to the complex organisms that exist today (Butterfield, 2000). Evidence of microbial mats has been found in Mesoproterozoic carbonates, shales and sandstones (Schieber, 1998). Blue-green algae (cyanobacteria) were the primary source of O₂ during this time—terrestrial plants had not yet evolved (Schopf, 1974; Hughes et al., 1995).

It was during this time that the Nonesuch Formation was deposited (Kelly and Nishioka, 1985; Davis and Paces, 1990; Hieshima and Pratt, 1991). The sediments of this shale were laid down in the middle of a failing rift, and also deposited were the tiny remains of primitive life forms. Both sediments and corpses were buried, compacted and heated until the silt became stone and the organic remains were transformed into hydrocarbons. The Nonesuch Fm is one of few Precambrian formations with significant amounts of what is likely syngenetic oil (Schopf, 1974).

There are not many fossils available from the Proterozoic—a high percentage of the biomass in this period was bacterial or algal in origin and lacked hard parts that could be preserved, and even the organic material that was preserved was often subject to deformation or obliteration as its host rock was metamorphosed (McKirdy, 1974). Although stromatolite fossils are uniquely abundant in the Proterozoic and Archean rock record (Schieber, 1998; George et al., 2008; Shaw, 2008), and eukaryote microfossils have been found in rocks as old as 1400 Ma (Butterfield, 2000), most of the evidence for life from the Precambrian and before comes from microfossils, which are defined as fossils under four millimeters in length, or molecular fossils, also known as biomarkers (Peters et al., 2005).

The purpose of this study is to use the biomarkers present in the inclusion oil of the Nonesuch Formation to gain a more complete picture of oil generated in Mesoproterozoic strata and through this, of Mesoproterozoic life and environment. In addition to biomarkers, other hydrocarbon parameters will be used to estimate maturity of the inclusion oil. The information gained from this analysis will be supported by additional data collected using a variety of geochemical methods and compared with work performed previously by others on the Nonesuch Fm in order to determine migration and thermal history. The information obtained by studying all features of the oil inclusions is an important component used to support the interpretation of the biomarker data, particularly when working with oil from the Proterozoic, as oil of this age has not been studied as extensively as younger hydrocarbons.

1.2 Biomarkers

Biomarkers are complex organic molecules that are the chemical remains of organisms (Peters et al., 2005). They have been chemically modified from their original form through biodegradation and diagenesis, but still retain enough of their initial characteristics for their origins to be identified. The most useful biomarkers are typically unique to one or two different families of organisms, making it possible to identify the parent life form and to infer something about the characteristics of the original depositional conditions and the maximum thermal maturity of the source rock. Often, it is the ratio of two different biomarkers that is most useful rather than the concentration of a single compound. Some typical examples of this are the pristane/phytane (Pr/Ph—see Table 1 for additional common abbreviations used in this text) ratio to determine salinity (Peters et al., 2005) and the 20S/(20S+20R) ratio of C₂₉ steranes that is used as an indicator of thermal maturity (Hieshima et al., 1991).

Biomarkers are likely present in many sedimentary rocks where parent organism population was high and the depositional conditions were right, but they are best preserved where organic accumulation was high enough to produce petroleum deposits (Peters et al., 2005). Compounds that are typically used as biomarkers that are present outside of hydrocarbon deposits cannot be traced to their origins with as much certainty as those preserved in oil, as the biomarkers in petroleum are concentrated during the oil-generation process (Peters et al., 2005). The chief input controls for the biomarkers present in a given oil are the type of parent organism that they were generated from and the depositional conditions of the source rock (Peters et al., 2005), and so they can be used for oil-oil correlation, source rock correlation and migration patterns. In this study, the

biomarkers and biomarker ratios will be used to confirm that the oil in the Nonesuch Fm inclusions was formed in-place rather than migrating from a different source rock.

Deposition of hydrocarbon source rocks can happen under a variety of conditions, with the highest productivity occurring in low-energy depositional environments, such as lakes and shallow coastal waters (Hunt, 1979). The low-energy environment allows the remains of the organisms to settle on the sediment under the water and collect over time. While a very low-energy environment is ideal for the collection of the organic matter, the rate of deposition must be high enough to bury the organic matter before it is subjected to high levels of biodegradation, in which other organisms chemically process the soluble organic matter for their own nutrients (Killops and Killops, 2005). As the organic matter undergoes biodegradation and diagenesis, soluble material is consumed while the insoluble material remains unchanged and continues to reflect the structure of its parent molecules (Peters et al., 2005). This insoluble material is called kerogen, and during a process called catagenesis, in which it is exposed to higher temperature and pressure, it releases hydrocarbons. Kerogen can form either or both oil or gas, and the main phase formed is dependent on its biological origin and the maximum temperature reached—all kerogen will eventually form gas at high enough temperatures (Hunt, 1979). In general, the oil window for kerogen is between 100 and 150°C, the gas window is 150-230°C. These correspond to depths of approximately 1.5-3km for the oil window and 3-4km for the gas window, although the depths can vary based on local geothermal gradient, type of organic matter and a wide variety of factors (Peters et al., 2005). Above 230°C and below 4km, kerogen will metamorphose into graphite (Killops and Killops, 2005).

During catagenesis, the molecular structure of the biomarkers changes depending on the temperatures to which they are exposed; however, they retain enough similarity to their parent molecules to determine what type of organism they were derived from. It is also possible to determine both environment of deposition and the maximum temperature of catagenesis by examining biomarker composition and structural details. Biomarkers can be detected in oil or pyrobitumen (solidified or extremely viscous hydrocarbons) by using high-resolution geochemical techniques, typically gas chromatography-mass spectrometry (GC-MS). Oil inclusion analyses are especially useful for older formations, as the pore-space oil or bitumen has often been contaminated by later events or removed altogether over time. While inclusions may be destroyed by metamorphism, where they are intact they are typically uncontaminated and will contain a sample of fluid or oil with original characteristics (George et al., 1998).

Analysis of fluid inclusions by GC-MS is hardly a new idea, having first been performed in 1971 by Kvenvolden and Roedder, but it has been refined over the years with the development of more sensitive equipment and techniques, and the results found today are far more precise and detailed than those obtained in the 70s and 80s. Recently, inclusion oil analyzed from the Matinenda Formation, which has been dated at 2.45 Ga, has shown biomarkers which indicate both eukaryotic and cyanobacterial sources (George et al., 2008).

1.3 Nonesuch Formation

The Nonesuch Formation is part of the late Mesoproterozoic Mid-Continent Rift System (MCRS), a failed extensional system that extends for 2500km through southern Ontario, Michigan, northern Wisconsin, Minnesota, Iowa and the very western edges of Nebraska and Kansas, and is generally centered underneath Lake Superior (Ojakangas and Dickas, 2002) (Figure 1). The tensional stresses that created the rift were likely caused by normal extensional tectonics, forming a complex horst and graben sequence trending generally NE-SW with a smaller arm on the eastern side of the rift trending in a perpendicular direction. The area of greatest extent covers more than 5700km².

Volcanic sediments are present in the central graben of the rift, overlain with marine, lacustrine, deltaic and fluvial sedimentary rocks (Palacas, 1995). The volcanics and sedimentary units that are associated with the MCRS are collectively known as the Keweenaw Supergroup and are ~30km thick (Swenson et al., 2004). Rifting lasted for 100 million years before compressional forces from the convergence of the proto-North American plate and the Grenville Province allochthon took over and caused uplift throughout the area (Ojakangas and Dickas, 2002).

The Nonesuch Formation is located in the Keweenaw Supergroup (Northern Michigan and Wisconsin), and is part of the Oronto Group, which consists of three sedimentary units: the Copper Harbor Conglomerate, Nonesuch Formation and Freda Sandstone and is approximately 7 km thick in total. The Nonesuch Fm is the middle unit and is on average about 200m thick. These three units were deposited as infill in the Mid Continent Rift System and are dated at ~1.1 Ga. They overlay the Portage Lake

Volcanics, a sequence of more than 200 lava flows, each ranging from 10-20m thick with sedimentary deposits interbedded (Bornhorst, 1997). Just under the Copper Harbor Conglomerates are the Porcupine Volcanics, the youngest volcanics associated with the rift (Ojakangas and Dickas, 2002),

The Nonesuch Fm is composed of varying layers of sandstone, shale and siltstone. Although there has been some argument as to whether its depositional environment is marine (Ojakangas et al., 2001) or some form of lacustrine (Hieshima and Pratt, 1991; Suszek, 1997), visual inspection of the formation shows crossbedding, ripple marks and interbedding of shale and sandstone, none of which are consistent with a marine setting. Hieshima and Pratt (1991) after examining the sulfur/carbon ratios of the extractable organic matter, concluded that the organic matter was derived from algal and bacterial origins, and the environment of deposition was dominated by saline water rather than non-saline. Halite has also been found in the Nonesuch Fm by Mauk (2011, pers. comm.), providing more evidence for a saline depositional environment. While this might lend credence to the marine depositional hypotheses, combined with the depositional features observed it indicates a shallow marine setting, likely an estuary or similar environment, though Uchytel et al. (1999) speculate that the Nonesuch Fm was deposited in a lacustrine environment with input from water of varying salinity based on their calculations of the activation energy for the transformation of Nonesuch Fm kerogen into hydrocarbons.

Below the Nonesuch Fm is the Copper Harbor Conglomerate, which was deposited in an arid terrestrial climate (Imbus et al., 1988) and shows fluvial characteristics, and above the Nonesuch Fm is the Freda Sandstone, which is also fluvial

in origin, though the two formations show significant differences in environment of deposition. The Copper Harbor Conglomerate is typically composed of medium sand to cobbles and, while generally fining upward, is not very well-sorted, suggesting that the area of deposition was not far from the source of the grains. The Freda Sandstone, by contrast, is composed mostly of fine-grained sand with some silt- and clay-size grains with small fining-upward sequences, typical of a meandering river sequence (Swenson et al., 2004). These three units together are indicative of a transgressive-regressive sequence, with retrogradation during the time the Nonesuch Fm was being deposited and progradation during the Freda Sandstone deposition (Swenson et al., 2004). It is likely that these units were deposited after rift extension ceased but prior to inversion of the system (Bornhorst, 1997).

From its base to a height of approximately five meters, the Nonesuch Fm hosts extensive stratibound copper deposits which were mined from 1880 until 1995 (Mauk and Hieshima, 1992). The copper is the result of hydrothermal fluid flow through the formation, although the conditions under which the copper precipitated are disputed and it was likely that there was more than one hydrothermal event and possibly more than one source of hydrothermal fluid (Mauk et al., 1992; Brown, 2006). The Nonesuch Fm was evaluated for hydrocarbon potential by Amoco and others, but it is not considered an economic deposit in that respect at this time (Uchytel et al., 1999). During their evaluation, Amoco and others shot seismic lines over several areas of the rift, giving a more comprehensive picture of the structure of the system and leading to several new studies of its architecture and characteristics (Thomas and Teskey, 1994; Ojakangas and Dickas, 2002).

The Nonesuch Formation has been extensively studied in the past because it is unusual to find Mesoproterozoic sedimentary rocks that are unmetamorphosed, and rarer still to find significant amounts of organic matter preserved in them (George et al., 2008). Most of the studies that have been previously undertaken on the organic matter have looked at the bitumen and petroleum from seeps in either the White Pine Mine or the Copper Range Mine, although Kelly and Nishioka (1985) examined the oil inclusions in late calcite veins to determine whether any relationship existed between the copper deposit and organic matter, with the conclusion that the copper was deposited later than the source rock and had locally replaced the organic matter in the area. Kelly and Nishioka (1985) also concluded that the oil in the Nonesuch Fm is the same age or only very slightly younger than the rock itself, suggesting that the rift area was stable enough during the time of deposition for burial of the Nonesuch Fm to hydrocarbon generation depth to occur. The calcite in the veins studied by Kelly and Nishioka (1985) was dated at 1047 ± 35 Ma by Ruiz et al. (1984) using Rb-Sr, and this can be used as a minimum age for the oil (Kelly and Nishioka, 1985). At one point, this was the oldest confirmed case of surviving liquid hydrocarbons (Mancuso et al., 1989). Pratt et al. (1991) examined the amounts of sterane and triterpane biomarkers in pyrobitumen extracted from Nonesuch Fm cores in Michigan and Wisconsin as well as seep petroleum from the White Pine Mine using MRM GC-MS and found significant similarities between the pyrobitumen of the Nonesuch Fm and the seep oil. This together with Kelly and Nishioka's 1985 study suggests that the inclusion oil was sourced by the Nonesuch Fm and so can be used as a sample of the original conditions of the Nonesuch Fm hydrocarbons.

More recently, Mauk and Burruss (2002) used gas chromatography on inclusion oil from White Pine to search for evidence of water washing, concluding that the alteration of the oils, particularly of the C₁-C₁₇ fraction, was caused by water washing rather than biodegradation or phase separation. Mauk and Hieshima (1992) and Mauk et al. (1992) also studied the organic matter-copper relationship as well as the relationship of deformation to copper mineralization, and concluded that the copper had likely precipitated out of the hydrothermal fluid because the organic matter caused reduction of the fluid based on the association of the copper with both the organic matter and faults in the area (Ho and Mauk, 1996; Brown, 2006). Mauk and Hieshima (1992) suggest that the petroleum in the area used thrust faults as fluid flow conduits and that hydrocarbon generation and maturation may have been aided by faulting and hydrothermal activity in the area rather than caused by burial alone.

In 2007, Hegarty et al. studied the extractable oil from a black shale in Idaho that is a temporal equivalent to the Nonesuch Formation, estimating maximum temperatures from vitrinite reflectance and apatite fission track analysis. The equivalency of the two formations was determined using a reconstruction of burial history by Witzke (1990 in Hegarty et al., 2007), and although the Idaho shale is thicker and more feldspathic than the Nonesuch Fm, there are enough similarities between the two formations that it is probable they were simultaneously deposited through similar mechanisms. Hegarty et al. (2007) concluded that the oil in the Idaho shale reached its highest maturity 200-300 million years ago, with the implication that the oil is much younger than the shale, and not truly Precambrian in origin. Their conclusion of the age of maximum maturity is based on the distribution of lengths of the fission tracks. The 200-300 Ma age obtained

by Hegarty et al. (2007) is directly contradictory to the study done by Kelly and Nishioka (1985), who observed oil residue in the copper-bearing veins as well as indentations caused by pyrobitumen in the native copper itself, and Mauk and Hieshima (1992), who found a diagenetic relationship between the copper and the oil, all of which suggests that the oil is at least as old as copper mineralization. The copper that is most clearly associated with the organic matter is said to have precipitated no later than the last episode of major uplift in the basin which occurred 30 Ma at most after the rifting ceased, giving it a youngest possible age of 1000 Ma (Mauk and Hieshima, 1992). Because the Idaho shale that Hegarty et al. (2007) evaluated was several hundred miles away from the Nonesuch Fm, it is possible that both analyses are correct and the oil was generated at different times in different areas. The equivalent formations in Idaho are currently buried much deeper than their northern counterparts (Swenson et al., 2004), and may have at some point undergone a secondary round of catagenesis, leading to a younger oil signature.

As of yet, there has not been a study of the inclusion oil in the Nonesuch Fm that uses low-detection-limit GC-MS techniques and is able to compare the biomarkers and maturity indicators in the inclusion oil to those previously found in the pore-space oil and bitumen. The intention of this study is to implement those techniques and draw a conclusion concerning the relationship (or lack thereof) between the original oil and the pore-space organic matter. This study will also allow better knowledge of the timing and phases of oil migration and maturation (if more than one exist) by using fluid inclusion petrography and microthermometry to estimate entrapment temperatures of the fluid inclusions.

Table 1: List of abbreviations commonly used in this text.

FI	Fluid inclusion
GC	Gas chromatography
MS	Mass spectrometry
T _h	Temperature of homogenization
Pr	Pristane
Ph	Phytane
MCRS	Mid-Continent Rift System
DBT	Dibenzothiophene
PHEN	Phenanthrene
SIM	Single ion monitoring
DCM	Dichloromethane
BIR	Big Iron River
LIR	Little Iron River
PIR	Presque Isle River
TMN	Trimethylnaphthalene
TeMN	Tetramethylnaphthalene
PMN	Pentamethylnaphthalene

Chapter 2: Methods

2.1 Sampling

Samples were collected from both outcrop and archived core. The outcrop samples were taken from three different sites in Northern Michigan: The Big Iron River, the Little Iron River (both near Silver City, MI) and the Presque Isle River (near Porcupine Mountains State Park, Ontonagon County). Sampling procedures were very similar for all three sites. The Nonesuch Formation outcrops along river beds and banks, and the entire unit is exposed stratigraphically from base to top heading from north to south along the Big Iron River and Little Iron River and south to north along the Presque Isle River. Samples were taken at approximately regular intervals with particular attention to visible veins, secondary copper minerals or other unusual features. At the Big Iron River site, the whole section of Nonesuch Formation was exposed and samples were taken from the top to the base, 17 in total. At the Little Iron River, the sandstone and some of the massive shale sections were exposed, and samples were taken where possible, 14 total. The last outcrop location, the Presque Isle River, had only a small section of Nonesuch Formation in outcrop, all in the cupriferous zone of the Lower Nonesuch Fm. Fifteen samples were collected here, most from the Nonesuch Fm but also a few from the upper section of the Copper Harbor Fm.

Eighteen thin sections were made from the outcrop samples, five of them single-polished sections for normal viewing and the other thirteen double-polished in order to

better study fluid inclusions. Sixteen thin sections were also made from five cores drilled in the White Pine Mine area in the 1980s and currently archived at Michigan Technological University, Houghton, MI (Figure 2). Of these, fifteen were double-polished and one was single-polished. Samples for the thin sections were taken from parts of the core and hand samples that were considered most likely to contain fluid inclusions, such as veins and sandstone layers with visible organic material, although a few thin sections were made from the shale layers in order to study the mineralogy of the formation.

A few of the thin sections also required epoxy to be injected because of their fragility. While studying the oil inclusion fluorescence, it was found that the type of epoxy used was also fluorescent under UV light; however, the epoxy fluorescence was a much brighter blue than the inclusions and generally this did not mask the inclusions except in rare cases where the sample was especially porous and the brightness of the epoxy made it difficult to see the dimmer inclusions.

2.2 Petrography and Microthermometry

Oil inclusions were identified in twelve thin sections (out of 34 total) by fluorescence under ultraviolet light at a wavelength of 365nm (Figure 3). The timing of the oil migration and entrapment was determined using the classical relationships as defined by Goldstein and Reynolds (1994). Inclusions present in fractures that cut across grain boundaries were assumed to have been entrapped later than deposition and cementation, whereas inclusion trails that were cut off by grain boundaries were assumed to be already in place. In veins, inclusions termed primary are associated with the growth planes of

crystals and are assumed to be syngenetic to vein formation and those called secondary are present in fractures within the vein and are assumed to be later. Different colors of fluorescence were observed and recorded, as they can be signs of different thermal maturities (George et al., 2001).

Five of the thin sections with oil inclusions were chosen, based on the size and abundance of the inclusions, for microthermometry. Three of these were core samples (30R 2263, 28G 539 and 40K 2088) and two were samples collected from river outcrops of the Nonesuch Fm (LIR 14 and BIR 16). The thin sections were removed from their glass slides using acetone and were carefully broken into fragments small enough to be viewed in the stage used for microthermometry. An additional outcrop sample, BIR 6 was also originally selected and photographed, but when acetone was applied, the epoxy released from the slide but did not dissolve off of the thin section, causing it to curl in on itself and rendering it impossible to view under the microscope. It was determined that because the inclusions in this sample were contained in calcite, a solvent strong enough to dissolve the epoxy was also likely to dissolve most of the sample.

Microthermometry was performed using a Linkam THMS 600 Stage attached to an Olympus BX51 microscope. Samples were heated to a maximum of 250°C and a minimum of -40°C at a rate of no faster than 15°C/minute. When it was apparent that the inclusion in question was nearing its homogenization temperature, heating was slowed to a rate of 2-5°C/minute. Heating was discontinued as soon as homogenization was observed or the temperature reached 250°C (150°C in some samples), as heating the sample above this temperature might cause deformation of the calcite hosting inclusions causing changes to inclusion volume and hence give false temperature readings

(Prezbindowski and Tapp, 1991). Because of the nature of the heating apparatus, this would also cause other fluid inclusions in each fragment to become deformed as well. In cases where 250°C was reached before homogenization, the inclusion was recorded as having a homogenization temperature of “>250°C”. Cooling runs were conducted after all heating runs on the sample were complete, as freezing can also cause inclusion deformation. Cooling was stopped when it was apparent that no liquid remained in the inclusion.

Microthermometry was also performed on saline aqueous inclusions in three of the same samples: LIR 14, 30R 2263 and BIR 16 (the two remaining microthermometry samples were not included in the saline analysis because they did not show any non-oil inclusions.) The saline inclusions were also heated until homogenization and then cooled until solidified in order to estimate entrapment temperatures and compositions. This technique has been used previously by El-Desouky et al., 2008 to determine salinities and Ca content of aqueous inclusions in the Democratic Republic of Congo. The oil and aqueous homogenization temperatures were compared to gain a better overall understanding of the conditions at the time of entrapment.

2.3 GC-MS

GC-MS analysis of the FI oil was performed at the CSIRO Petroleum laboratory, Sydney, Australia, on a Hewlett Packard 5890 gas chromatograph interfaced to a VG AutoSpecQ Ultima (electron energy 70 eV; electron multiplier 250 V; filament current 200 μ A; source temperature 250 °C) tuned to 1000 resolution. Chromatography was

carried out on a fused silica column (60 m x 0.25 mm i.d.) coated with DB5MS polymer, using a splitless injection technique. The FI oil, final outside rinse and laboratory system blank samples were analyzed using three different single ion monitoring (SIM) programs: SIRV_INCA, SIRV_INCB and SIRV_INCC. (Ahmed and Volk, internal report).

SIM GC-MS was chosen for the analysis of the inclusion oil. This type of GC-MS has been used in previous studies for the detection of biomarkers in fluid inclusions (George et al., 2004a; George et al., 2007). Molecules that fall into the group of undetermined composition because of their low abundance in comparison to the other elements present in a normal GC-MS analysis can often be defined using this technique, making it ideal for this study (George et al., 2007). The inclusions entrapped in a calcite vein from Core 30R (sample 30R 2263, Figure 4) were selected for analysis based on their abundance and large average size. The inclusions present in this vein are generally very large, up to ~30 μ m, and most show yellow fluorescence under UV light. The 4g sample of vein and immediately adjacent wall rock contains both oil and aqueous inclusions of at least one primary and one secondary generation. The sample was fragmented into 2mm pieces and cleaned using several rounds of ultrasonication (5-10 minutes) in methanol and dichloromethane (DCM). Six outside rinses of the sample were analyzed by GC-MS to show that no contamination was present on the outside of the sample prior to crushing, and a system blank showed that there was no contamination present within the glassware or GC-MS system itself. There was some difficulty in obtaining a clean blank sample—several sources of possible contamination were investigated before it was concluded that the contamination must have come from the DCM distillation process. Once the distillation equipment was decontaminated using

hydrofluoric acid and the DCM was re-purified, the clean blank analysis was obtained. Although Brocks et al., 2008 states that when a crushed sample will be analyzed, the actual crushing of rock must be part of the system blank process, both George et al, 2007 and Dutkiewicz et al., 2007 were able to obtain satisfactory analyses by only running the outside rinse DCM through the crushing mechanism.

The sample was crushed offline in DCM using a stainless steel crushing cylinder for 10 minutes, allowed to rest for 10 minutes and then crushing was continued for an additional 10 minutes. The oil and DCM were extracted from the rock powder in the cylinder, and the cylinder was cleaned with an additional 25mL of DCM. Squalane was used as the internal standard and was added to all outside rinses, system blanks, and the fluid inclusion oil with varying concentrations. The solvent containing the oil and the internal standard was reduced on a rotary evaporator and then blown down using purified nitrogen taking care not to dry the sample in order to preserve the low molecular weight hydrocarbons. The concentrate was then filtered through a pipette packed with alumina and silica gel and evaporated down to ~200 μ L for injection into the GC-MS system, again taking care to avoid drying the sample. The initial GC-MS run of the oil found that there was an exceptionally high amount of oil obtained from the inclusions, likely due to the large size and quantity of the inclusions in the sample. This caused too high of a concentration of target molecular compounds compared to the internal standard for an accurate analysis. This problem was mitigated by performing a second GC-MS run on the oil using a higher concentration of squalane in order to precisely compare the relative peaks on the chromatogram.

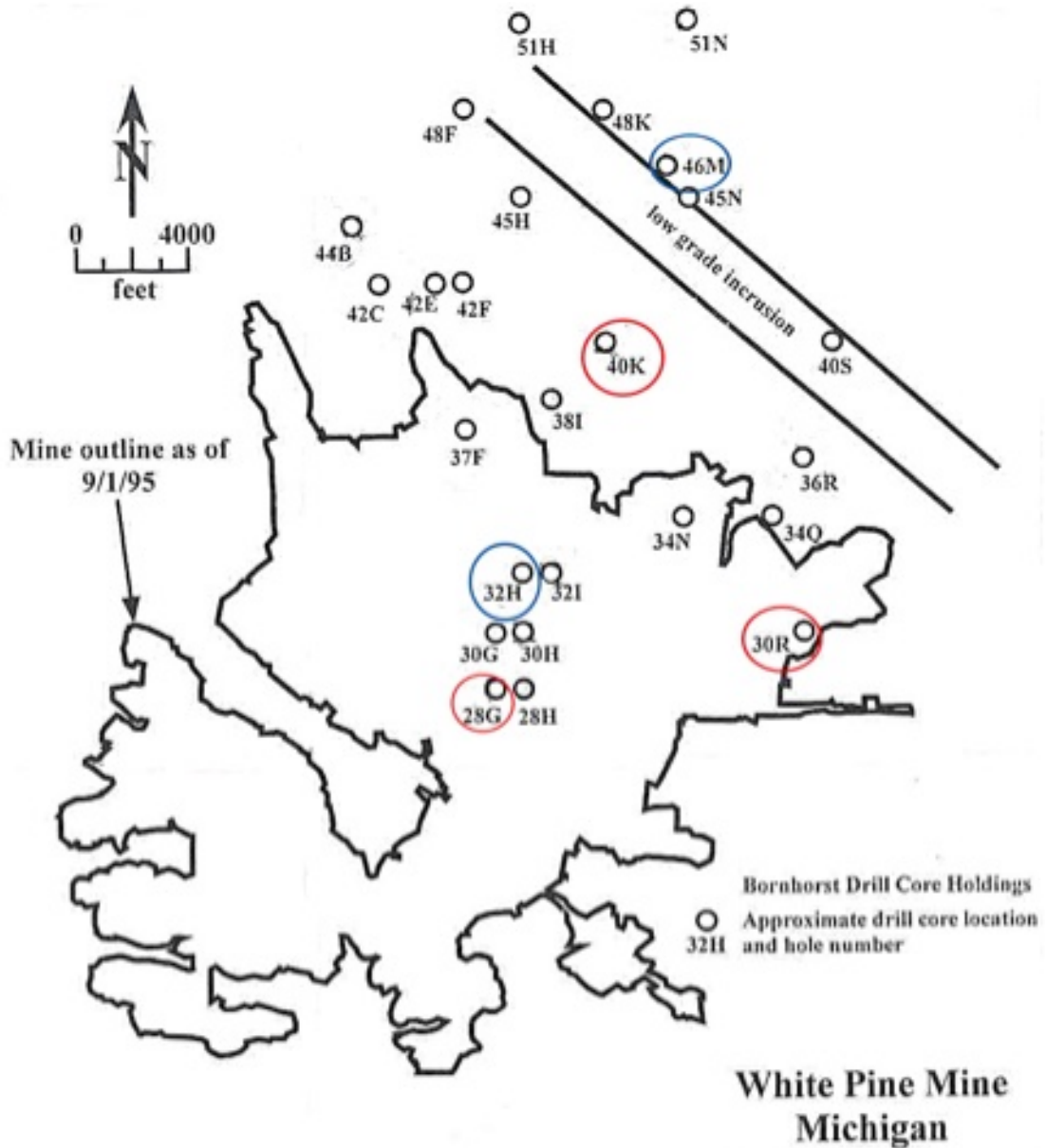


Figure 2: Map showing location of cores taken from the White Pine Mine area. Locations circled in red were used for microthermometry while locations circled in blue were sampled but only used for petrography. The sample used for GC-MS work was taken from core 30R. Mine outline defines the area of economic ore.



Figure 3: Micrograph from sample 30R 2263 showing the visible difference in fluorescence of oil inclusions, aqueous inclusions and epoxy under UV light. Field of view in this micrograph is 0.35mm.

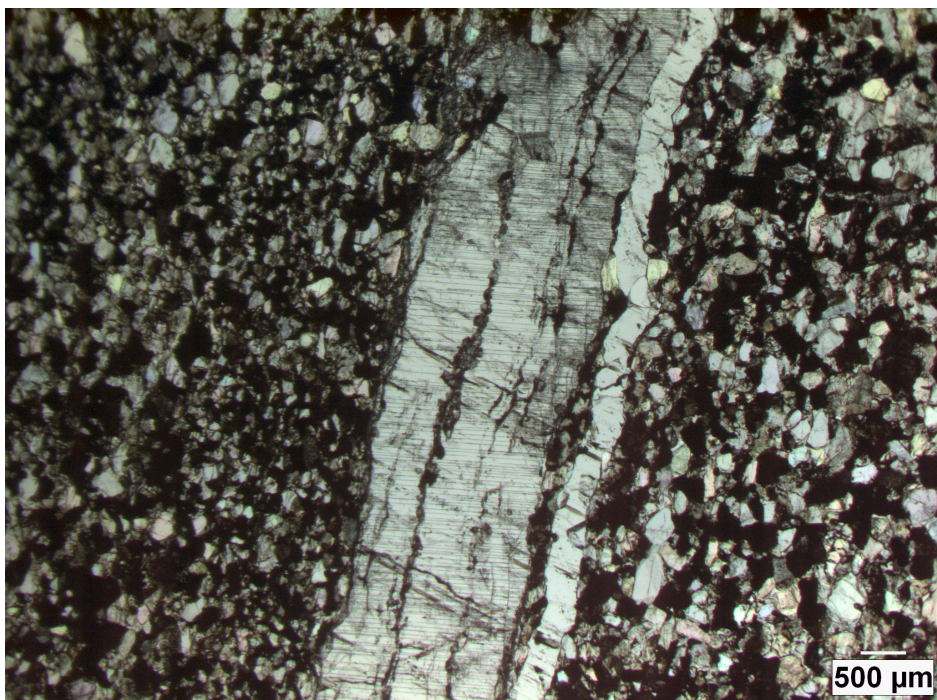


Figure 4: Laminated calcite vein in sample 30R 2263 from which inclusion oil was extracted for GC-MS analysis.

Chapter 3: Results

3.1 Petrography results

3.1.1 Nonesuch Formation Petrography and Sedimentology

Suszek (1997) thoroughly mapped the Nonesuch from top to base in outcrop at the Big Iron River site (Figure 5a), but Ensign et al. (1968) was the first to create a detailed stratigraphic section of the Nonesuch Fm (Figure 5b). In their stratigraphy, which is considered the definitive section by most other Keweenaw researchers, the Nonesuch Fm is split into two large sections: the Upper Nonesuch Fm, which is comprised of all but the basal ~20m of the formation, and the Lower Nonesuch Fm, which is comprised of the lowest 20m of formation and contains most of the copper-bearing minerals. The Lower Nonesuch Fm is split into three units (the Upper Shale, Upper Sand and Parting Shale) and then into 14 subunits (Figure 5b). In outcrop, it is difficult to see all of the various units noted Ensign et al.'s (1965) stratigraphic column (Figure 5b), but these are distinguishable in cores.

Though the Nonesuch Formation is occasionally referred to as the Nonesuch Shale, this is a misnomer. The sediments of the formation range from clay all the way to coarse sand. In general, the formation is dark grey to green colored silt with bitumen flecks visible to the eye. In the cores, which were taken from the Marker Bed to the upper part of the Copper Harbor Fm (just below the base of the Nonesuch Fm), these are more abundant in some layers than others, although they can be found throughout. There

are some oxidized sections throughout the core with a red to red-brown color, more predominantly near the top and the base of the Nonesuch Fm (King, 2009).

The Upper Nonesuch Fm mainly consists of siltstones and shales which are typically grey in color and calcite- or chlorite-cemented (King, 2009). Several layers and single bedding planes within layers have a bleached or greenish color and are laminated, and these are typically calcite-cemented. The coarse silt to fine sand sized grains, where present, are primarily quartz and calcite, with some feldspar, lithic clasts and trace amounts of other minerals including chlorite and epidote. The shale is fissile in many areas and breaks apart in layers 0.5-3cm thick. Bedding is present in some of these and is parallel to layering and graded. Mudcrack-like structures and ripple marks are present in some layers, as are ball and pillow structures. At the Big Iron River location approximately 800m downstream from the top of the Nonesuch Fm, syneresis cracks are present on a bedding plane (Figure 6). These structures are often thought to be created by salinity changes during deposition (Köykkä and Lamminen, 2011), which would provide more evidence for a near-shore marine environment, although Pratt (1998) argues that syneresis cracks are caused by earthquake activity, which also could have occurred in the rift system during deposition and later thrusting. Large calcite nodules, 15-20cm across and 5-10cm thick are present near the top of the Nonesuch Fm—these typically occur across layers in massive sections approximately one meter in thickness. Some of the nodules are cut by calcite veins with variable azimuths. Small (0.5-2cm) quartz, calcite and quartz-calcite veins cross the tops and sides of the layers in varying directions. Slightly lower in the formation, joints become more prominent in perpendicular directions, approximately 160° and 125°. Approximately 600m from top of the Nonesuch

Fm at the Big Iron River outcrop, calcite veins 2-3cm wide are present along these joints and will switch from one azimuth to the other as joints cross. The layer with these veins also contains the large calcite nodules mentioned previously. The joints continue throughout the rest of the section, and approximately 50m below the layer containing the calcite nodules, irregular bands of breccia 0.5-4cm thick appear. These brecciated bands are cut by the joints and in some areas there is up to 3cm of offset across joints. There is no clear pattern to the breccia bands—they vary in direction and size and also crosscut each other. Just below the brecciated sections is the top of the cupriferous zone. Chalcocite and native copper are visible on bedding planes and the copper-containing units tend to be more fissile than other units. Below these units the veins become wider, up to 5cm, trend at 185° at the Big Iron River site, and the surrounding rock is locally bleached for 2-3cm on either side of the vein. The veins are composed of quartz and/or calcite, and at least one vein was observed that also contained pyrite near the base of the Nonesuch Fm. Some of the veins have smaller veins attached that extend in perpendicular directions to the main vein.

The Marker Bed, at the top of the Lower Nonesuch Fm, is the most notable of the Nonesuch Fm units, standing out because of the small, diagenetic calcite nodules that are present (Figure 7). These typically range from 0.3-2.0mm in diameter, significantly larger than the grains in the sample, which are silt-sized. The nodules are often slightly elongated in the direction of bedding. These growths were likely present prior to matrix cementation as the grains in the shale are arranged around them but do not appear to be deformed or replaced.

At the contact between the Nonesuch Fm and the Copper Harbor Fm, sandstone and siltstone layers are interbedded, with the sand grains progressively becoming coarser. At the Presque Isle River contact, the sandstone changes in color from red to green just below the Nonesuch Fm/Copper Harbor Fm contact, and copper-bearing minerals are present just above the contact, though not in the greenish sandstone below the contact. Most of the copper minerals are contained in the Parting Shale unit of the Lower Nonesuch Fm, particularly in the Lower Transition subunit, although in this section, copper mineralization is visible for approximately 20m and continues past the Marker Bed unit, which is higher in the section than copper is typically found. There is also a blue-green, well-cemented conglomerate present just above the Marker Bed in this area with clasts up to 3cm across which has not been described previously. Copper minerals are present in and just slightly above this conglomerate.

There are many copper-bearing minerals in the Nonesuch Fm, particularly in the Lower Nonesuch Fm. An extensive study of Nonesuch Fm mineralogy was conducted by Brown (1971) who reported finding many different copper and iron sulfides including pyrite, chalcopyrite, chalcocite, bornite, hematite, djurleite and native copper. Most of the copper mineralization in the Nonesuch Fm occurs as chalcocite (Brown, 1971), although a notable amount of native copper is also visible in outcrop and hand samples.

3.1.2 Fluid inclusion petrography

Fourteen out of the 30 thin sections made contain oil inclusions (see Appendix A for list of thin sections). The inclusions, both oil and aqueous, are two-phase, liquid and vapor, with a gas bubble that typically comprises 5-10% of the volume of the inclusion,

although a few inclusions are notable for their very small or large gas bubbles. Mauk and Burruss (2002) observed three-phase inclusions (oil, gas and water) in veins they studied, but none are evident in the fourteen oil-containing thin sections from this study. The oil inclusions are mostly differentiated from the aqueous inclusions by fluorescence, although some do show a light brown color under normal light.

Out of the 14 samples that contained oil inclusions, three also contained copper-bearing minerals. BIR 6 was the stratigraphically highest sample to contain oil inclusions; this sample was collected from the Upper Nonesuch Fm, approximately 600m from the top of the formation where malachite was present along joints. There were only four thin sections made from the Upper Nonesuch Fm; of these, BIR 6 was the only one to contain oil inclusion. The other oil inclusion-bearing samples were from the Lower Nonesuch Fm, where they were found throughout the unit and particularly in the Marker Bed, of which every thin section made contained oil inclusions. The stratigraphically lowest samples to contain oil inclusions were collected from the top of the Copper Harbor Fm. It is possible that the lower sections of the Copper Harbor Fm could also contain oil inclusions; however for this study samples were only collected to ~5m below the top of the formation.

There are several different sites in which oil inclusions are present. They are largest and most abundant in the quartz-calcite vein from sample 30R 2263 (from the top of the Copper Harbor Fm) and the calcite vein of LIR 14 (likely from the Nonesuch Fm, collected from an excavation pile along the Little Iron River), and are present as both blue and yellow-fluorescing inclusions. In these veins, primary and pseudosecondary inclusions were observed in calcite crystals, and secondary inclusions were observed

throughout the vein. In thin sections made from sandstone layers of the Nonesuch Fm and the top of the Copper Harbor Fm (M46½ 2662, PIR 7, PIR 10, 30R 2221 and 28G 574), the inclusions are present mostly in oil-stained calcite grains in the matrix and are uniformly bright blue in color approximately 1-5 microns in size. The bitumen on the calcite grains also fluoresces in some cases, making it difficult to see the oil inclusions.

In shale (32H 951) and siltstone (40K 2140), the inclusions are extremely small, usually less than 1 micron, and it is difficult to tell exactly what site they belong to, whether it is matrix grains or cement. These inclusions are also typically bright blue in color, although a few rare orange inclusions were also present.

In two of the samples (BIR 16 and 28G 539), oil inclusions are present in the diagenetic calcite nodules of the Marker Bed. The orientation of inclusions in growths is highly irregular—in some nodules, the inclusions are in radial trails (Figure 8), in others they are present as smaller spherical clusters within the calcite itself, though not necessarily surrounding the growth center (Figure 9) and in some cases they are in trails cutting through the nodule but not radially (Figure 10). All three of these orientations occur in the same sample, though in individual nodules inclusion character is limited to one of the three options. All of the inclusion trails stop at the edges of the calcite. A third thin section (PIR 5) has visible nodules but they do not contain oil inclusions—instead, in this thin section, there are oil inclusions present only in the matrix calcite grains, and these are very small (<1 micron) and rare.

3.2 Microthermometry results

Thirty oil inclusions in each microthermometry sample were analyzed. In cases where inclusions differed in character throughout the sample (e.g., some inclusions in the matrix and others in a vein, yellow and blue inclusions), the inclusions chosen for analysis were split according to proportion in the sample. In addition to the oil inclusions, fifteen saline inclusions from two samples were analyzed (the other samples did not have visible aqueous inclusions). Individual oil-bearing inclusion homogenization temperatures for each sample are shown in Table 2.

Sample 40K 2088 had two distinct types of inclusions: those in the siltstone (both in grains and cement) and those in diagenetic calcite nodules present throughout the sample. All the inclusions present were oil—no saline inclusions were found. Oil fluorescence was mostly yellow with some blue inclusions. Fifteen inclusions of each type were heated. The maximum temperature allowed for heating was 150°C because of the fragility of the calcite (Prezbindowski and Tapp, 1991), but where the inclusion phases were not homogenized by 150°C, an estimate was made as to whether the inclusion was close to homogenization or not. This estimate was based on the behavior of the gas bubble in the inclusion and the overall appearance. It was observed during the study and has been observed in the past by Goldstein and Reynolds (1994) and Grimmer et al (2003) that the gas bubbles in liquid rich fluid inclusions become smaller and generally more active as the inclusion is heated. Typically, just before homogenization, the gas bubble is barely visible and appears to be vibrating at a high speed; therefore, a qualitative estimate as to whether or not an inclusion is close to homogenization may be made by observing both bubble size (close to or much smaller than its size at room

temperature) and movement (similar or higher-energy movement when compared to its behavior at room temperature). In the cases where the gas bubble in a given inclusion at 150°C was both much smaller and more energetic than at room temperature, it is described as being “close” to homogenization. In cases where the gas bubble was generally unchanged or only slightly smaller in size with similar bubble movement at 150°C when compared to room temperature, it is described as “not close” to homogenization. In the case of very light oils that homogenize close to their critical point, Grimmer et al (2003) observed that the volume of the gas phase did not decrease steadily during heating; however, in this study, the gas phase in all inclusions was observed to decrease at a steady rate, though the rate itself varied by inclusion.

The homogenization temperatures of oil inclusions in sample 40K 2088 ranged from 104°C to 231°C (Figure 11). In the calcite growths, the temperatures ranged from 100-231°C while the siltstone-hosted inclusions had a homogenization range of 104-222°C. For many of the siltstone-hosted inclusions, heating was stopped at 150°C; however there were several inclusions very close to homogenization at 150°C and for these the heating was continued until homogenization as it was unlikely to significantly damage the calcite until ~250°C. However, the majority of the inclusions that homogenized at >150°C were not close to homogenization at this temperature. Because of this, the true upper limit of the range may be higher than the values recorded.

Sample 28G 539 has a quartz and calcite shale matrix with spheroidal calcite nodules similar to those in sample 40K 2088. The growths present in this sample have a more deformed character than those in 40K 2088, however, appearing flattened, occasionally to the point of running veinlike across the thin section, although these are

distinguished from typical veins by their high opacity and grainy texture. In addition to the pseudo-veins, there is a quartz-calcite vein in this sample approximately 300 μ m wide and running perpendicular to bedding with a smaller vein branching off and running parallel to bedding. There are inclusions present in the vein, but they are too small for microthermometrical analysis. There are also some inclusions in the siltstone grains and cement of this sample, in a variety of colors from yellow to blue, however most inclusions are in the calcite growths. Also similarly to 40K 2088, most of these inclusions are bright blue, although a few are dim orange. Inclusions throughout the sample are mostly isolated or in very small clusters rather than trails. There are no visible aqueous inclusions in this sample.

The homogenization temperatures range from 50 to >150°C in a generally even distribution although there is a noticeable mode between 100 and 110°C (Figure 12). Overall, the range is lower than that of other samples with only 6 inclusions with homogenization temperatures beyond 150°C, and of these 6, only 4 were considered not close to homogenization at 150°C.

Sample LIR 14 has both oil and saline inclusions. Most of the oil inclusions have blue fluorescence although some exhibit yellow fluorescence. The inclusions in this sample are located in a quartz-calcite vein oriented parallel to bedding (azimuth of orientation is unknown as this sample was collected from an excavation pile along the Little Iron River), typically as primary inclusions around edges of grains, although they can also be found as pseudosecondary and secondary trails or small clusters. Yellow inclusions especially tend to occur in clusters rather than trails, although they are present in all three classes. Aqueous inclusions are also present in the vein. Homogenization

temperature for yellow inclusions ranges from 62°C to >250°C, with a distinct mode around 110-130°C (Figure 13) and a mean of 128°C. Homogenization temperatures for blue inclusions ranges from 73°C to >250°C, with the majority between 130-170°C and a mean of 152°C. Saline inclusions show final ice melting points ranging from -6 to -45°C (Figure 14) and homogenization temperatures ranging from 140 to >250°C (most not close to homogenization at 250°C) with one outlier homogenized at 75°C (Figure 15).

Sample 30R 2263 shows mostly uniform blue-yellow fluorescing inclusions with a very few inclusions that show color variations. The blue-yellow inclusions occur in trails, clusters and isolated inclusions, whereas the differently colored inclusions are only present in isolation. Some of the inclusion trails have much dimmer, more mustard-yellow fluorescence, appearing to be somewhere in between a mobile and solid phase based on their appearance and the existence of solid brown inclusions within the same trail. Inclusions are very abundant in this sample, almost all contained in a laminated calcite vein approximately 2mm across running through the sample parallel to bedding (Figure 4). They are dense toward one end of the vein, and sparse at the other, in both intragranular trails (Figure 16) and transgranular trails (Figure 17). Some inclusion trails cross very slightly over the edge of the vein. In general, the inclusion trails are parallel to the vein, with occasional small trails branching off at 90° from the main trails. In some grains, the inclusions are so abundant that it is difficult to make out individual trails and so a trail azimuth could not be established (Figure 18). In several trails, the inclusions are elongate along the trail direction. In addition to the oil inclusions, there are also numerous solid and aqueous inclusions present in the vein. There are very few oil inclusions found in the sample outside of the vein and those that are outside are mostly

very close to the edge of the vein. The homogenization temperature of the oil inclusions ranges from 65°C to >250°C, with uneven distribution that is skewed toward the higher end temperatures (Figure 19). The mean of the homogenization temperatures of the blue-yellow inclusions (227°C) was noticeably higher than that of the yellow inclusions (163°C). The aqueous inclusions homogenize from 170 to >250°C (Figure 20) and have final ice melts between -24 and -1°C, with one anomalous outlier with a final melting point of 15°C (Figure 21). The melting ranges for this sample are very broad, with some ice melting slowly over a span of 40 degrees from first visible liquid to last visible solid with eutectic melts between -60 and -70°C, suggesting more complex salts than a simple CaCl₂-NaCl combination (Goldstein and Reynolds, 1994; Munz 2001). The single inclusion that melted with a range of -15 to 15°C may contain methane clathrate as the behavior of this inclusion was similar to that of clathrates observed by Murphy and Roberts (1997) and would hence be an indicator that dissolved methane is present in some of the aqueous inclusions.

In Sample BIR 16, the inclusions are mostly present as intragranular clusters and isolated inclusions in silt-sized quartz clasts (Figure 22). Trails are short, infrequent and do not cross grain boundaries, in some cases not even reaching from edge-to-edge of a grain. They are highly variable in color of fluorescence, from dim yellow to bright blue, often showing variation within the same cluster or trail. There is a quartz-calcite vein in this sample that runs perpendicular to bedding, but, in contrast to sample 30R 2263, there are no inclusions present within the vein. The inclusions tend to be more abundant in silt-sized grains than in fine sand-sized ones. There are no visible aqueous inclusions present in the sample.

The homogenization temperatures of the oil inclusions range 94°C to >150°C (Figure 23). As in the case of sample 40K 2088, the sample was not heated past 150°C to preserve the integrity of the calcite. Most of the inclusions with temperatures greater than 150°C were not close to homogenization at that temperature. The temperature distribution up to the 150°C limit is generally uniform with 3-13% of the inclusions homogenizing per 10° increase in temperature. Almost half the inclusions were not close to homogenization at 150°C, but it is impossible to say if they would have continued to homogenize gradually with increasing temperature or if all would have homogenization temperatures similar to one another.

3.3 GC-MS results

3.3.1 General characteristics of inclusion oil

The *n*-alkanes in the sample are present in very high concentration with 106µg recovered (26µg/g calcite), overwhelming much of the other data that would normally be available from SIM GC-MS. The amount of hydrocarbons obtained from the inclusions is abnormally high compared to other FI extractions for GC-MS work (Ahmed, 2009, pers. comm.), although the percentage of *n*-alkanes in the sample is not surprising given that it is likely of Precambrian origin (McKirdy, 1974). Typical sterane and hopane biomarkers were undetectable in this analysis, although they were found in a study by Pratt et al. (1991) using multiple reaction monitoring GC-MS on extracted bitumen from Nonesuch Fm cores.

The GC-MS chromatogram of partial *m/z* 85 shows a normal distribution of *n*-alkanes ranging from C₈ to C₃₆ and peaking at C₁₇ (Figure 24) with no preference for odd

or even carbon chain lengths (Carbon Preference Indices [CPIs] are all ~1). The pristane/phytane ratio is high (2.99), however the pristane/*n*-C₁₇ ratio is very low as is the phytane/*n*-C₁₈ ratio (0.24 and 0.09 respectively). Isoprenoids ranging from iC₁₃-iC₁₈ are present in low concentrations relative to *n*-alkanes and can be seen on partial *m/z* 85 and 113. No β-carotane was recorded in *m/z* 125. The aromatic plots, partial *m/z* 106, 120 and 134 show numerous alkylbenzenes. Several trimethylbenzenes (TMBs) are present, with 1,2,4-TMB at the highest concentrations. On the partial *m/z* 134 chromatogram, many peaks are present, although probably the most important of these are the tetramethylbenzenes (TeMBs), of which 1,2,3,5-TeMB is the most concentrated, followed by 1,2,3,4-TeMB and 1,2,4,5-TeMB.

Partial *m/z* 128 shows the presence of naphthalene and partial *m/z* 142 shows 1- and 2-methylnaphthalene (MN) with a slight preference toward 2-MN. There are several dimethylnaphthalenes (DMNs) visible in partial *m/z* 156, the most abundant of which is 1,6-DMN. 1- and 2-ethylnaphthalene (EN) are also present in this chromatogram. Partial *m/z* 170 and 184 show many different stereoisomers of trimethylnaphthalenes (TMNs) and tetramethylnaphthalenes (TeMNs), with the largest peaks at 1,3,5- + 1,4,6-TMN and 1,2,4,6- + 1,2,4,7- + 1,4,6,7-TeMN respectively. There are pentamethylnaphthalenes (PMNs) present in the partial *m/z* 198 chromatogram, though they are noticeably less abundant than the TMNs and TeMNs. The highest concentration of these is the 1,2,3,5,6-PMN.

Both phenanthrene (PHEN) and anthracene are present on partial *m/z* 178, and there are four methylphenanthrenes (MP) visible on partial *m/z* 192. Of these, 9-MP is by far the most abundant in the sample. Several dimethylphenanthrenes (DMPs) are present

on m/z 206, the highest peak of which is caused by the combination of 1,3- + 3,10- + 2,10- + 2,6-DMP. There are no C_3 alkylphenanthrenes present, although there is a peak on m/z 284 that may be retene, although it is more likely n -alkane interference. Similarly, there is a peak on the partial m/z 183 and 198 chromatograms that may be cadalene, but again is probably caused by n -alkane interference.

Biphenyl (Bp) is present in the sample, as are methylbiphenyls (MBp), dimethylbiphenyls (DMBp) and ethylbiphenyls (EBp). 2-MBp is the most concentrated of the MBps, and 2,3'- and 3,3'-DMBp are the most abundant of the DMBps. 3- and 4-EBp are the only ethylbiphenyls present, both in fairly low concentration in comparison to the DMBps when viewed on the partial m/z 182 chromatogram. 2- and 4-methyldiphenylmethane are present on this chromatogram as well, also in low concentration relative to the DMBps.

A small fluorene peak is present on partial m/z 166 chromatogram, and fluoranthene and pyrene are visible on the m/z 202 chromatogram. Methylfluorenes (MFIs) are present on the partial m/z 180 plot with 1-Mfl in much higher concentration than the other MFIs. No methylfluoranthenes or methylpyrenes could be distinguished in the sample.

Dibenzothiophene (DBT) is present in the sample and shows a clear peak on partial m/z 184. There are also three distinct peaks for methyldibenzothiophenes (MDBTs) on m/z 198, the highest of which is 4-MDBT. There are also several dimethyldibenzothiophene (DMDBTs) peaks on chromatogram m/z 212, with 4,6-DMDBT, 3,6-DMDBT and 2,6-DMDBT showing particularly high peaks.

There was no obvious unresolved complex mixture (typically seen as an unidentifiable “hump” of data that is shorter than resolvable peaks) on any of the scans. The presence of such a mixture is characteristically seen on chromatograms of oil that has undergone biodegradation (George et al., 1998), which is consistent with Mauk and Burruss’ (2002) conclusion that the oils were water washed but not biodegraded.

3.3.2 Thermal maturity indicators

Most of the aromatic ratios in the inclusion oil indicate an early- to peak-oil window maturity, approximately corresponding to temperatures of 100-130°C. There is 1,2,5-TMN present in the sample, which suggests that it did not reach high maturity, as this is the first of the TMNs to break down during heating (Alexander et al., 1988). The three methylnaphthalene ratios described by van Aarssen et al. (1999) using TMN, TeMN and PMN all indicate a mid-oil window maturity with values at 0.49, 0.47 and 0.30 respectively. A visual representation as compared to the example of van Aarssen et al. (1999) can be seen in Figure 25. The calculated vitrinite reflectance (%R) is 0.8%, also suggesting a mid-oil window maturity (George et al., 2004b).

Early oil-window maturity indicators include the ethylnaphthalene ratio (ENR, 0.59) (George et al., 1998), the dimethylphenanthrene ratio (DPR; $[3,5\text{-}+2,6\text{-DMP}+2,7\text{-DMP}]/[1,3\text{-}+3,9\text{-}+2,10\text{-}+3,10\text{-DMP}+1,6\text{-}+2,9\text{-}+2,5\text{-DMP}]$, 0.15) (George et al., 2004) and the dimethylnaphthalene ratios (DMRs), for example DMR-x ($[2,6\text{-}+2,7\text{-DMN}]/1,6\text{-DMN}$, 0.66) (George et al., 1998). The inclusion oil contains no 1,8-dimethylnaphthalene (DMN), which is the least thermally stable of the dimethylnaphthalenes (George et al., 1998), although this is somewhat expected given that most other studies of the Nonesuch

Formation have found low but not extremely low temperatures. Brown (1971) studied the thermal stability of sulfide minerals present in the area and found pink bornite present as a pseudomorph of pyrite and also found small amounts of djurleite, both in the transition between the Cu-rich and Fe-rich parts of the Nonesuch Fm; the thermal stability of these minerals suggests a maximum temperature of $\sim 100^{\circ}\text{C}$. Similarly, Nishioka (1983, as reported in Ho and Mauk, 1996) observed monoclinic chalcocite in veins which is only stable up to $\sim 103^{\circ}\text{C}$. However, Mauk and Hieshima (1992) caution that copper sulfides are not necessarily a reliable geothermometer based on the work of Barton and Skinner (1979, as reported in Mauk and Hieshima, 1992) on rapid re-equilibration of copper sulfide minerals. Ho et al. (1990), using pyrolysis of organic matter from mineralized Nonesuch Fm samples, found T_{max} values of $450\text{-}460^{\circ}\text{C}$, indicating peak-oil window maturity.

3.3.3 Biomarkers

Several of the traditional specific biomarkers (eg. hopanes and steranes) were not detected in this sample because of *n*-alkane interference. However, there is still some biological information that can be inferred from the alkanes and aromatic compounds that were measured.

In general, the *n*-alkane distribution is typical of other Proterozoic oils. *n*-C₁₇ is commonly the most abundant of the alkanes in Precambrian hydrocarbons, and it is suggested that it is derived from cyanobacteria (McKirdy, 1974), although that interpretation may not be valid in this study because, while *n*-C₁₇ is at the peak of the

distribution, it does not stand above the general trend of the *n*-alkanes. The small clusters of peaks that represent iC_{14-18} monomethylalkanes on the m/z 85 chromatogram show a preference for mid-chain substituted isomers. These isomers, when present in equal or greater concentrations than the end-chain substituted isomers, are also a biomarker for cyanobacteria (Volk et al., 2005a; George et al., 2008).

The terrigenous/aquatic ratio (TAR, $[C_{27} + C_{29} + C_{31}]/[C_{15} + C_{17} + C_{19}]$), which compares *n*-alkanes normally formed from higher plants to those typically formed by algae, is very low (0.18). Though this ratio can be affected by high temperatures, breaking down the terrestrially-sourced higher-end carbon chains, it is also thought that terrigenous sources add a relatively higher beginning concentration of *n*-alkanes (Peters et al., 2005), so the extremely low value of this ratio at these maturities suggests that there was little to no higher-plant input, as expected for a Mesoproterozoic oil. In addition, there is a very small amount of 1,2,7-TMN present, with a ratio of 0.17 relative to 1,3,7-TMN, showing that the organic matter was likely deposited before the evolution of angiosperms (George et al., 1997). The low DMPR-x ratio (1,7-DMP/1,7-+1,3-+3,9-+2,10-+3,10-DMP) of 0.14 suggests no resin input in the sample (Alexander et al., 1988). 1,2,5-TMN, though it can be an indicator of resins from higher plants (Alexander et al., 1988) is also thought to be a product of cyanobacteria in some oils (Grice et al., 2001 in Peters et al., 2005), and is present here in moderate concentrations. There were no biomarkers found that suggest life forms typically found in the later Precambrian such as those derived from late Neoproterozoic sponges or diverse eukaryotes (Love et al, 2009). Pratt et al. (1991) did find evidence for eukaryotic input in their biomarker data, but they

attribute it to an algal source and do not claim that it is more diverse than expected for the Mesoproterozoic.

The dibenzothiophene/phenanthrene (DBT/PHEN) ratio is very low, 0.06, and this along with the low MDBT/MP ratio indicates a low-sulfur source rock (George et al., 1997; Dutkiewicz et al., 2004). When the DBT/PHEN ratio is paired with the Pr/Ph ratio, the resulting point plots just on the line between a marine/lacustrine shale and a fluvio-deltaic source rock (Figure 26; Hughes et al., 1995). According to Peters et al. (2005), Pr/Ph values below 2 are indicative of a marine source whereas Pr/Ph values between 1-3 are generally from a lacustrine source. The sample Pr/Ph value of 2.99 would then support the hypothesis that the Nonesuch Fm, while it may have had some saline input (Hieshima and Pratt, 1991; Uchytel et al., 1999), was deposited in a lacustrine environment.

3.3.4 Comparison with other Nonesuch Formation studies

The information obtained from the SIM GC-MS analysis was compared with similar pore-space oil and bitumen data and also against GC-MS data from previous studies of the Nonesuch shale to determine whether the oil in the fluid inclusions is related to the preserved organic matter in the pore spaces or is from a different source entirely (Table 3).

The Pr/Ph ratio and *n*-alkane distribution of the FI oil from 30R 2263 was essentially identical to sample 188-01 analyzed by Mauk and Burruss (2002) from a calcite vein from the upper Nonesuch Fm in the White Pine Mine area, and the Pr/*n*-C₁₇ and Ph/*n*-C₁₈ values are also within 0.02 of the ratios obtained in this study. The

distributions of *n*-alkanes on the chromatograms from their other samples were similarly bell-shaped, but with a peak typically slightly lower, between C₉ and C₁₅. When compared with their sample set (Figure 27), the 30R 2263 oil appears to have undergone moderate water washing.

The FI *n*-alkane GC-MS plot in this study is comparable to one obtained by Ho et al. (1989), who studied the total extractable material from unmineralized portions of the upper shale of the Nonesuch Fm, and to two gas chromatograms from Uchytíl et al. (1999), one analyzing oil from a Nonesuch Fm core and the other seep oil from the White Pine mine (Figure 28). Both of Uchytíl's GC results are slightly skewed to the higher-end carbon chains, though the peak is at C₁₇ for both and the upper limits of the alkanes are in the C₂₈-C₃₂ range. It is reasonable to assume that some of the lighter alkanes from Uchytíl's samples may have been lost due to evaporation during the GC preparation process, as observed by Ahmed and George, 2004.

The Pr/Ph and Pr/*n*-C₁₇ and Ph/*n*-C₁₈ ratios of 30R-2263 is similar to the extracted bitumen analyzed by Ho and Mauk (1996), particularly their sample 192 (Pr/Ph = 2.75, Pr/*n*-C₁₇ = 0.17, Ph/*n*-C₁₈ = 0.07), a hand sample from the "lower sandstone" (actually the upper part of the Copper Harbor Conglomerate) in the southwest area of the White Pine Mine. These ratios are also similar to the ratio obtained by Hieshima and Pratt (1991) using the extractable oil and bitumen of the Nonesuch Fm. The Pr/Ph ratio is much closer to the ratios from their samples originating in Michigan (avg. 3.2) than those originating in Wisconsin (avg. 1.98); however, the Pr/*n*-C₁₇ and Ph/*n*-C₁₈ ratios from the fluid inclusions are closer to the Wisconsin samples, though the Wisconsin ratios are still slightly higher. Their saturated hydrocarbon analysis conducted on oil from oil seeps at

the Copper Range mine, however, had a similar character to the FI oil in that the Pr and Ph were in very small amounts when compared to the *n*-alkanes, although their *n*-alkane distribution was skewed more toward the lower-MW chains than the FI distribution (Figure 29). Mauk and Hieshima (1992) showed similar skewed distributions in their GC work on seep petroleum from the White Pine copper mine with peaks at *n*-C₁₅ in the northeastern part of the mine and *n*-C₁₃ in the southwestern area. They also found a higher percentage of *n*-alkanes compared to Pr and Ph in the petroleum seeps than in the extracted bitumen from the mine.

Table 2: Oil inclusion homogenization temperatures obtained from microthermometry. Approximate averages were calculated arithmetically using a value of 275°C for measurements of >250, 200°C for measurements of >150 (not close), 175°C for measurements of >150 (close) and 160°C for measurements of >150 (very close). Full microthermometry data is available in Appendix B.

40K 2088	LIR14	30R2263	BIR 16	28G 539
158	62	234	103	59
104	74.3	>250 (x10)	111	100
111.5	198	167.4	120	109
119	121	199	94	124
170	123	193.3	>150 (not close)	109
222	123	183	>150 (not close)	115
116	126	224	>150 (not close)	>150 (not close)
143	145	>250	>150 (not close)	>150 (not close)
137	111	177	>150 (not close)	>150 (not close)
155	>250	172.4	109	72
>150	93	102.1	115	103
>150	115.8	85	122	>150 (close)
>150	156	102	101	>150 (not close)
>150	131	200.9	140	75
>150	86.6	65	>150 (close)	77
163	142	93	>150 (not close)	93
171	105	107.6	>150 (not close)	140
182	109	166.5	>150 (not close)	103
138	73	163	138	110
141	93	219.2	140	50
113	167	128	113	56
180	>250	148.9	>150 (not close)	>150 (very close)
155	>250	234	>150 (not close)	108
168	150	244	>150 (not close)	143
170	152	231	150	83
205	155	239	>150 (very close)	108
231	165	96.2	>150 (close)	92
142	88	104	143	116
100	133	106	>150 (close)	108
133	>250	216.1	>150 (not close)	135
Average 156.75	Average 143.26	231	Average	110
		233	159.47	Average
		233.5		117.19
		Average 196.32		

Table 3: Comparison of GC-MS data from sample 30R 2263 with other Nonesuch Fm studies.

Study	Pr/Ph	Pr/n-C17	Ph/n-C18
30R 2263	2.99	0.24	0.09
Hieshima & Pratt 1991 Michigan	3.2	0.86	0.36
Hieshima & Pratt 1991 Wisconsin	1.98	0.41	0.24
Hieshima & Pratt 1991 Oil Seep	1.66	0.25	0.12
Pratt et al., 1991 - Core	2.5-6	0.4-0.9	
Pratt et al., 1991 - Seeps	"similar"	0.15	
Mauk and Burruss 2002 #188-01	2.98	0.22	0.08
Mauk and Burruss 2002 - average	2.29	0.3	0.13

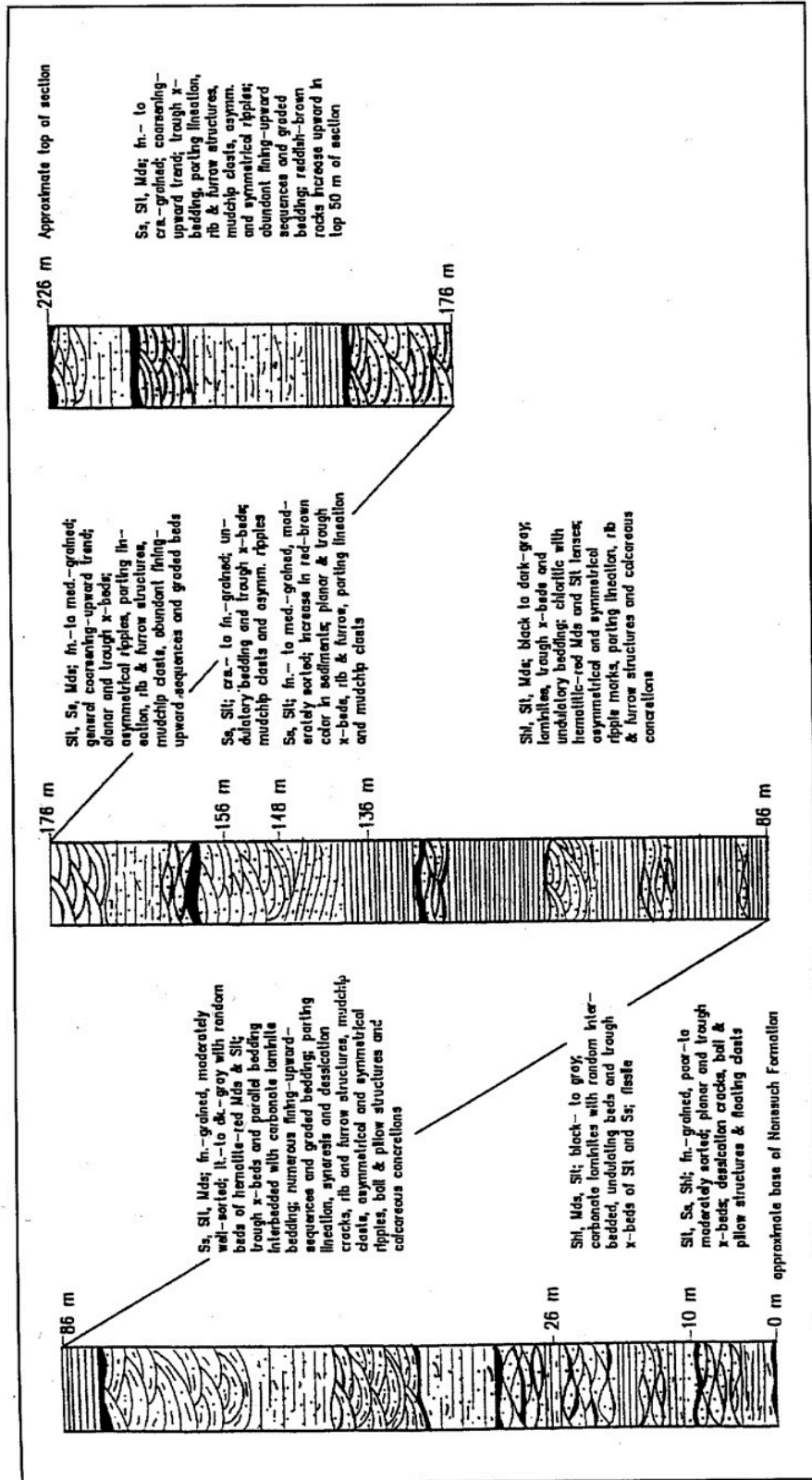


Figure 5a: Full stratigraphic section of the Nonesuch Formation at the Big Iron River outcrop from Suszek (1997). Thickness in this area is ~250m. Detailed section of the lower 20m of the Nonesuch Fm is shown in Figure 5b.

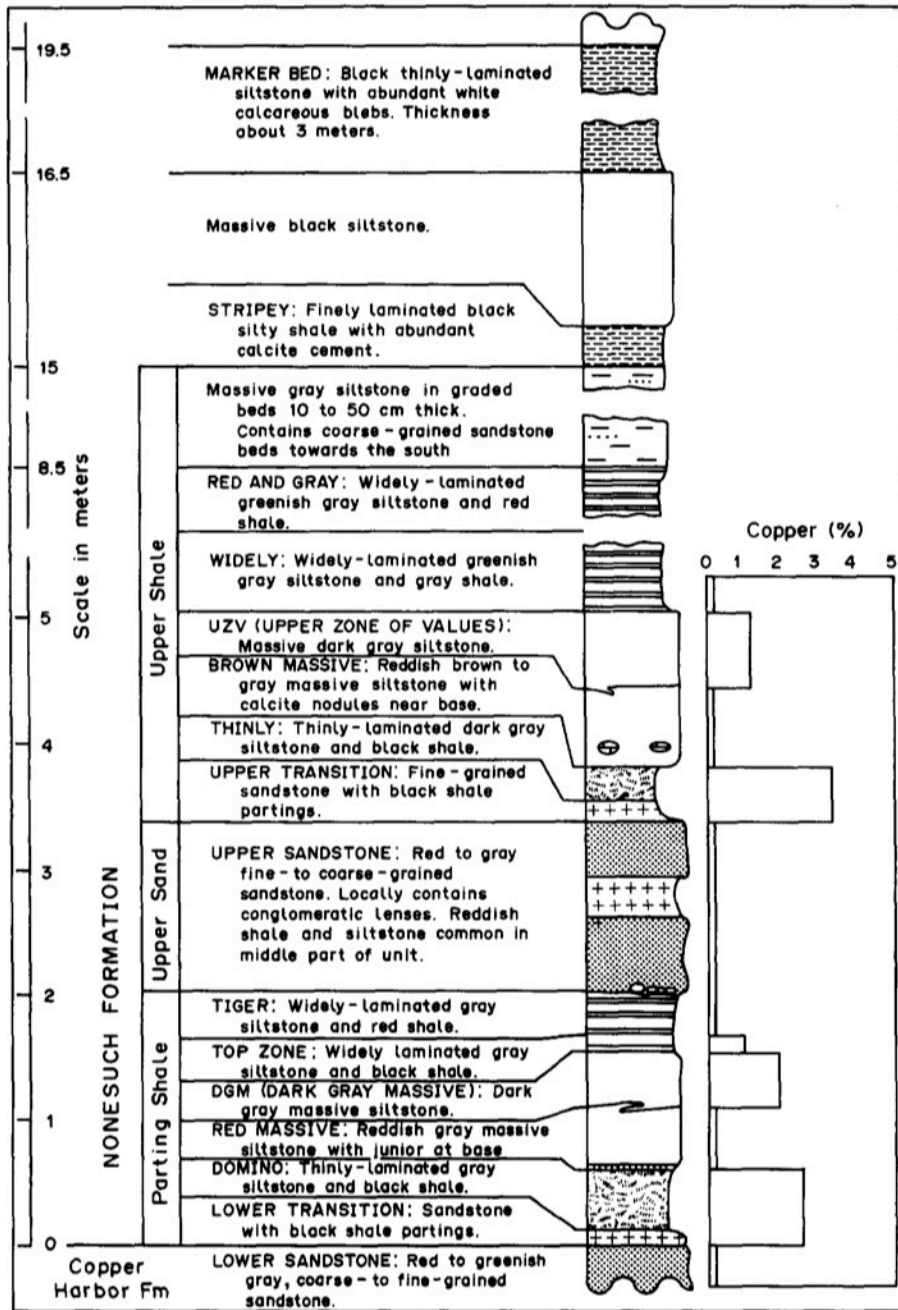


Figure 5b: Stratigraphic section of the Nonesuch Formation by Ensign et al. (1968) with percent copper added by Mauk and Hieshima (1992). The lower ~20m of the Nonesuch Fm has been extensively divided into small sections, but the upper part (shown in Figure 5a) has been given general divisions only.



Figure 6: Syneresis cracks on a bedding surface in the Upper Nonesuch Formation in outcrop at the Big Iron River approximately 300m downstream of Bonanza Falls (corresponds to 136-86m section in Figure 5b).



Figure 7: Spherical calcite nodules in thin section from sample 40K 2088.

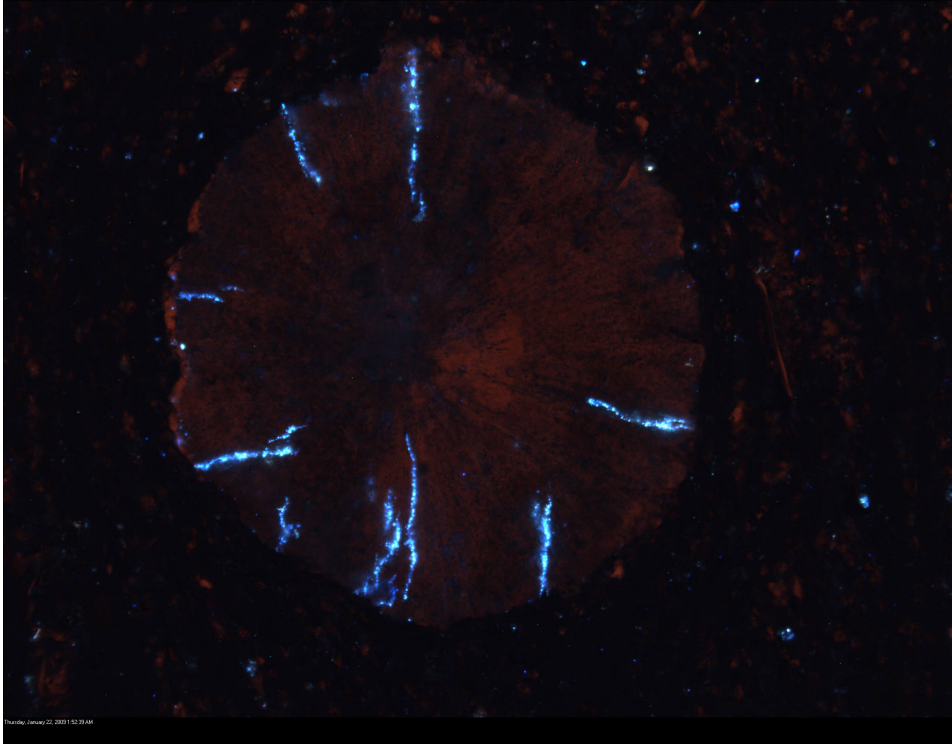


Figure 8: Radial trails of oil inclusions in calcite nodule from sample 40K 2088 under UV light. Field of view in this micrograph is 1.5mm.

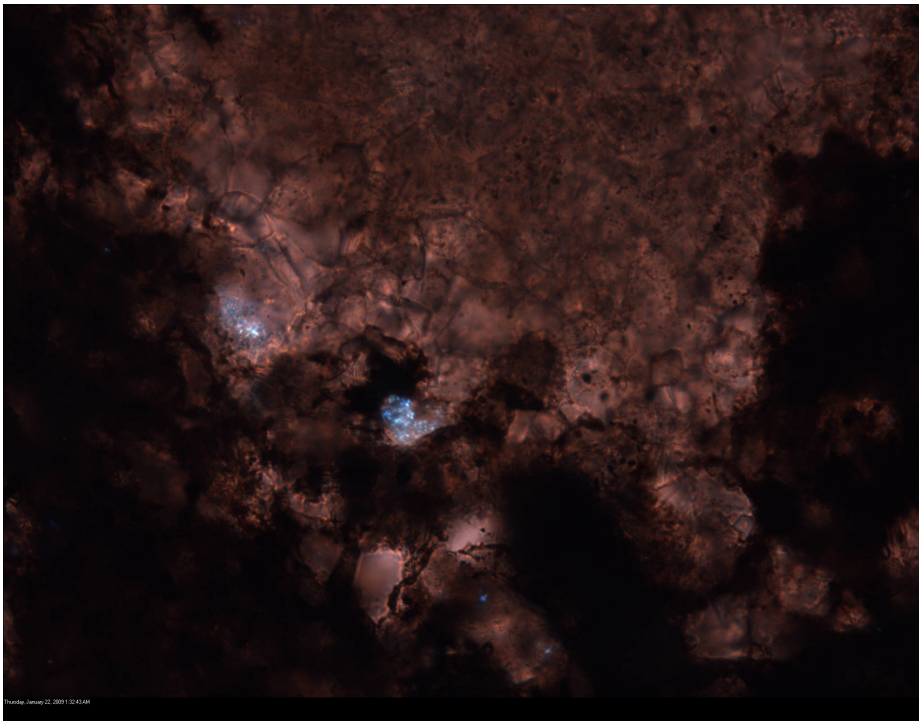


Figure 9: Small clusters of oil inclusions in calcite nodule from sample 40K 2088 under UV light. Field of view in this micrograph is 0.35mm.

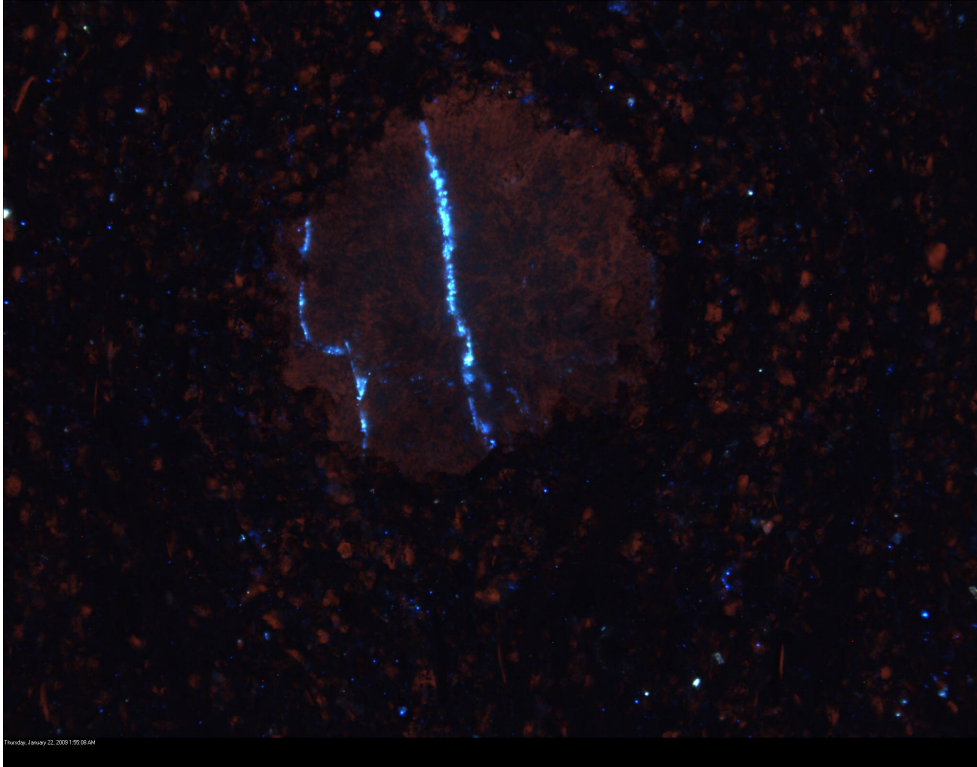


Figure 10: Non-radial trail of oil inclusions in calcite nodule from sample 40K 2088 under UV light. Field of view in this micrograph is 1.5mm.

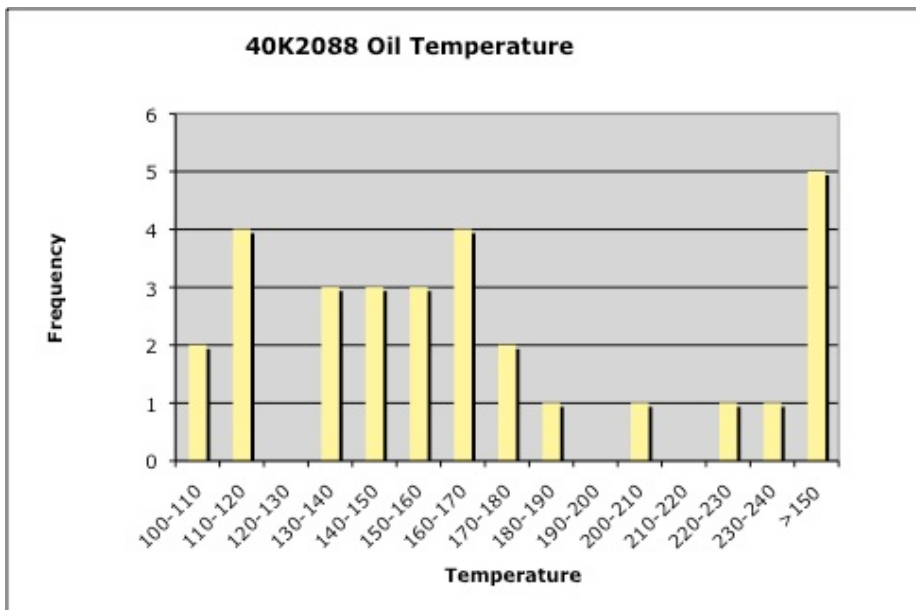


Figure 11: Histogram of oil inclusion homogenization temperatures from sample 40K 2088. Temperatures are in °C. In some instances where the oil inclusions appeared to be near homogenization, heating was continued until they homogenized. Otherwise, heating was stopped at 150°C.

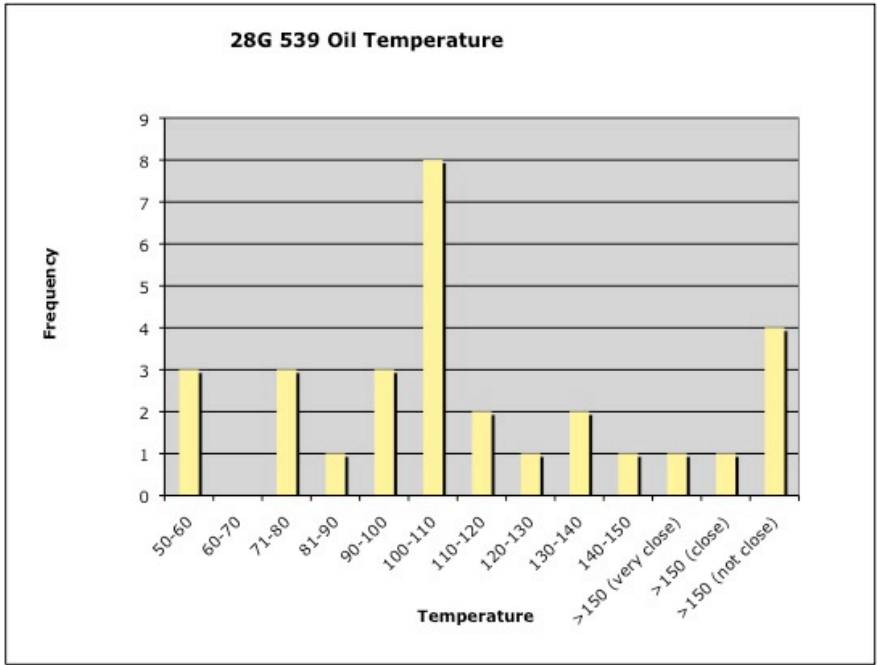


Figure 12: Histogram of oil homogenization temperatures from sample 28G 539. Temperatures are in °C. Qualitative estimates of how near an inclusion was to homogenization were made when heating reached 150°C. This sample was not heated beyond 150°C.

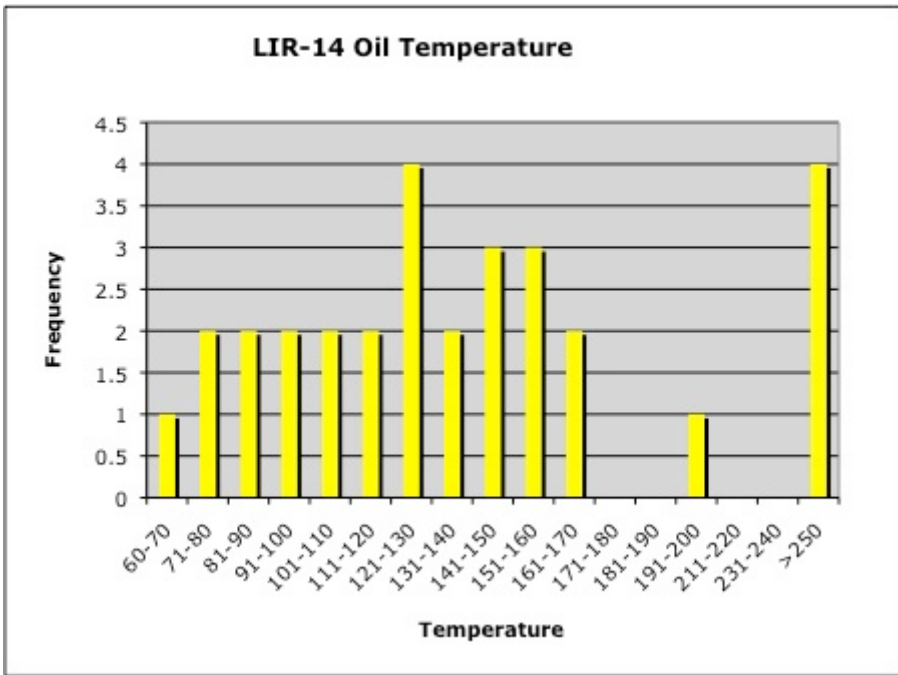


Figure 13: Oil homogenization temperatures for sample LIR 14. Temperatures are in °C. The sample was not heated beyond 250°C although there were several inclusions that had not yet homogenized at this temperature.

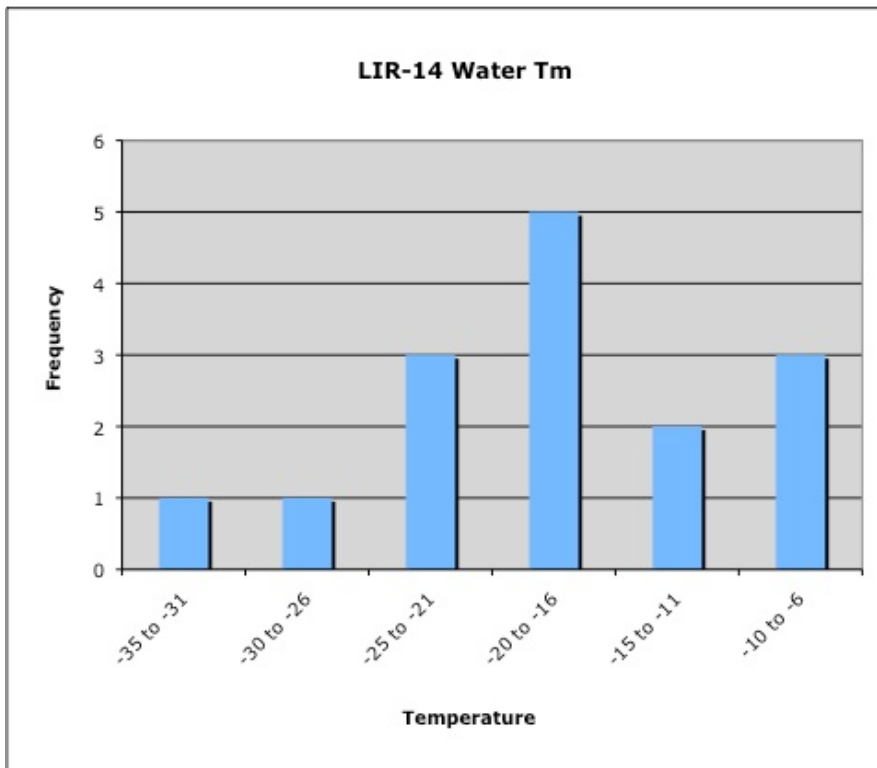


Figure 14: Histogram of final melting points of aqueous inclusions in sample LIR 14. Temperatures are in °C.

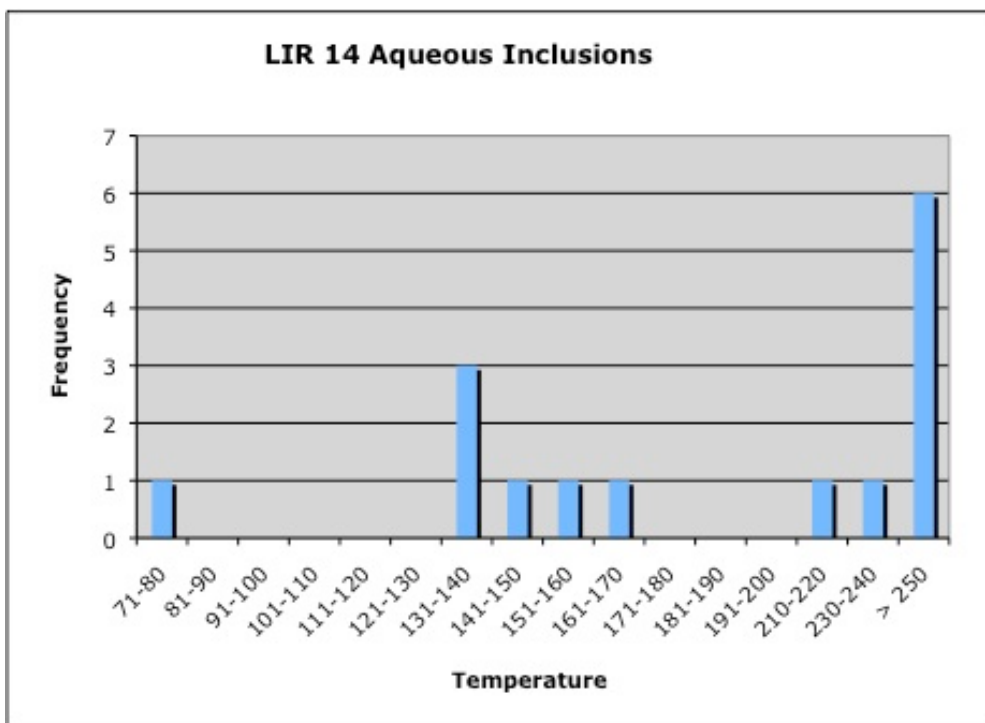


Figure 15: Histogram showing homogenization temperatures for aqueous inclusions in sample LIR 14. Temperatures are in °C.

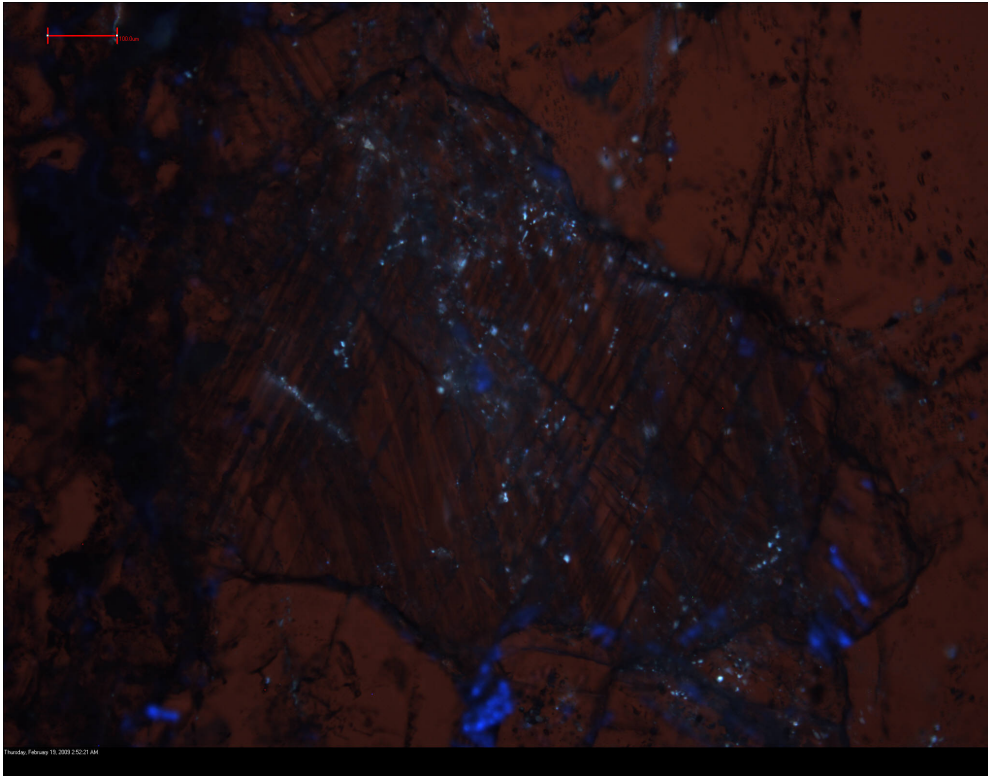


Figure 16: Intragranular oil inclusion trails in vein calcite from sample 30R 2263 under UV light. Field of view in this micrograph is 1.5mm.

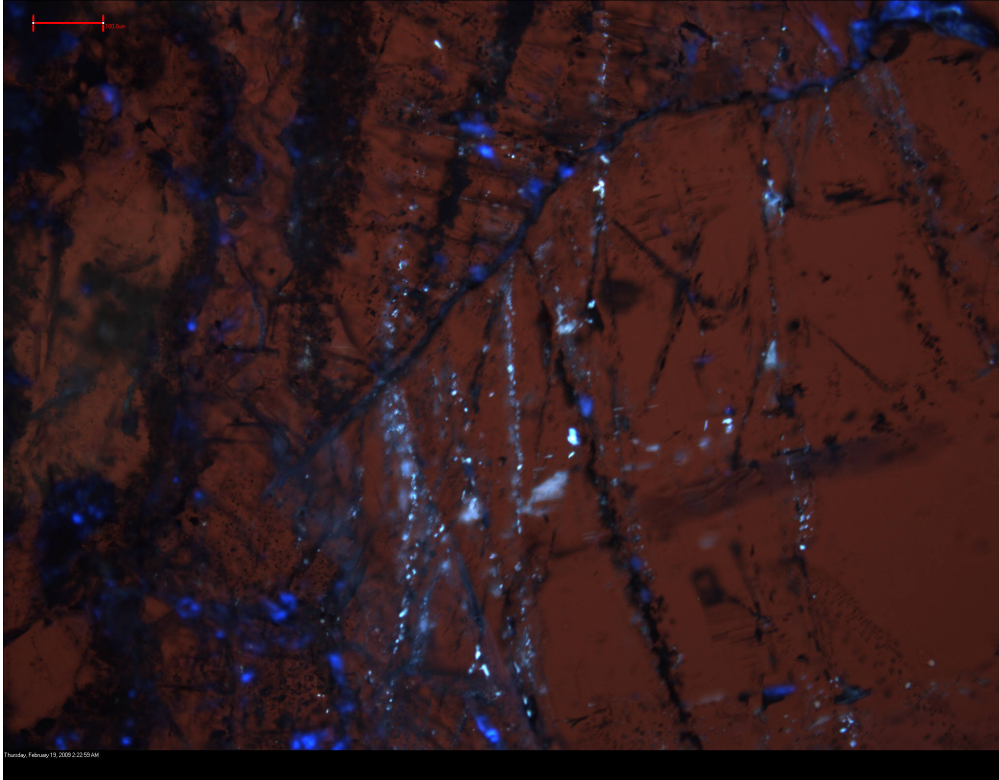


Figure 17: Transgranular oil inclusion trails in vein calcite from sample 30R 2263 under UV light. Field of view in this micrograph is 1.5mm.

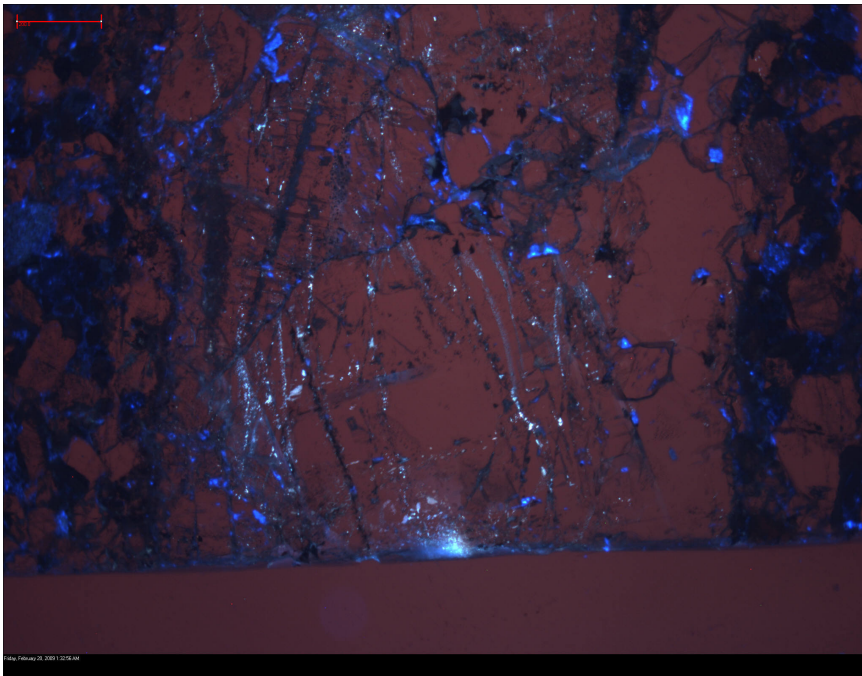


Figure 18: Area in calcite vein of sample 30R 2263 under UV light where oil inclusion trails are so numerous it is difficult to determine trail azimuths. Field of view in this micrograph is 3.5mm.

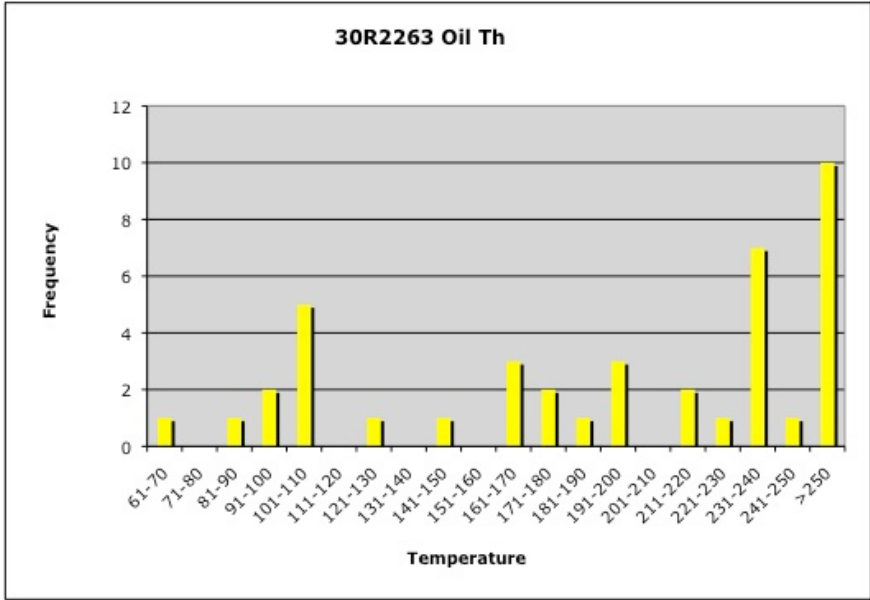


Figure 19: Histogram of oil inclusion homogenization temperatures in sample 30R 2263. Temperatures are in °C.

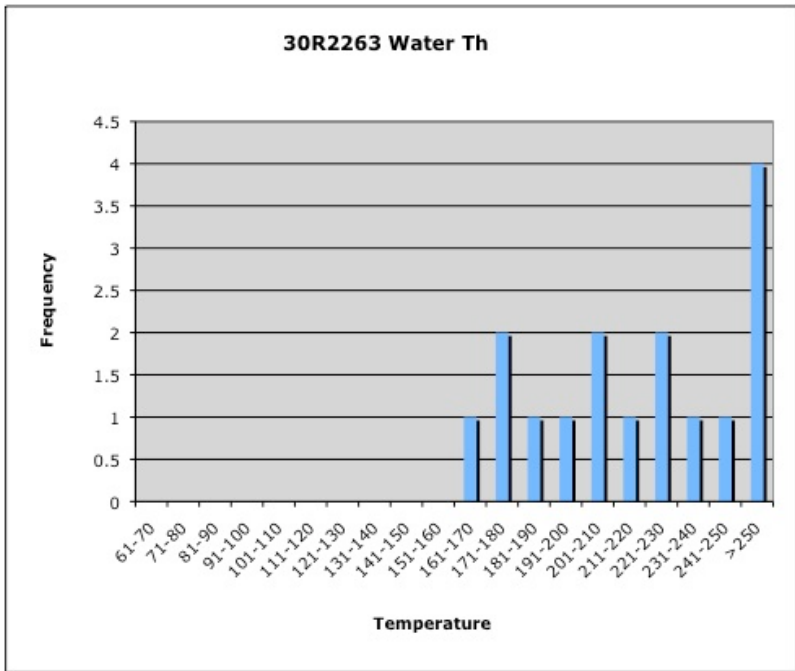


Figure 20: Histogram of homogenization temperatures of aqueous inclusions in sample 30R 2263. Temperatures are in °C.

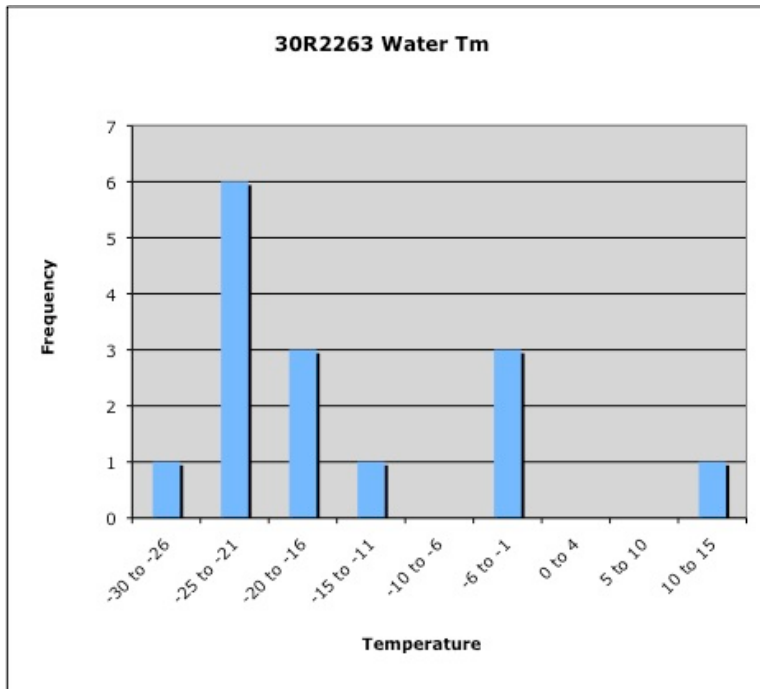


Figure 21: Histogram of final melting point of aqueous inclusions in sample 30R 2263. Temperatures are in °C.

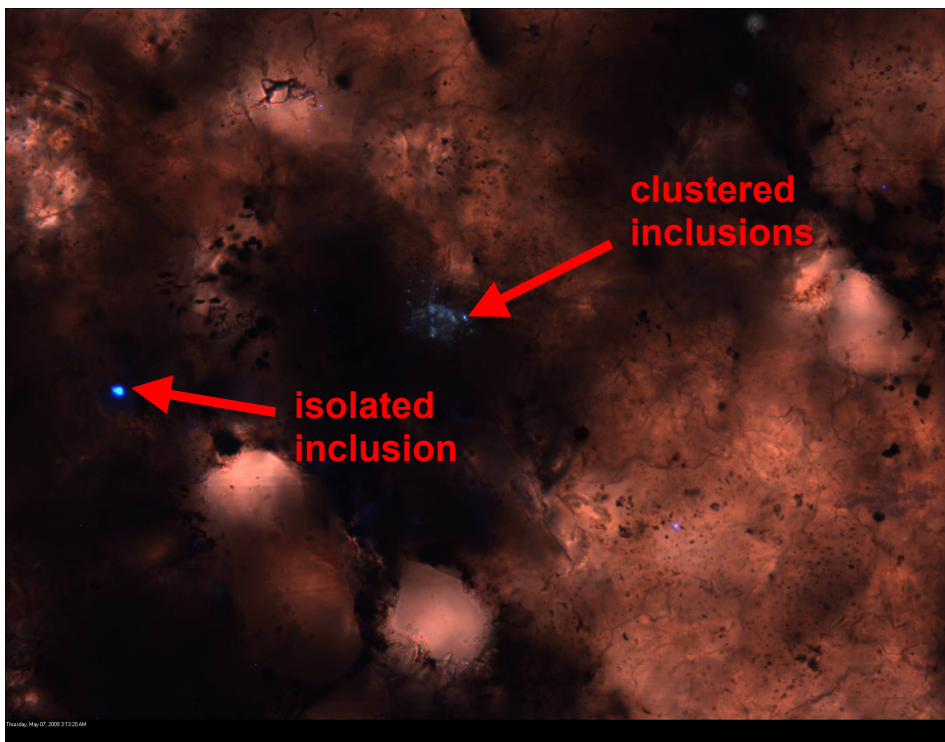


Figure 22: Micrograph from sample BIR 16 showing isolated and clustered oil inclusions in matrix minerals under UV light. Field of view in this micrograph is 1.5mm.

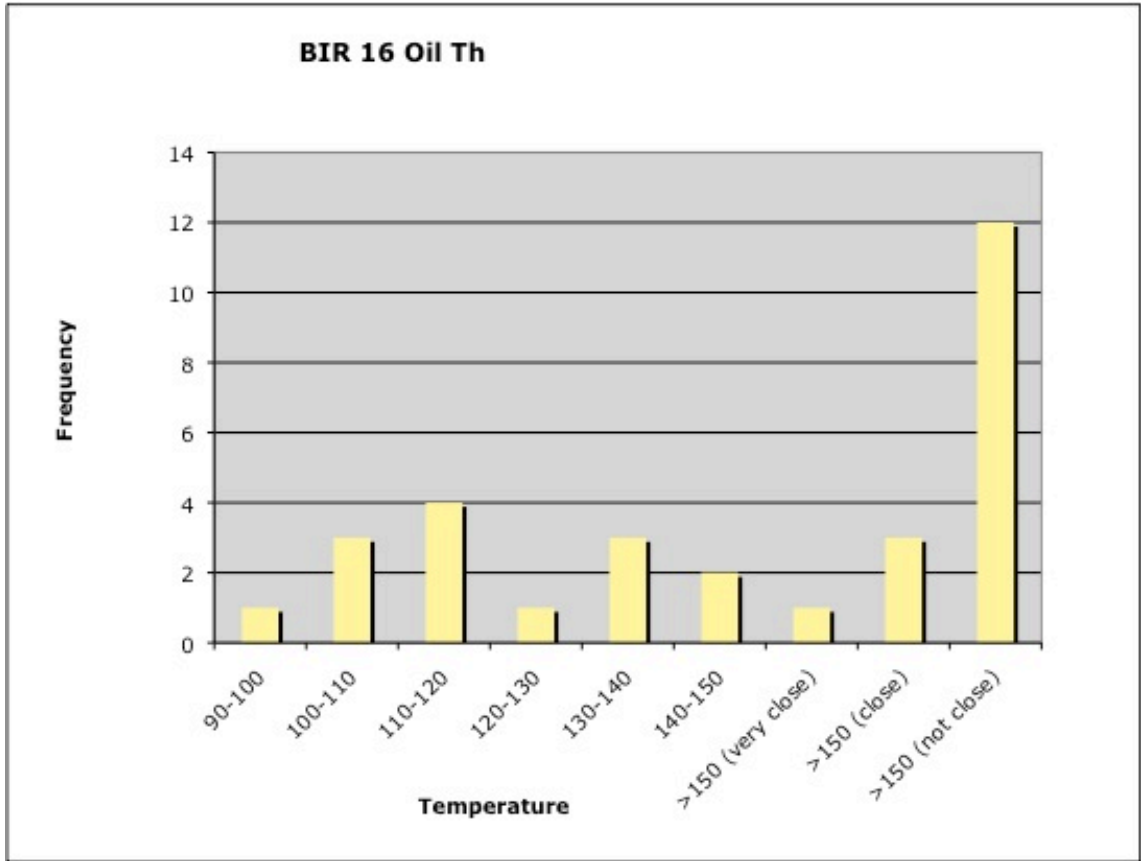


Figure 23: Histogram of oil inclusion homogenization temperatures in sample BIR 16. Temperatures are in °C. The sample was only heated to 150°C and a qualitative estimate was made to determine how “close” a given inclusion was to homogenization.

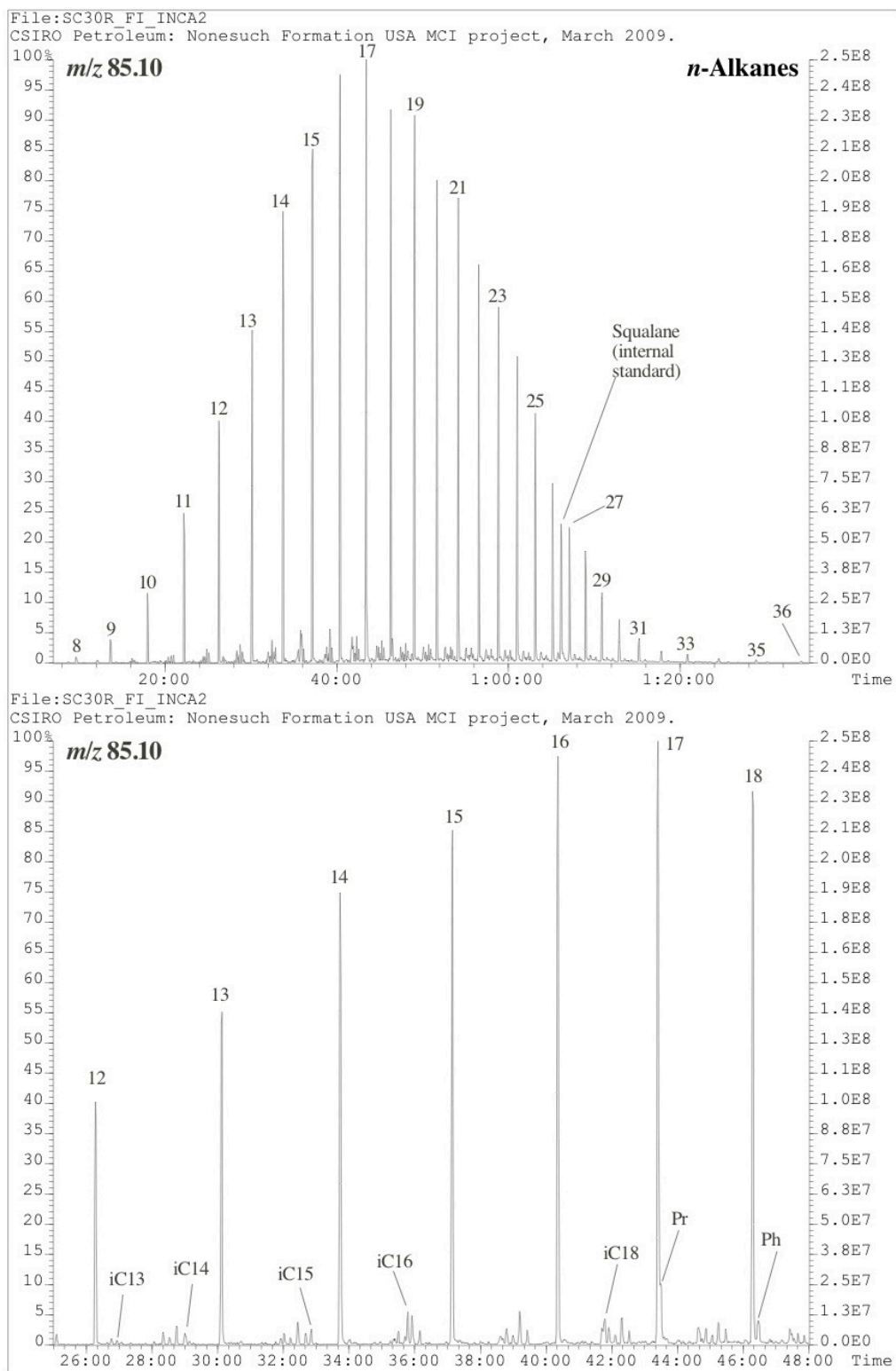


Figure 24: Partial *m/z* 85 chromatogram of sample 30R 2263 showing *n*-alkane distribution as well as isoprenoids (iC_{xx}), pristane (Pr) and phytane (Ph). Numbers refer to chain length. Distribution of *n*-alkanes is normal with a maximum at *n*-C₁₇.

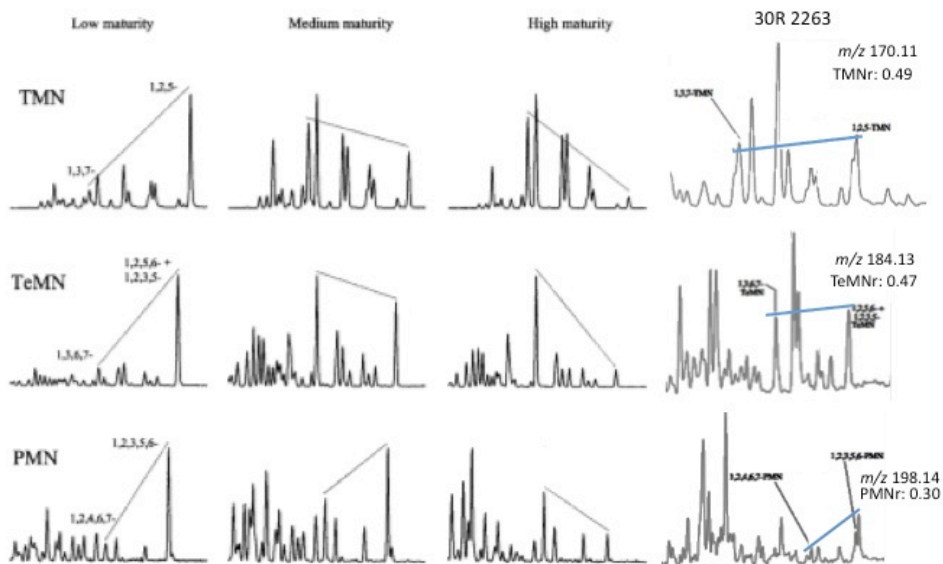


Figure 25: Comparison between low, medium and high maturity distributions for TMN, TeMN and PMN from van Aarssen et al. (1999) and distributions of TMN, TeMN and PMN from GC-MS chromatograms of sample 30R 2263.

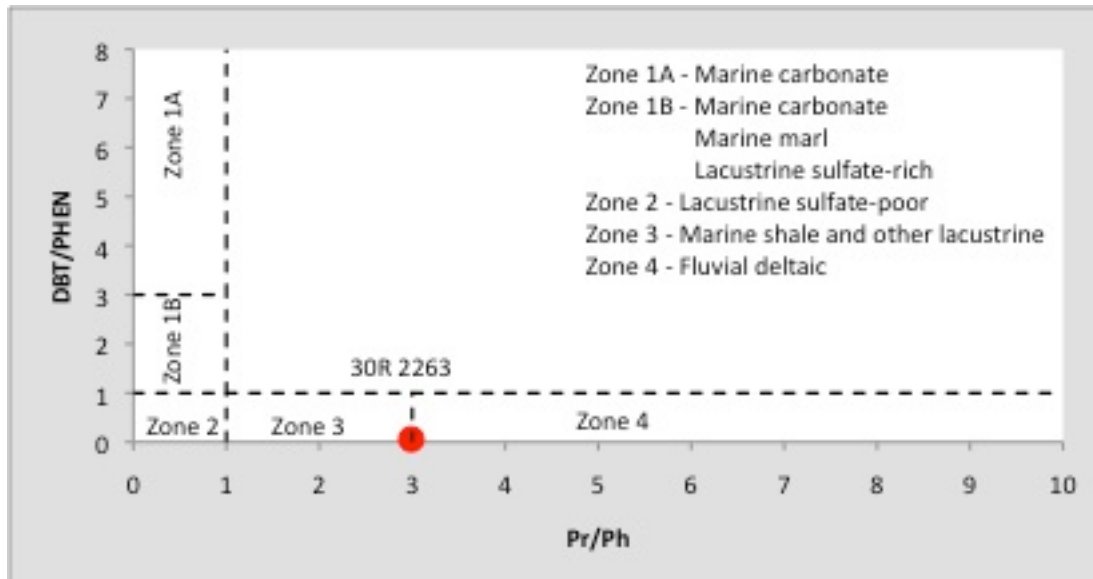


Figure 26: Graph of dibenzothiophene/phenanthrene (DBT/PHEN) vs. pristane/phytane (Ph/Pr). The red dot represents where the 30R 2263 values plot on this graph, directly between the zones of “Marine Shale and other Lacustrine (Zone 3)” and “Fluvial Deltaic (Zone 4).” Graph and definitions from Hughes et al., 1995.

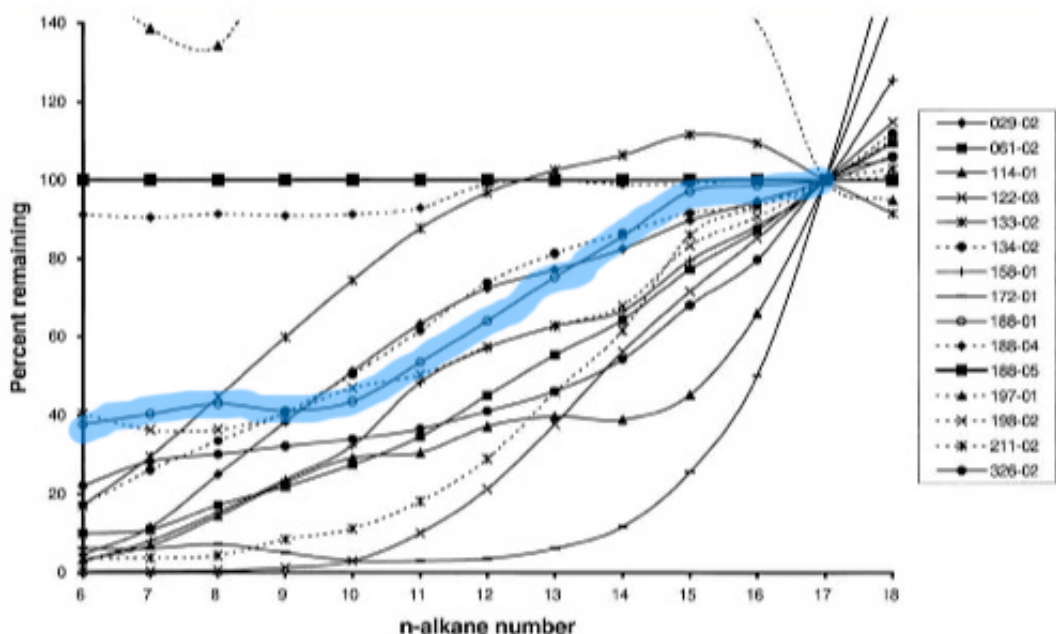


Figure 27: Graph from Mauk and Burruss (2002) showing water washing of various Nonesuch Fm samples compared to an unaltered standard. Samples that have undergone more water washing will plot towards the lower part of the graph as they have a lower remaining percentage of each *n*-alkane. Although it was not possible to directly plot data from 30R 2263 on the graph as Mauk and Burruss (2002) did not publish the *n*-alkane values of their standard, the high similarity between the chromatogram for 30R 2263 and the chromatogram for their sample 188-01 (highlighted in blue) would likely lead to similar positioning on the graph and thus a similar degree of water washing.

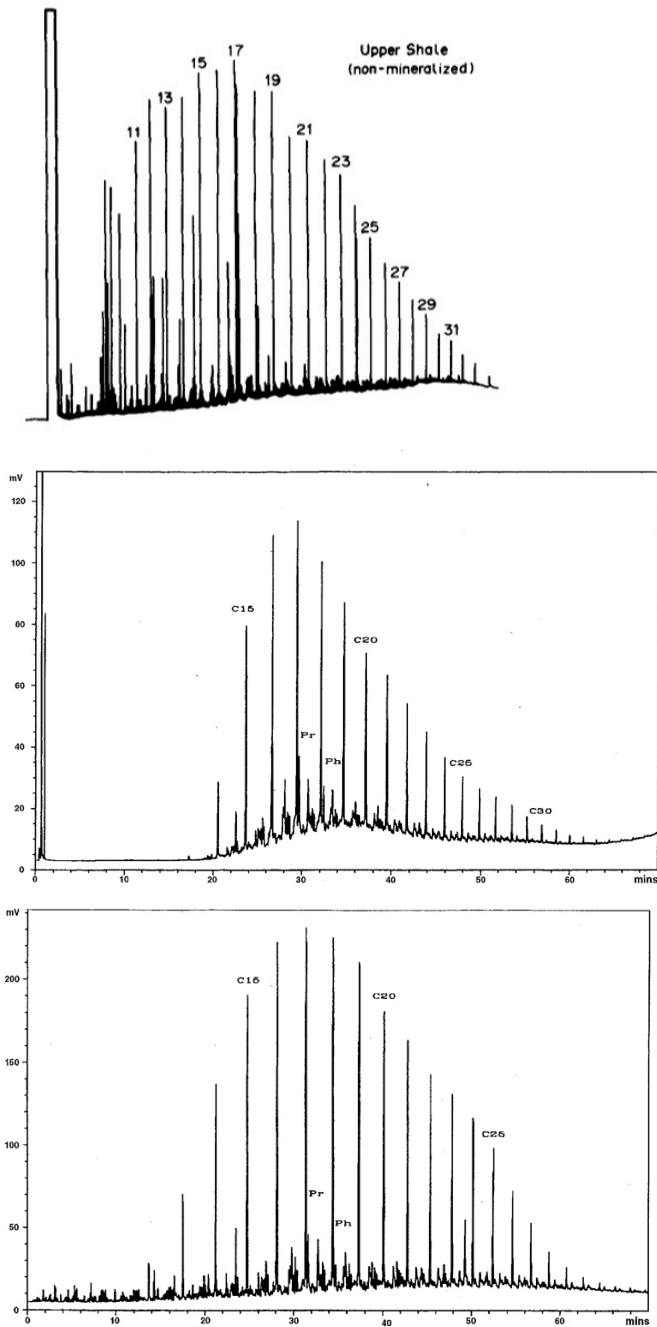


Figure 28: Chromatographic fingerprints of the Nonesuch Fm whole oil. The topmost chromatogram is from Ho et al. (1989) and is from a sample of unmineralized shale from the White Pine Mine. The other two chromatograms are from Uchytel et al. (1999). The middle chromatogram is from a sample of the Bear Creek W-26 borehole and the lower chromatogram is from the seep oil at White Pine Mine. The seep oil in particular has a very similar fingerprint to the 30R 2263 chromatogram.

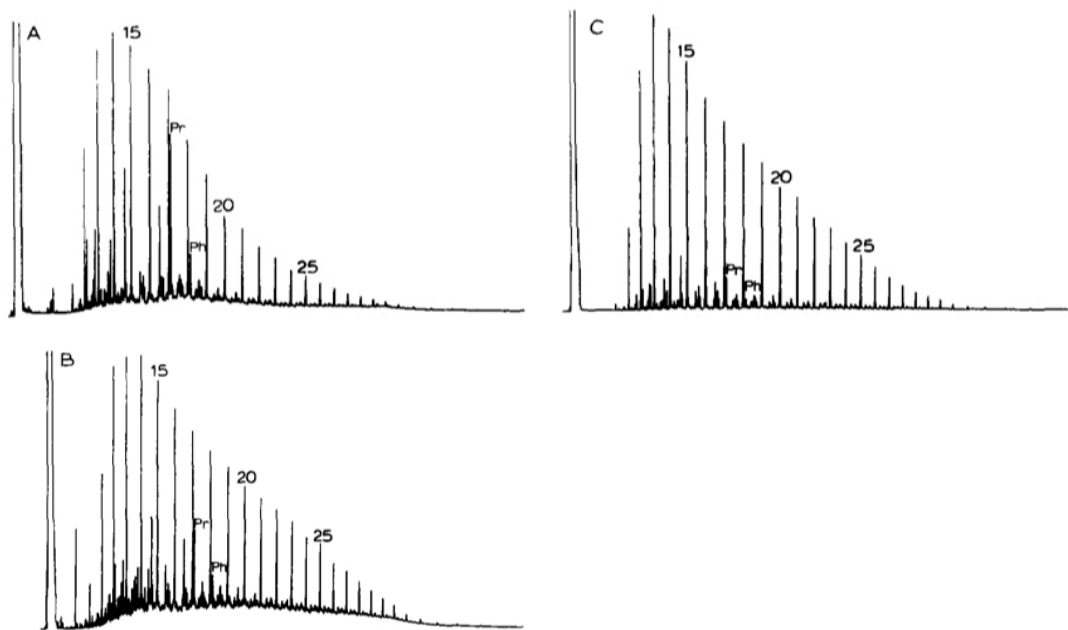


Figure 29: Whole oil gas chromatograms from Hieshima and Pratt (1991). Chromatogram A shows saturated hydrocarbon fractions of bitumens from Michigan, B shows saturated hydrocarbon fractions from bitumens in Wisconsin, and C shows the saturated hydrocarbon fraction from seep oil at the Copper Range Mine. The seep oil chromatogram (C) as a whole is the most similar to the data from 30R 2263, but the Pr/Ph ratio of 30R 2263 is most similar to that of their sample from Michigan (A).

Chapter 4: Discussion

4.1 Biological source and migration

The biogenic source of the oil is likely Proterozoic based both on the findings of this study and those of previous studies. Primary oil inclusions were found in vein calcite dated at 1047 +/- 35 Ma (Kelly and Nishioka, 1985) that is syngenetic with copper mineralization and thrust faulting that occurred during the Grenville Orogeny based on the textural relationship of the pyrobitumen, solid oil inclusions and native copper mineralization (Kelly and Nishioka, 1985; Mauk et al., 1992; Mauk and Hieshima, 1992; Li et al., 1995) and the geochemical fingerprint of the oil is Precambrian in appearance particularly when the *n*-alkane distribution, lack of even-odd preference and low DBT/PHEN ratio are taken into account. The presence of TMNs and TeMNs plus limited unresolved complex mixture in the GC-MS data shows little biodegradation effect on the oil, and a TeMNR value higher than the PMNR value supports this (George et al., 1998; van Aarssen et al., 1999). This agrees with the findings of Mauk and Burruss (2002) who also observed the presence of naphthalenes in the oil.

The similarities between the geochemical fingerprint of the oil inclusions and those obtained by other authors from the pyrobitumen and seep oil of the Nonesuch Fm (Ho et al., 1989; Hieshima and Pratt, 1991; Mauk and Hieshima, 1992; Ho and Mauk, 1996; Uchytel et al., 1999; Mauk and Burruss, 2002) support the hypothesis that the hydrocarbons were sourced from the Nonesuch Fm rather than higher, later deposits as

mentioned (though not supported) by Barghoon et al. (1965). The Nonesuch Fm is also the only sedimentary rock in the Keweenawan Supergroup that is not described as a sandstone, making it the only possible source rock in the basin. Mauk and Hieshima (1992) also postulate that the oil matured outside the White Pine area in a deeper part of the Nonesuch Formation closer to the rift axis, then migrated into White Pine during thrust faulting along with hydrothermal fluids. Their temperature estimates for maturation during deeper burial are 140-300°C, the upper limit of which is significantly higher than what would be expected from the geochemical ratios obtained through GC-MS of this study, which indicates early- to peak-oil window maturity (100-130°C). There is also no difference in homogenization temperatures between vein inclusions and inclusions occurring outside of veins, which would be expected if the oil migrated at higher temperatures along faults and fractures. Mauk and Hieshima's (1992) scenario cannot be completely ruled out as they state that if migration occurred during and was related to thrusting, the oil in the northeastern area of the mine (where Core 30R was drilled; see Figure 2) would show lower maturity than that in the southwestern domain. The microthermometry temperatures show no significant difference moving southwest across the mine—the highest peak in the distribution of T_h data for the most southwestern core used in this study, 28G 539, occurs at 101-110°C, the lowest peak temperatures of any of the samples. However, this core is still somewhat northeast of what Mauk and Hieshima (1992) describe as the southwestern domain of the mine and it is possible that significantly higher microthermometry temperatures would be obtained from samples taken from that domain.

4.2 Maturity and thermal history

The maturity of the inclusion oil ranges from low- to mid-oil window maturity based on the GC-MS maturity markers. The yellow fluorescence color that is present in at least some inclusions in all samples also indicates early- to peak-oil window maturity, as fluorescence color/maturity studies have found that, while blue fluorescence is found in oils with a range of maturities, yellow fluorescence is a reliable indicator of fairly immature petroleum (George et al., 2001; Chang and Huang, 2008).

The temperature at which the oil and its gas bubble homogenized during microthermometry was used as an estimate of the minimum temperature of entrapment of the inclusions, although by examination of a P-T diagram for two-phase oil inclusions, it can be seen that the actual trapping temperature of a given inclusion would be likely slightly higher than the homogenization temperature (Munz, 2001; Thiéry et al., 2002).

The range of oil inclusion homogenization temperatures seems surprisingly wide, especially given that the maximum temperature of the Nonesuch Formation has been studied using several different methods that all give a result close to 100°C (Mauk and Burruss, 2002). However, Hegarty et al. (2007), in their study of a Nonesuch Fm temporal equivalent in Iowa, found that the sediments there had undergone a later event of heating at approximately 200-300, which they concluded had increased the local temperature to above 200°C. This agreed with the findings of Barker (1990 as reported in Hegarty et al., 2007), whose fluid inclusion studies of units near the Nonesuch Fm equivalent led to the conclusion of a minimum paleotemperature of ~200°C. Mauk and

Hieshima (1992) also support a secondary phase of heating and copper mineralization, although they suggest it occurred during the compressional stage of structural development, no later than 30 Ma after sediment deposition. They state that the hydrothermal fluids at this stage were likely higher in temperature than the primary stage of mineralization, but they cap their estimates at 100°C based on previous Nonesuch Fm work by other authors. Brown (2006) suggests that the later stage copper mineralization could have happened at metamorphic-grade temperatures while still preserving the original sedimentary features of the Nonesuch Fm. Although Brown (2006) does not mention a precise higher temperature for the hydrothermal fluid, the maximum temperature determined from the Portage Lake basalts with the highest degree of metamorphism was 280 +/- 40°C (Livnat et al., 1983 as reported in Brown, 2006). Price and McDowell (1993) also determined that paleotemperatures of the Nonesuch Fm had ranged from 100-190°C, although their method utilizes illite and smectite, which Essene and Peacor (1995) criticized as an inaccurate geothermometer. Brown's (1971) study of sulfide minerals gives a maximum possible temperature of ~100°C; however, the DBT/PHEN and MDBT/MB ratios found via GC-MS suggest a low-sulfur environment for the oil generation (George et al., 1997; Dutkiewicz et al., 2004), so it is possible that cooling to temperatures less than 100°C occurred prior to the introduction of copper sulfide minerals into the system.

The aqueous inclusion homogenization temperatures (T_h) are possible evidence for higher maximum temperatures in the history of the rocks. Munz (2001) states that in a system where there are both aqueous and oil inclusions present, the T_h of the aqueous inclusions is more reliable than the T_h of the oil, as the oil inclusions will always contain

an essentially invisible third phase, water, making the final state of homogenization that of oil and water homogenization, which, due to the very small amount of water in the inclusion, is unobservable. The aqueous inclusions likely contain some methane in addition to the two visible phases, however the water and methane phases will homogenize prior to the water and vapor, and therefore the visible homogenization is also the final miscibility of the fluids. For both LIR 14 and 30R 2263, the homogenization temperature range of the aqueous inclusions was smaller and had a higher average than the T_h of the oil inclusions (Figure 30).

If the Nonesuch Formation was at one point heated to higher temperatures, regardless of timing of the heating (providing it occurred after entrapment of the inclusion fluids), the homogenization temperature may reflect the highest temperature experienced by the formation, and not the original entrapment temperature (Prezbindowski and Tapp, 1991; Goldstein and Reynolds, 1994). If the overheating did not reach too high a temperature or was a short event geologically, it may also be the case that some of the inclusions would have re-equilibrated and others would not, giving a wide range of temperatures that represent both the original entrapment and the subsequent heating event (Goldstein and Reynolds, 1994). The re-equilibration is caused by stretching of the host calcite due to increasing internal pressure of the inclusions as the temperature increases. When looking at the histograms of the Nonesuch Formation data, it is clear that the distribution for each sample is bimodal, with the lower peak occurring between 100-130°C. This is particularly noticeable on the histogram of the combined sample data (Figure 31), where there is an obvious mode at 101-110°C. In the past, in areas of study where re-equilibration is suspected to have occurred, the lower mode of

bimodal distributions of T_h has been used as an estimate for the original entrapment temperatures (Dutkiewicz et al., 2003). This would likely be an accurate assignment in this case, as an entrapment temperature of 101-110°C agrees with most previous work on the Nonesuch Formation (e.g., Hieshima and Pratt, 1991; Mauk and Hieshima, 1992; Ho and Mauk, 1996), as well as the maturity data obtained from GC-MS on sample 30R 2263.

There are other possible explanations for the higher homogenization temperatures. The inclusions could have leaked at some point in time, which would cause lower pressures within the inclusions and thus higher T_h . The included oil could also have degraded over time, causing an apparent shift to higher maturation parameters. This would also result in a shift towards blue fluorescence as the complex aromatic molecules are broken down and higher T_h due to hydrocarbon cracking within the inclusions.

For samples that were heated beyond 150°C (LIR 14, 30R 2263 and 40K 2088), there is a third, typically smaller mode at 160-170°C. This could indicate that there were two heating events that caused re-equilibration; possibly two later stages of hydrothermal activity, or one stage of hydrothermal activity 30my after sedimentation as suggested by Mauk and Hieshima (1992) and then a Paleozoic stage of tectonic-related heating at 200-300 Ma as suggested by Hegarty et al. (2007).

The combined aqueous inclusion homogenization temperatures (Figure 32) are also bimodal, with a lower mode at 131-140°C and a higher mode of >250°C. Per Munz's (2001) statement regarding entrapment temperatures being represented more accurately by aqueous inclusions, it is possible that the lower mode is a indicator of the true entrapment temperature of the Nonesuch Formation oil. The higher end of this

range, 140°C is slightly higher than estimated by previous studies of the Nonesuch Formation, but is not out of the range of uncertainties. The combined aqueous T_h distribution also shows a small bump between 150-170°C, but it is not as prominent as in the oil T_h graph. The general skew of the aqueous inclusions towards higher temperatures could be explained by the difference in compressibility between water and oil—oil is more compressible than water (bulk modulus of oil ≈ 1.5 depending on weight, bulk modulus of water ≈ 2.15 -2.35 depending on salinity), and this could mean that the aqueous inclusions would be quicker and in general more likely to re-equilibrate than oil inclusions, which in this case would mean that the original entrapment temperature is better estimated by the homogenization temperatures of the oil inclusions.

A T_h vs. sample depth plot (Figure 33), which is a suggested method from Prezbindowski and Tapp (1991) for determining the extent of re-equilibration of inclusions shows some correlation between the depths of the core samples and their average homogenization temperatures, but the outcrop samples do not follow this pattern and the overall number of samples available for use (5) cannot give an accurate correlation; however, the scatter is not so great on the graph as to rule out the possibility of a burial effect on T_h . Use of this plot assumes that folding in the area occurred prior to the major burial in the Phanerozoic, which is shown by Mauk and Hieshima (1992).

There is a possibility that the sample inclusions were re-equilibrated artificially during the microthermometry analysis, which could have caused artificially high homogenization temperatures and is a possible explanation for values obtained above the 130°C maximum expected for the Nonesuch Fm. Quartz-hosted inclusions would not have been affected even at the maximum temperatures used in this study, although a

comparison of homogenization temperatures between quartz-hosted and calcite-hosted inclusions is not possible because the hosting mineral was not recorded at the time of microthermometry.

In attempting to determine homogenization temperatures, the samples in some cases were heated beyond the 140°C minimum cutoff for re-equilibration of inclusions in calcite (Goldstein and Reynolds, 1994). However, because heating was conducted carefully, kept to relatively low rates (no more than 15°C/minute and slower than this near homogenization) and particularly because heating was stopped as soon as homogenization occurred or the maximum temperature was reached (150°C in some samples, 250°C in others), this is unlikely to be the case. Additionally, no evidence of ongoing re-equilibration was observed during microthermometry (e.g., sudden change in bubble size or appearance of inclusions). If the inclusions in the samples had not previously been subjected to heating beyond the 100-130°C maximum temperatures as suggested by Brown (1971), Mauk et al. (1992) and Ho et al. (1991), the inclusions would have homogenized at or below these temperatures and there would have been no need for increased heating. At worst, it is possible that heating the samples beyond 150°C during microthermometry caused additional re-equilibration of some of the calcite-hosted inclusions, which would lead to an artificial skew toward higher temperatures in the histograms of the data. However, while an alteration in the percentages of the lower- and higher-temperature inclusions may lead one to conclude that the higher-temperature event lasted for a longer time period than in actuality, it does not affect the conclusion of the existence of such an event.

4.3 Interpretation of oil maturation history

Hegarty et al. (2007) did not rule out the possibility of at least some Proterozoic hydrocarbon generation, and if it were indeed the case that the oil was originally generated 1100 Ma but then re-heated to higher temperatures at 200-300 Ma, the results of the combined GC-MS and microthermometry may show similar characteristics to those obtained from 30R 2263: A general geochemical oil fingerprint similar to other Proterozoic oils (McKirby, 1974; Hughes et al., 1995; Volk et al., 2005; George et al., 2008) but a range of homogenization temperatures representing both the Proterozoic and Mesozoic heating events. Due to the nature of fluid inclusions, the oil contained in them should be more pristine than the pyrobitumen and seep oil from the source rock. There is a question of why the maturity indicators from the GC-MS would show an early- to peak-oil window maturity if it is the case that the oil was heated beyond this temperature (peak-oil window maturity occurs at approximately 130°C); a possible reason for this is that the second, higher heating event did not last for a long time period. Hegarty et al (2007) proposed that the 200-300 Ma heating event could have been caused by an additional 1850m of paleoburial (and subsequent erosion), which would have not been considered a short event; however, they also mention that collision on the tectonic plate margin that occurred in this time period may also have been responsible for a higher geothermal gradient, and they state that the methods used in their study constrain thermal history but not structural or depositional history.

Previous studies have also shown that inclusion oil that is reheated can retain its original maturity characteristics despite heating beyond its original formation temperature (Dutkiewicz et al., 2003; George et al., 2008). This, along with the possibility of heating

event that occurred during a short time period, would lend an explanation to all of the combined data—the low-temperature copper sulfide minerals noted by Brown (1971) would not have had time to destabilize, the biomarkers that indicate maturity and T_{\max} values obtained through pyrolysis would have remained relatively unchanged, though possibly develop a slight skew toward a more mature oil and Hegarty et al.'s (2007) conclusion that secondary, higher heating event occurred would also be correct. If hydrothermal fluid temperatures approached the maximum $280 \pm 40^{\circ}\text{C}$ suggested by Livnat et al. (1983 as reported in Brown, 2006), this would be consistent with the highest microthermometry values obtained ($>250^{\circ}\text{C}$). Because of the fragile nature of fluid inclusions hosted in carbonate minerals, even a short period of heating would likely cause re-equilibration of some inclusions, and additional evidence for a shorter heating event is that not all the inclusions appear to have re-equilibrated—there are several in each sample that exhibit temperatures closer to the Proterozoic estimates. The variable yellow to blue fluorescence color exhibited by some of the inclusions is also possible evidence for overprinting, and the presence of both yellow- and blue- fluorescing inclusion in the same sample is additional evidence that the Nonesuch Fm was deposited in a saline environment as proposed by several authors (Pratt and Hieshima, 1991; Ojakangas et al., 2001), as the change in fluorescence color from yellow to blue with heating happens over a much wider temperature range than in a non-saline environment (Chang and Huang, 2008).

4.4 Conclusions

- 1) The environment of deposition of the Nonesuch Fm is still unclear, as there are indicators for both a lacustrine and marine source. When used together, the DBT/PHEN vs. Pr/Ph ratios from sample 30R 2263 indicate either a marine shale, lacustrine or fluvial source (Hughes et al., 1995), but the Pr/Ph ratio taken alone indicates a lacustrine environment (Peters et al., 2005). Evidence for a saline environment in this study is limited to the presence of yellow- and blue-fluorescing inclusions in the same sample, which is more likely to occur in oil from a marine shale than a lacustrine shale (Chang and Huang, 2008). Previous work by Ojakangas et al. (2001), Hieshima and Pratt (1991) and Uchytíl et al. (1999) has shown compelling evidence for at least some saline input and Uchytíl et al. (1999) hypothesized that the depositional environment was lacustrine with varying amounts of salinity. The limited data provided by this study supports this interpretation, as there is evidence present for both a lacustrine and saline environment. A marginal estuary or lagoon would also fit the data.
- 2) Based on the biomarker data found in sample 30R 2263, it is likely that the Nonesuch Fm inclusion oil was locally sourced from cyanobacteria and algae (algal biomarkers were not seen in this study but were found by Pratt et al., 1991) during the Mesoproterozoic and trapped as inclusions during diagenesis at approximately 1.05 Ga as previously suggested by Kelly and Nishioka (1985) or up to 30my after deposition of the Nonesuch Fm in the case of the vein-hosted inclusions as suggested by Mauk and Hieshima (1992). Entrapment likely occurred during initial oil formation and maturation based on inclusion

homogenization temperatures and previous work on the relationship between the oil and copper mineral precipitation (Kelly and Nishoka, 1985; Mauk and Hieshima, 1992; Ho et al., 1992).

- 3) During initial maturation, temperatures reached peak-oil window conditions, approximately 100-130°C as evidenced by the maturity ratios calculated from the GC-MS data and the lowest mode in the distribution of microthermometrical data.
- 4) Post-entrapment, the inclusions were subjected to at least one additional and likely short period of heating, possibly close to the time of deposition (Mauk and Hieshima, 1992) or around 200-300 Ma (Hegarty et al., 2007), which increased local temperatures to 200-250°C (Brown, 2006; Hegarty et al., 2007), which caused re-equilibration of some of the fluid inclusions, the evidence for which was seen during microthermometry analysis.

4.5 Further work on oil inclusions

There were several biomarkers that were not detected during GC-MS of the inclusions from 30R 2263 but had been found previously by Pratt et al. (1991). In the 30R 2263 oil, it is likely that these biomarkers were obscured by the high amounts of *n*-alkanes in the sample and a possible method for detection would be molecular sieving followed by another GC-MS analysis, which would remove the *n*-alkanes from the oil and presumably allow better definition of the remaining compounds (Volk, 2009, pers. comm.). However, this is a technique that is typically performed on 5mg or more of oil and it is unknown whether it would be successful on inclusion oil (Ahmed, 2011, pers. comm.). The inclusions from 30R 2263 yielded 0.1mg of oil, which is considered a very

high amount from fluid inclusions, so it is unlikely that a 5mg sample of inclusion oil can be obtained from the Nonesuch Fm.

Also, it is likely that another sample would have to be found for this analysis. The majority of the calcite vein from 30R 2263 was crushed for the GC-MS procedure and, as the sample was taken from a core, it would be difficult to return to the original site of coring to obtain more of this specific vein. The oil used in the original GC-MS analysis in 2009 was preserved, but it is the experience of the CSIRO Petroleum laboratory that oil kept for this amount of time is subject to outside contamination and it is unlikely that subsequent analyses could provide valid information about the oil (Ahmed, 2011, pers. comm.).

If a suitable sample containing similar oil could be found, an attempt at the above molecular sieving procedure would be recommended in order to provide additional biomarker information.

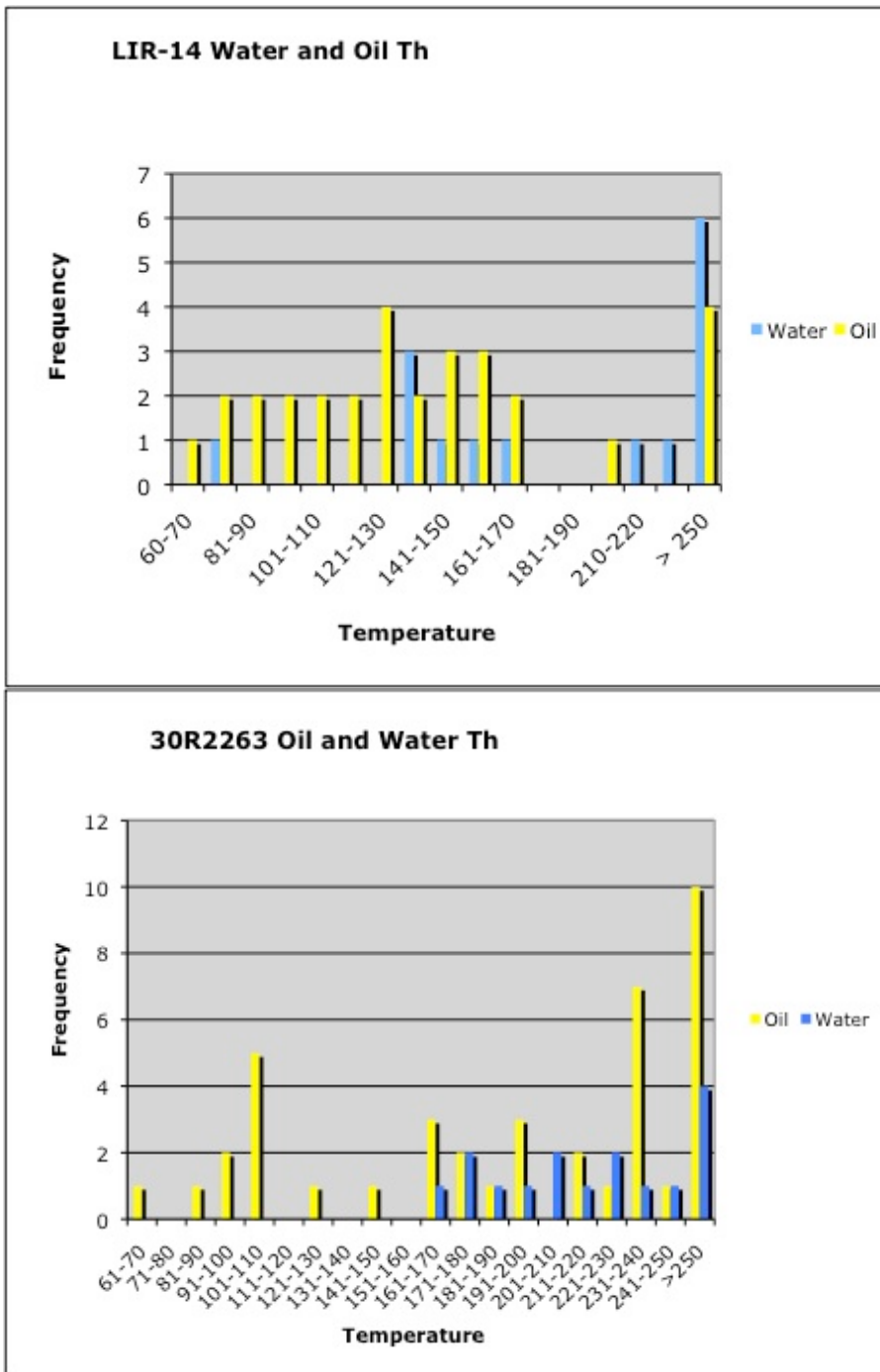


Figure 30: Histograms showing the combined oil and aqueous inclusion homogenization temperatures. Note that the water T_h range is smaller and has a higher average than the oil T_h range for both samples.

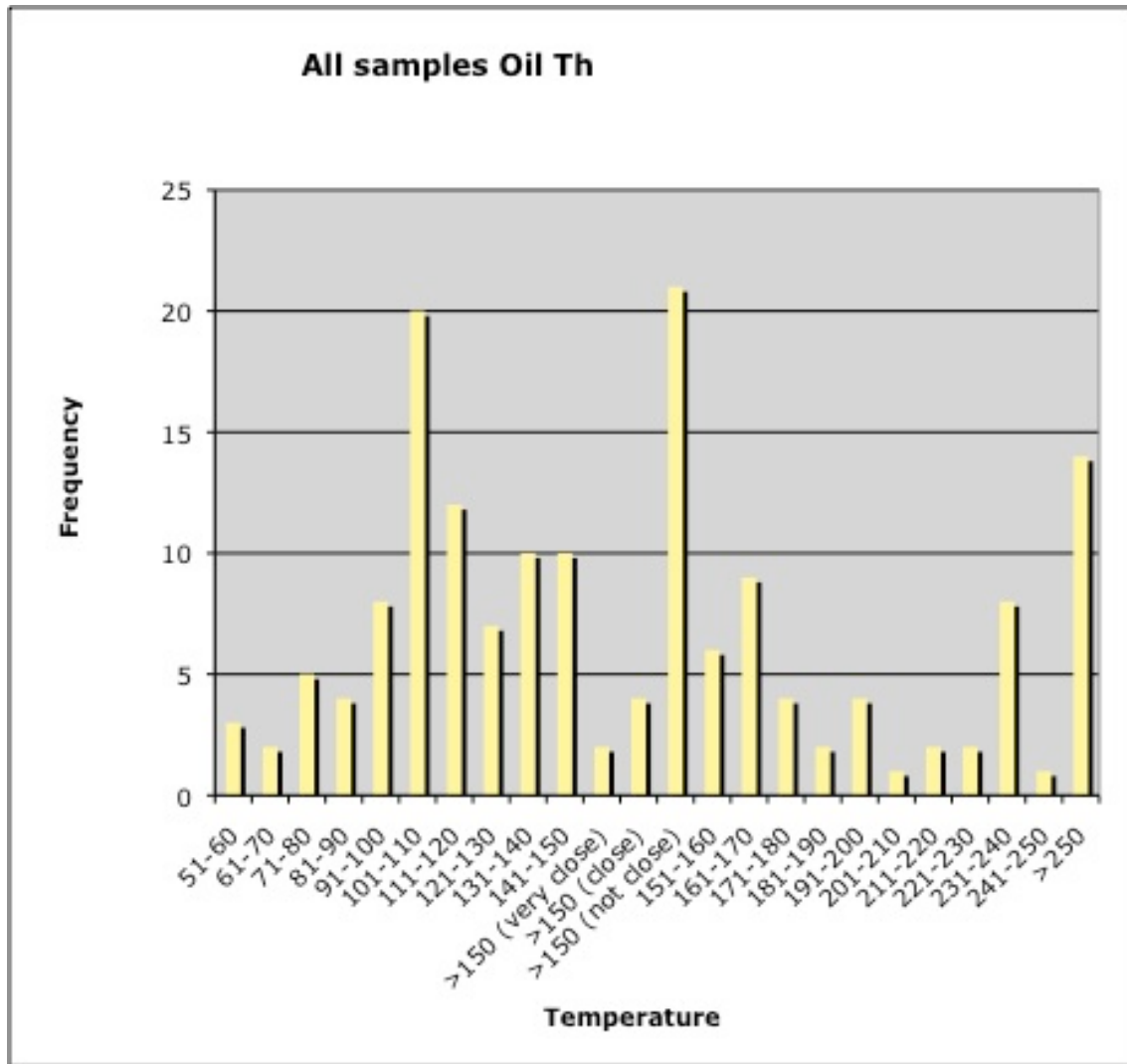


Figure 31: Histogram showing combined oil T_h data for all microthermometry samples (all temperature units are °C). The mode at 101-110°C likely represents the original entrapment temperature of the oil while the higher modes likely represent temperatures at which inclusions later re-equilibrated. Note that the highest peak, >150 (not close) likely belongs closer to the higher-temperature side of the graph, however, there is uncertainty in the correct placement and it is also probable that most of the inclusions represented by this peak would not homogenize at precisely the same temperature, so it should be used only to show that there is an additional skew toward the higher-temperature side of the graph. The smaller mode at 161-170°C may indicate a third re-equilibration event occurring between the original entrapment and highest-temperature heating.

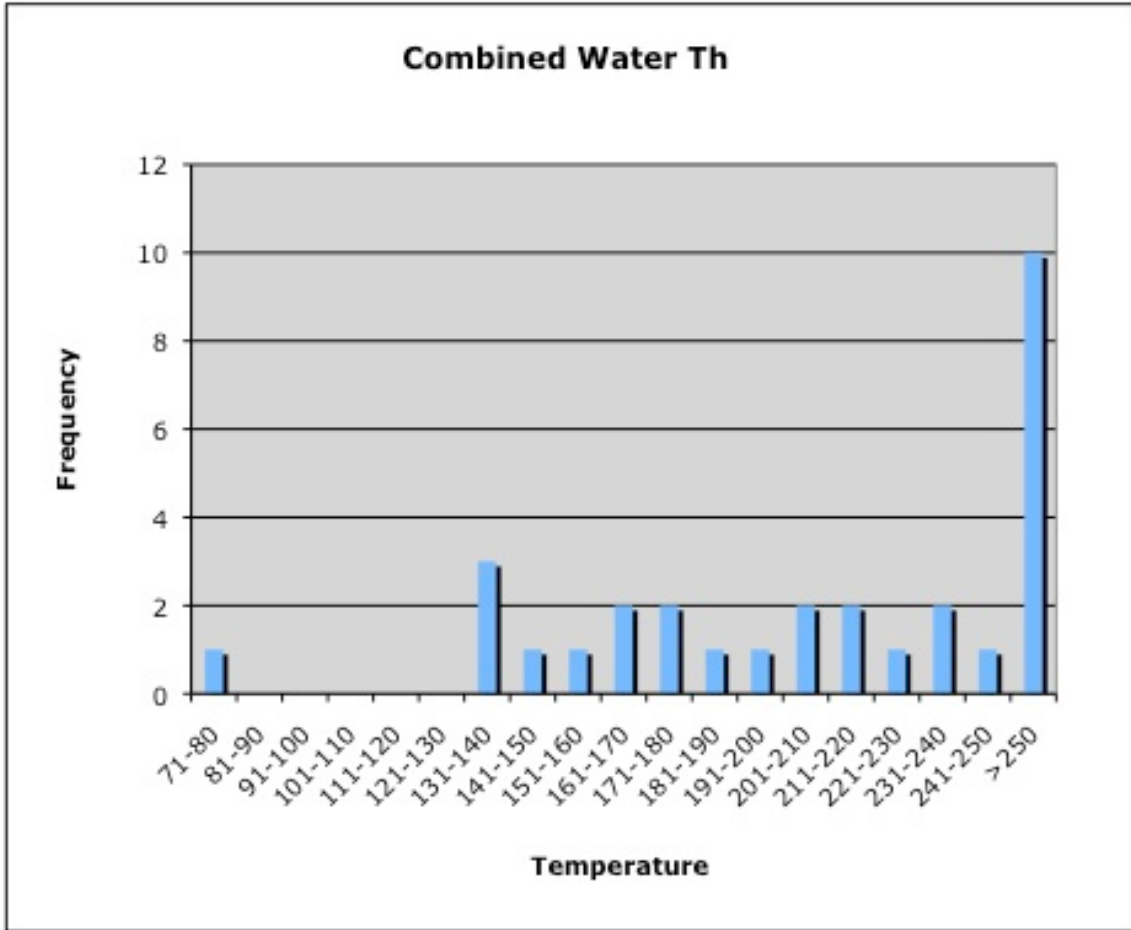


Figure 32: Histogram of combined water homogenization temperatures from both LIR 14 and 30R 2263 (all temperature units are °C). The distribution (with one outlier at 75°C) has a noticeably higher average than the oil homogenization temperatures. This is likely due to easier re-equilibration of aqueous inclusions compared to oil inclusions, and so while the homogenization temperatures of the aqueous inclusions may be used for the minimum temperatures reached by the system, the original entrapment temperature is likely better represented by oil inclusion homogenization temperatures.

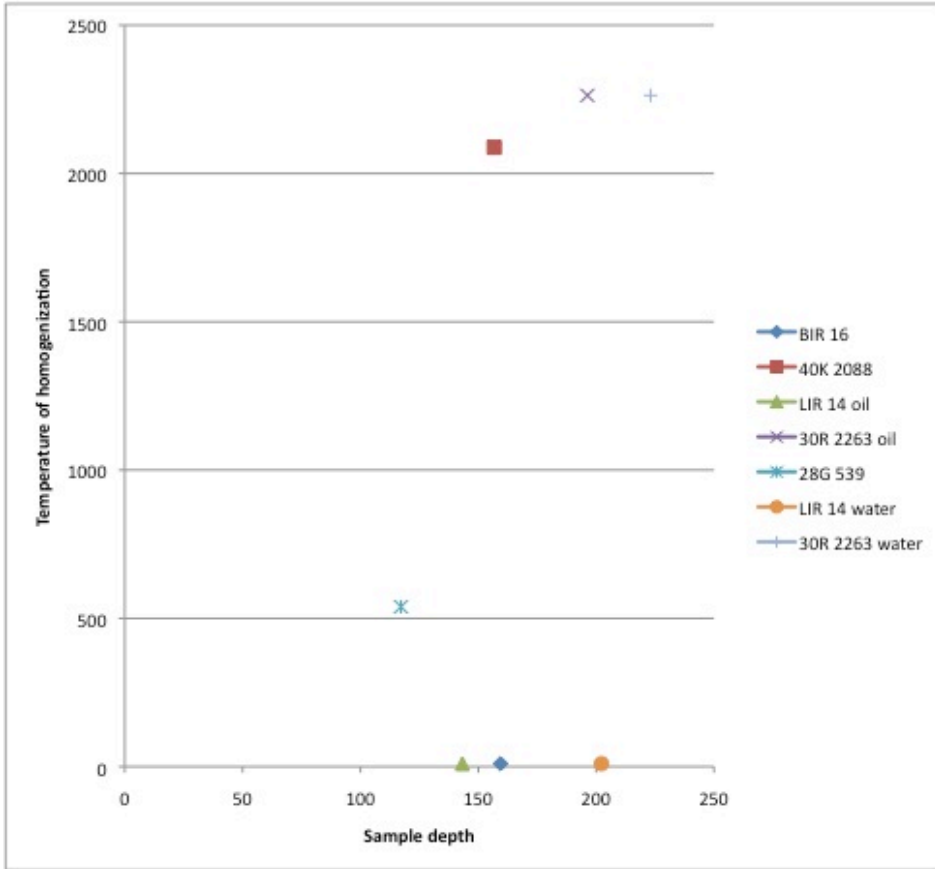


Figure 33: Graph of average T_h (°C) vs. sample depth as suggested by Prezbindowski and Tapp (1991) as a method of determining whether T_h is influenced by burial depth. There is no visible correlation between the outcrop samples.

5. References cited

Alexander, R.; Larcher, A.V.; Kagi, R.I., 1988. The use of plant-derived biomarkers for correlation of oils with source rocks in the Cooper/Eromanga Basin system, Australia. *The Apea Journal* 28: 310-324.

Barghoon, E.S.; Meinschein, W.G.; Schopf, J.W., 1965. Paleobiology of a Precambrian Shale. *Science* 148(3669): 461-472.

Bornhorst, T.J., 1997, Tectonic context of native copper deposits of the North American Midcontinent Rift System, in Ojakangas, R.W., Dickas, A.B., and Green, J.C., eds., *Middle Proterozoic to Cambrian Rifting, Central North America*: Boulder, Colorado, Geological Society of America Special Paper 312.

Brown, A.C., 1971. Zoning in the White Pine copper deposit, Ontonogon County, Michigan. *Economic Geology* 66: 543-573.

Brown, A.C., 2006. Genesis of native copper lodes in the Keweenaw District, Northern Michigan: a hybrid evolved meteoric and metamorphogenic model. *Economic Geology* 101: 1437-1444.

Butterfield, N.J.; 2006. *Bangiomorpha pubescens* n. gen., n. sp.: implications for the evolution of sex, multicellularity, and the Mesoproterozoic/Neoproterozoic radiation of eukaryotes. *Paleobiology* 26(3): 386-404.

Chang, Y.; Huang, W., 2008. Simulation of the fluorescence evolution of “live” oils from kerogens in a diamond anvil cell: Application to inclusion oils in terms of maturity and source. *Geochimica et Cosmochimica Acta* 72: 3771-3787.

Davis, D.W.; Paces, J.B., 1990. Time resolution of geologic events on the Keweenawan Peninsula and implications for development of the Midcontinent Rift system. *Earth and Planetary Science Letters* 97: 54-64.

Dutkiewicz, A.; Ridley, J.; Buick, R., 2003. Oil-bearing CO₂-CH₄-H₂O fluid inclusions: oil survival since the Palaeoproterozoic after high temperature entrapment. *Chemical Geology* 194: 51-79.

- Dutkiewicz, A.; Volk, H.; Ridley, J.; George, S.C., 2004. Geochemistry of oil in fluid inclusions in a middle Proterozoic igneous intrusion: implications for the source of hydrocarbons in crystalline rocks. *Organic Geochemistry* 35: 937-957.
- Dutkiewicz, A.; Volk, H.; George, S.C.; Ridley, J.; Buick, R., 2006. Biomarkers from Huronian oil-bearing fluid inclusions: An uncontaminated record of life before the Great Oxidation Event. *Geology* 34(6): 437-440.
- El-Desouky, H.A.; Muchez, P.; Tyler, R., 2008. The sandstone-hosted stratiform copper mineralization at Mwitapile and its relation to the mineralization at Lufukwe, Lufilian foreland, Democratic Republic of Congo. *Ore Geology Reviews* 34: 561-579.
- Ensign, Jr., C.O.; White, W.S.; Wright, J.C.; Patrick, J.L.; Leone, R.J.; Hathaway, D.J.; Trammell, J.W.; Fritts, J.J.; Wright, T.L., 1968. Copper deposits in the Nonesuch Shale, White Pine, Michigan, In: J.D. Ridge (Editor), *Ore Deposits of the United States 1933-1967, Vol. I (Graton-Sales Volume)*. Am. Inst. Min. Metall. Pet. Eng., New York, N.Y. pp. 459-488.
- Essene, E.J.; Peacor, D.R., 1995. Clay mineral thermometry—a critical perspective. *Clays and Clay Minerals* 43(5): 540-553.
- George, S.C.; Krieger, F.W.; Eadington, P.J.; Quezada, R.A.; Greenwood, P.F.; Eisenberg, L.I.; Hamilton, P.J.; Wilson, M.A., 1997. Geochemical comparison of oil-bearing fluid inclusions and produced oil from the Toro sandstone, Papua New Guinea. *Organic Geochemistry* 26(3/4): 155-173.
- George, S.C.; Lisk, M.; Summons, R.E.; Quezada, R.A., 1998. Constraining the oil charge history of the South Pepper oilfield from the analysis of oil-bearing fluid inclusions. *Organic Geochemistry* 29(1-3): 631-648.
- George, S.C.; Ruble, T.E.; Dutkiewicz, A.; Eadington, P.J., 2001. Assessing the maturity of oil trapped in fluid inclusions using molecular geochemistry data and visually-determined fluorescence colours. *Applied Geochemistry* 16: 451-473.
- George, S.C.; Ahmed, M.; Liu, K.; Volk, H., 2004a. The analysis of oil trapped during secondary migration. *Organic Geochemistry* 35: 1489-1511
- George, S.C.; Lisk, M.; Eadington, P.J., 2004b. Fluid inclusion evidence for an early, marine-sourced oil charge prior to gas-condensate migration, Bayu-1, Timor Sea, Australia. *Marine and Petroleum Geology* 21: 1107-1128.
- George, S.C.; Volk, H.; Ahmed, M., 2007a. Geochemical analysis techniques and geological applications of oil-bearing fluid inclusions, with some Australian case studies. *Journal of Petroleum Science and Engineering* 57: 119-138.

George, S.C.; Volk, H.; Dutkiewicz, A.; Ridley, J.; Buick, R., 2008. Preservation of hydrocarbons and biomarkers in oil trapped inside fluid inclusions for >2 billion years. *Geochimica et Cosmochimica Acta* 72: 844-870.

Goldstein, R.H.; Reynolds, T.J., 1994. Systematics of fluid inclusions in diagenetic minerals. SEPM.

Grimmer, J.O.W.; Pironen, J.; Teinturier, S.; Mutterer, J., 2003. Recognition and differentiation of gas condensates and other oil types using microthermometry of petroleum inclusions. *Journal of Geochemical Exploration* 78-79: 367-371.

Hegarty, K.A.; Foland, S.S.; Cook, A.C.; Green, P.F.; Duddy, I.R., 2007. Direct measurement of timing: Underpinning a reliable petroleum system model for the Mid-Continent rift system. *AAPG Bulletin* 91(7): 959-979

Hieshima, G.B.; Pratt, L.M., 1991. Sulfur/carbon ratios and extractable organic matter of the Middle Proterozoic Nonesuch Formation, North American Midcontinent rift. *Precambrian Research* 54: 65-79.

Hieshima, G.B.; Summons, R.E.; Pratt, L.M., 1991. Thermal maturity of the 1.05 Ga Nonesuch Formation, North American Midcontinent Rift: biomarker ratios and hopane and sterane stereoisomers. *AAPG Bulletin* 75(3): 595.

Ho, E.S.; Mauk, J.L., 1996. Relationship between organic matter and copper mineralization in the Proterozoic Nonesuch Formation, northern Michigan. *Ore Geology Reviews* 11: 71-88

Ho, E.S.; Meyers, P.A.; Mauk, J.L., 1990. Organic geochemical study of mineralization in the Keweenaw Nonesuch Formation at White Pine, Michigan. *Advances in Organic Geochemistry 1989, Organic Geochemistry* 16(1-3): 229-234

Hughes, W.B.; Holba, A.G.; Dzou, L.I.P., 1995. The ratios of dibenzothiophene to phenanthrene and pristane to phytane as indicators of depositional environment and lithology of petroleum source rocks. *Geochimica et Cosmochimica Acta* 59(17): 3581-3598.

Hunt, J.M., 1979. *Petroleum Geochemistry and Geology*. Oxford: Freeman.

Imbus, S.W.; Engel, M.H.; Elmore, R.D.; Zumberge, J.E., 1988. The origin, distribution and hydrocarbon generation potential of organic-rich facies in the Nonesuch Formation, Central North American Rift System: A regional study. *Advances in Organic Geochemistry 1987, Organic Geochemistry* 13(1-3): 207-219.

Javaux, E.J.; Marshal, C.P., 2006. A new approach in deciphering early protist paleobiology evolution: Combined microscopy and microchemistry of single Proterozoic acritarchs. *Review of Palaeobotany and Palynology* 139: 1-15.

- Kelly, W.C.; Nishioka, G.K., 1985. Precambrian oil inclusions in late veins and the role of hydrocarbons in copper mineralization at White Pine, Michigan. *Geology* 13: 334-337.
- Killops, S.; Killops, V., 2005. *Introduction to Organic Geochemistry*. Oxford: Blackwell Publishing.
- King, N., 2009. Using copper mineralization to evaluate small-scale controls on mudstone permeability in the Nonesuch Formation. M.S. Thesis, Colorado State University, Fort Collins, CO.
- Köykkä, J.; Lamminen, J., 2011. Tidally influenced clastic epeiric sea at a Mesoproterozoic continental margin, Rjukan Rift Basin, southern Norway. *Precambrian Research* 185: 164-182.
- Kvenvolden, K.A.; Roedder, E., 1971. Fluid inclusions in quartz crystals from South-West Africa. *Geochimica et Cosmochimica Acta* 35: 1209–1229.
- Li, G.; Mauk, J.L.; Peacor, D.R., 1995. Preservation of clay minerals in the Precambrian (1.1 Ga) Nonesuch formation in the vicinity of the White Pine Copper Mine, Michigan. *Clays and Clay Minerals* 43(3): 361-376.
- Love, G.D.; Grosjean, E.; Stalvies, C.; Fike, D.A.; Grotzinger, J.P.; Bradley, A.S.; Kelly, A.E.; Bhatia, M.; Meredith, W.; Snape, C.E.; Bowring, S.A.; Condon, D.J.; Summons, R.E., 2009. Fossil steroids record the appearance of Demospongiae during the Cryogenian period. *Nature* 457: 718-721.
- Mauk, J.L.; Burruss, R.C., 2002. Water washing of Proterozoic oil in the Midcontinent rift system. *AAPG Bulletin* 86(6): 1113-1127.
- Mauk, J.L.; Hieshima, G.B., 1992. Organic matter and copper mineralization at White Pine, Michigan, U.S.A. *Chemical Geology* 99: 189-211.
- Mauk, J.L.; Kelly, W.C.; van der Pluijm, B.A., 1992. Relations between deformation and sediment-hosted copper mineralization: Evidence from the White Pine part of the Midcontinent rift system. *Geology* 20: 427-430.
- Mancuso, J.J.; Kneller, W.A.; Quick, J.C., 1989. Precambrian vein pyrobitumen: evidence for petroleum generation and migration 2 Ga ago. *Precambrian Research* 44: 137-146.
- McKirdy, D.M., 1974. Organic geochemistry in Precambrian research. *Precambrian Research* 1: 75-137.

- Munz, I.A., 2001. Petroleum inclusions in sedimentary basins: systematics, analytical methods and applications. *Lithos* 55: 195-212.
- Murphy, P.J.; Roberts, S., 1997. Melting and nucleation behavior of clathrates in multivolatile fluid inclusions: evidence of thermodynamic disequilibrium. *Chemical Geology* 135: 1-20.
- Ojakangas, R.W.; Morey, G.B.; Green, J.C., 2001. The Mesoproterozoic Midcontinent Rift System, Lake Superior Region, U.S.A. *Sedimentary Geology* 141-142: 421-442.
- Ojakangas, R.W.; Dickas, A.B., 2002. The 1.1-Ga Midcontinent Rift System, central North America: sedimentology of two deep boreholes, Lake Superior region. *Sedimentary Geology* 147: 13-36.
- Palacas, J.G., 1995. Superior Province: U.S. Geological Survey National Oil and Gas Assessment. <http://energy.cr.usgs.gov/oilgas/noga/index.htm>
- Peters K. E.; Walters C. C.; Moldowan J. M., (2005). *The Biomarker Guide*. Cambridge University Press.
- Prezbindowski, D.R.; Tapp, J.B., 1991. Dynamics of fluid inclusion alteration in sedimentary rocks: a review and discussion. *Organic Geochemistry* 17(2): 131-142.
- Price, K.L.; McDowell, S.D., 1993. Illite/smectite geothermometry of the Proterozoic Oronto Group, Midcontinent Rift system. *Clays and Clay Minerals* 41(2): 134-147
- Pratt, B.R., 1998. Syneresis cracks: subaqueous shrinkage in argillaceous sediments caused by earthquake-induced dewatering. *Sedimentary Geology* 117: 1-10.
- Pratt, L.M.; Summons, R.E.; Hieshima, G.B., 1991. Sterane and triterpane biomarkers in the Precambrian Nonesuch Formation, North American Midcontinent Rift. *Geochimica et Cosmochimica Acta* 55: 911-916.
- Ruiz, J.; Jones, L.M.; Kelly, W.C., 1984. Rubidium-strontium dating of ore deposits hosted by Rb-rich rocks, using calcite and other common Sr-bearing minerals. *Geology* 12: 259-262.
- Schieber, J., 1998. Possible indicators of microbial mat deposits in shales and sandstones: examples from the Mid-Proterozoic Belt Supergroup, Montana, U.S.A. *Sedimentary Geology* 120: 105-124.
- Schopf, J.W., 1974. The development and diversification of Precambrian life. *Origins of Life* 5: 119-135.
- Shaw, G.H., 2008. Earth's atmosphere – Hadean to early Proterozoic. *Chemie der Erde* 68: 235-264.

- Suszek, T., 1997. Petrography and sedimentation of the middle Proterozoic (Keweenaw) Nonesuch Formation, western Lake Superior region, Midcontinent Rift System. *Geological Society of America Special Paper 312*: 195-210
- Swenson, J.B.; Person, M.; Raffensperger, J.P.; Cannon, W.F.; Woodruff, L.G.; Berndt, M.E., 2004. A hydrogeologic model of stratiform copper mineralization in the Midcontinent Rift System, Northern Michigan, USA. *Geofluids 4*: 1-22.
- Thiéry, R.; Pironon, J.; Walgenwitz, F.; Montel, F., 2002. Individual characterization of petroleum fluid inclusions (composition and P-T trapping conditions by microthermometry and confocal laser scanning microscopy: inferences from applied thermodynamics of oils. *Marine and Petroleum Geology 19*: 847-859.
- Thomas, M.D.; Teskey, D.J., 1994. An interpretation of gravity anomalies over the Midcontinent Rift, Lake Superior, constrained by GLIMPCE seismic and aeromagnetic data. *Canadian Journal of Earth Sciences 31*:(4) 682-697
- Uchytel, S.J.; Steffensen, C.K.; Jarvie, D.M., 1999. Hydrocarbon potential of the middle Proterozoic Nonesuch Formation in northwestern Wisconsin and Michigan. *Wisconsin Geological and Natural History Survey*: 95-106.
- van Aarssen, B.G.K.; Bastow, T.P.; Alexander, R.; Kagi, R.I., 1999. Distributions of methylated naphthalenes in crude oils: indicators of maturity, biodegradation and mixing. *Organic Geochemistry 30*: 1213-1227.
- Volk, H.; George, S.C.; Dutkiewicz, A.; Ridley, J., 2005a. Characterisation of fluid inclusion oil in a Mid-Proterozoic sandstone and dolerite (Roper Superbasin, Australia). *Chemical Geology 223*: 109-135.

6. Appendices

6.1 Appendix A: Samples collected

Core 46½M:

Depth:	Unit of Nonesuch Formation:	Notable characteristics in sample:
2630	Upper Shale – Massive	Calcite-cemented, above orebody
2646	Upper Shale – Widely/Red and Green	Calcite-cemented sandstone from Widely, greenish color
2662	Upper Shale – Widely/Red and Green	Orebody sandstone with bitumen flecks
2664	Upper Shale – Widely/Red and Green	Orebody sandstone with bitumen flecks
2677	Copper Harbor Conglomerate	Top of Copper Harbor

Core 40K:

Depth:	Unit of Nonesuch Formation:	Notable characteristics of sample:
2088	Marker Bed	Calcite blebs from marker bed
2130	Upper Sandstone	Top of upper sandstone, bitumen flecks
2136	Upper Sandstone	Bottom of upper sandstone, bitumen
2140	Parting Shale	Chalcocite and native copper visible
2148	Copper Harbor/Nonesuch transition	Top of transition
2149	Copper Harbor/Nonesuch transition	Sampling of regular intervals through transition from green to red sandstone
2150	Copper Harbor/Nonesuch transition	
2151	Copper Harbor/Nonesuch transition	
2170	Copper Harbor	Bottom of core

Core 28G:

Depth:	Unit of Nonesuch Formation:	Notable characteristics of sample:
514	Marker Bed	Calcite vein
520	Marker Bed	Calcite vein
522	Massive black shale	Calcite nodules
539	Massive grey shale	Calcite vein and bitumen flecks
563	Upper Transition	Sandstone with sulfides and bitumen
571	Red Massive shale	Shale with sulfides
572	Domino	Shale with sulfides
574	Lower Transition	Sulfides with bitumen
578	Copper Harbor	Volcanic clasts, epidote

Core 32H:

Depth:	Unit of Nonesuch Formation:	Notable characteristics of sample:
899	Marker Bed	Calcite nodules
906	Massive grey siltstone	Deformation with calcite visible
943	Upper Sandstone	Middle of Upper SS, red color
951	Copper Harbor	Top of Copper Harbor

Core 30R:

Depth:	Unit of Nonesuch Formation:	Notable characteristics of sample:
2221	Massive grey siltstone	Clast with calcite in vugs
2237	Upper Sandstone	Greenish color, sulfides present
2249	Copper Harbor	Top of Copper Harbor
2255	Copper Harbor	Bleached red clasts
2263	Copper Harbor	Calcite vein

Big Iron River:

Number:	Notable characteristics of sample:	Unit of Nonesuch/Approx. walking distance from top of formation
BIR 1	From large nodule with calcite veins running through	Upper Nonesuch/50m
BIR 2	From large nodule without veins	Upper Nonesuch/50m
BIR 3	Dark grey shale with mudcrack structures	Upper Nonesuch/150m
BIR 4	Greenish colored shale	Upper Nonesuch/300m
BIR 5	Calcite vein along joints	Upper Nonesuch/600m
BIR 6	Malachite present along joint	Upper Nonesuch/600m
BIR 7	Stratabound copper in shale layers	Lower Nonesuch/700m
BIR 8		Lower Nonesuch/720m
BIR 9		Lower Nonesuch/740m
BIR 10		Lower Nonesuch/760m
BIR 11	Syneresis cracks on shale bedding plane	Lower Nonesuch/800m
BIR 12	Copper in red sandstone matrix	Lower Nonesuch/820m
BIR 13	Syneresis cracks on shale bedding plane	Lower Nonesuch/850m
BIR 14	Copper in same shale layer as syneresis cracks	Lower Nonesuch/850m
BIR 15	Large lithic nodule	Lower Nonesuch/880m
BIR 16	Quartz and calcite vein with pyrite visible	Lower Nonesuch/900m
BIR 17	Lithic nodule growing along discontinuous calcite vein	Top of Copper Harbor Fm/950m

Little Iron River:

Number:	Notable characteristics of sample:
LIR 1	Copper Harbor SS veins surrounded by bleaching
LIR 2	Parting Shale with native copper
LIR 3	Regular sampling between contact of Copper Harbor and Upper Sandstone
LIR 4	
LIR 5	
LIR 6	Regular sampling between Upper Sandstone and Massive Shale
LIR 7	
LIR 8	
LIR 9	Sample of Stripey
LIR 10	Black Massive shale
LIR 11	Sandstone from exploration rockpile with copper minerals
LIR 12	Shale from exploration rockpile with graphite
LIR 13	Sandstone from exploration rockpile with slickenlines
LIR 14	Sandstone from exploration rockpile with calcite vein

Presque Isle River:

Number:	Notable characteristics of sample:
PIR 1	Fissile shale near the base of the Nonesuch Fm, visible copper
PIR 3	Conglomerate in Nonesuch Fm
PIR 4	Shale bed with copper just above PIR 3 conglomerate
PIR 5	Just above last visible band of copper
PIR 6	Just below a conglomerate section
PIR 7	Sandy unit
PIR 8	Very fissile shale unit, abundant copper
PIR 9	Shale just below PIR 8, copper present
PIR 10	Green sandstone from very top of Copper Harbor
PIR 11	Sampled from between PIR 9 and 10, just above Copper Harbor, high amounts of native copper
PIR 12	Conglomerate in Copper Harbor
PIR 13	Border between green and red colors in Copper Harbor
PIR 14	Red colored Copper Harbor
PIR 15	From very base of Nonesuch Fm, no visible copper

Thin sections:

From sample:	Oil inclusions present?
46½M 2662	Yes (rare)
46½M 2630	No
40K 2088	Yes
40K 2136	No
40K 2140	Yes
40K 2151	No
30R 2221	Yes
30R 2263	Yes
32H 906	No
32H 943	No
32H 951	Yes (rare)
28G 522	Yes
28G 539	Yes
28G 563	No
28G 574	Yes
28G 578	No
BIR 1	No
BIR 4	No
BIR 6	Yes
BIR 7	No
BIR 16	Yes
LIR 1	No
LIR 2	No
LIR 7	No
LIR 11	No
LIR 12	No
LIR 14	Yes
PIR 1	No
PIR 3	No
PIR 5	No
PIR 7	Yes
PIR 10	Yes
PIR 12	No
PIR 14	No

6.2 Appendix B: Microthermometry data

LIR 14 Oil Th	Fluorescence color	LIR 14 Water Th	LIR 14 Water Tm
62	yellow	130	-21
74.3	yellow	145	-18
198	yellow	75	-19
121	yellow	>250	-16
123	yellow	>250	-10
123	yellow	140	-6
126	yellow	>250	-12
145	yellow	>250	-10
111	yellow	>250	-22
>250	yellow	>250	-17
93	yellow	225	-28
115.8	yellow	>250	-32
156	yellow	137	-25
131	yellow	154	-14
86.6	yellow	168	-16
142	blue	Average:	Average:
105	blue	202.27	-17.73
109	blue		
73	blue		
93	blue		
167	blue		
>250	blue		
>250	blue		
150	blue		
152	blue		
155	blue		
165	blue		
88	blue		
133	blue		
>250	blue		
Average	Yellow average		
143.26	127.71		
	Blue average		
	152.13		

30R2263 Oil Th	Fluorescence color	30R 2263 Water Th	30R 2263 Water Tm
234	blue-yellow	230	-1
>250	blue-yellow	210	-2
167.4	yellow	>250	-1
199	yellow	>250	-24
193.3	yellow	170	-22
183	yellow	177	-25
224	yellow	180	-24
>250	yellow	>250	15
177	yellow	215	-18
172.4	yellow	233	-21
102.1	yellow	>250	-24
85	yellow	184	-15
102	yellow	244	-28
200.9	yellow	210	-17
65	yellow	193	-17
93	blue-yellow	Average	Average
107.6	blue-yellow	223.07	-14.93
>250	yellow		
>250	yellow		
166.5	yellow		
163	yellow		
219.2	yellow		
128	yellow		
148.9	yellow		
234	yellow		
244	blue-yellow		
>250	blue-yellow		
231	blue-yellow		
239	blue-yellow		
>250	blue-yellow		
>250	blue-yellow		
96.2	yellow		
>250	yellow		
104	yellow		
106	yellow		
216.1	yellow		
>250	yellow		
>250	yellow		
231	blue-yellow	Yellow avg	
233	blue-yellow	162.61	
233.5	blue-yellow	Blue-yellow avg:	
		226.62	
Average:	196.32		

BIR 16 Oil Th	28G 539 Oil Th	40K 2088 Oil Th
103	59	158
111	100	104
120	109	111.5
94	124	119
>150 (not close)	109	170
>150 (not close)	115	222
>150 (not close)	>150 (not close)	116
>150 (not close)	>150 (not close)	143
>150 (not close)	>150 (not close)	137
109	72	155
115	103	>150
122	>150 (close)	>150
101	>150 (not close)	>150
140	75	>150
>150 (close)	77	>150
>150 (not close)	93	163
>150 (not close)	140	171
>150 (not close)	103	182
138	110	138
140	50	141
113	56	113
>150 (not close)	>150 (very close)	180
>150 (not close)	108	155
>150 (not close)	143	168
150	83	170
>150 (very close)	108	205
>150 (close)	92	231
143	116	142
>150 (close)	108	100
>150 (not close)	135	133
Average 159.47	110	Average
	Average 117.19	156.75

6.3: Appendix C: GC-MS data

Note: All figures and descriptions of data in this appendix were prepared using in-house software in 2009 by Manzur Ahmed and Herbert Volk, CSIRO Petroleum, Sydney Australia.

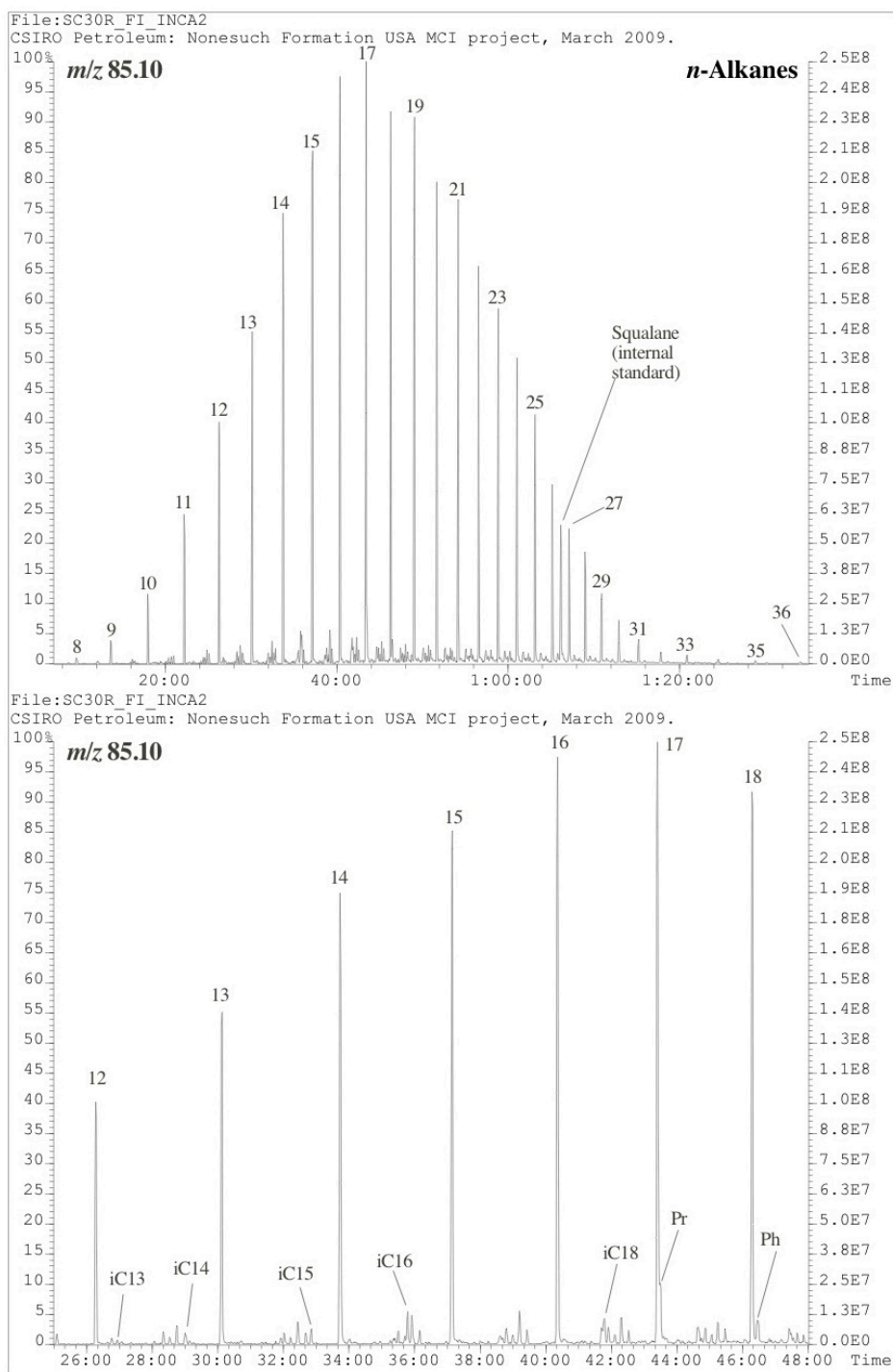


Figure B1: Partial m/z 85.10 mass chromatograms for the Well-30R, 2263 ft, Nonesuch Formation, Keweenaw Basin, USA MCI sample, showing the distribution of n -alkanes, methylalkanes and isoprenoids. Numbers refer to n -alkane chain length, Pr = pristane, Ph = phytane, iC13 = C₁₃ isoprenoid, etc.

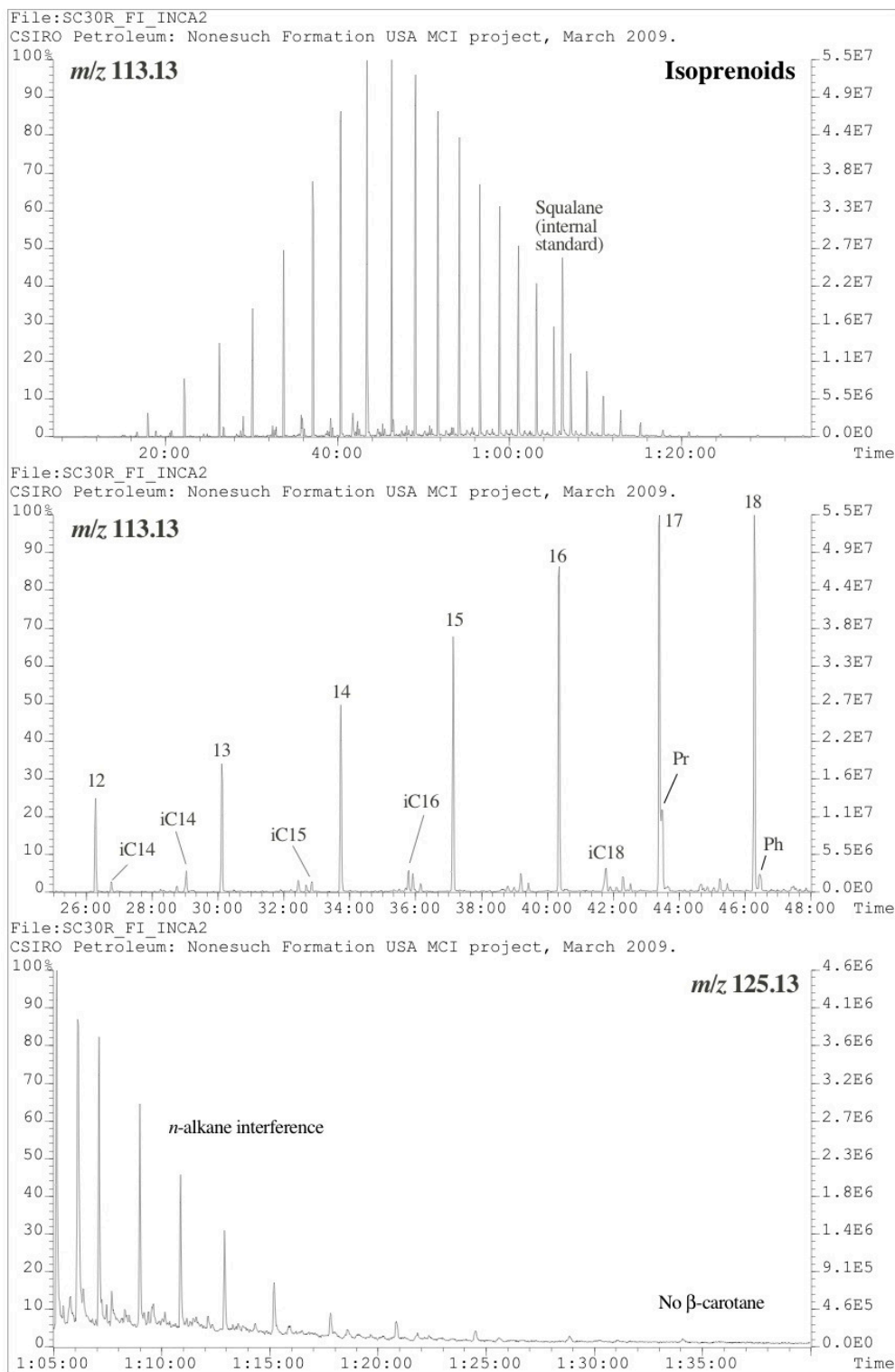


Figure B3: Partial m/z 113.13 and 125.13 mass chromatograms for the Well-30R, 2263 ft, Nonesuch Formation, Keweenaw Basin, USA MCI sample, showing the distribution of isoprenoids and β -carotane. Numbers refer to n -alkane chain length, Pr = pristane, Ph = phytane, iC13 = C₁₃ isoprenoid, etc.

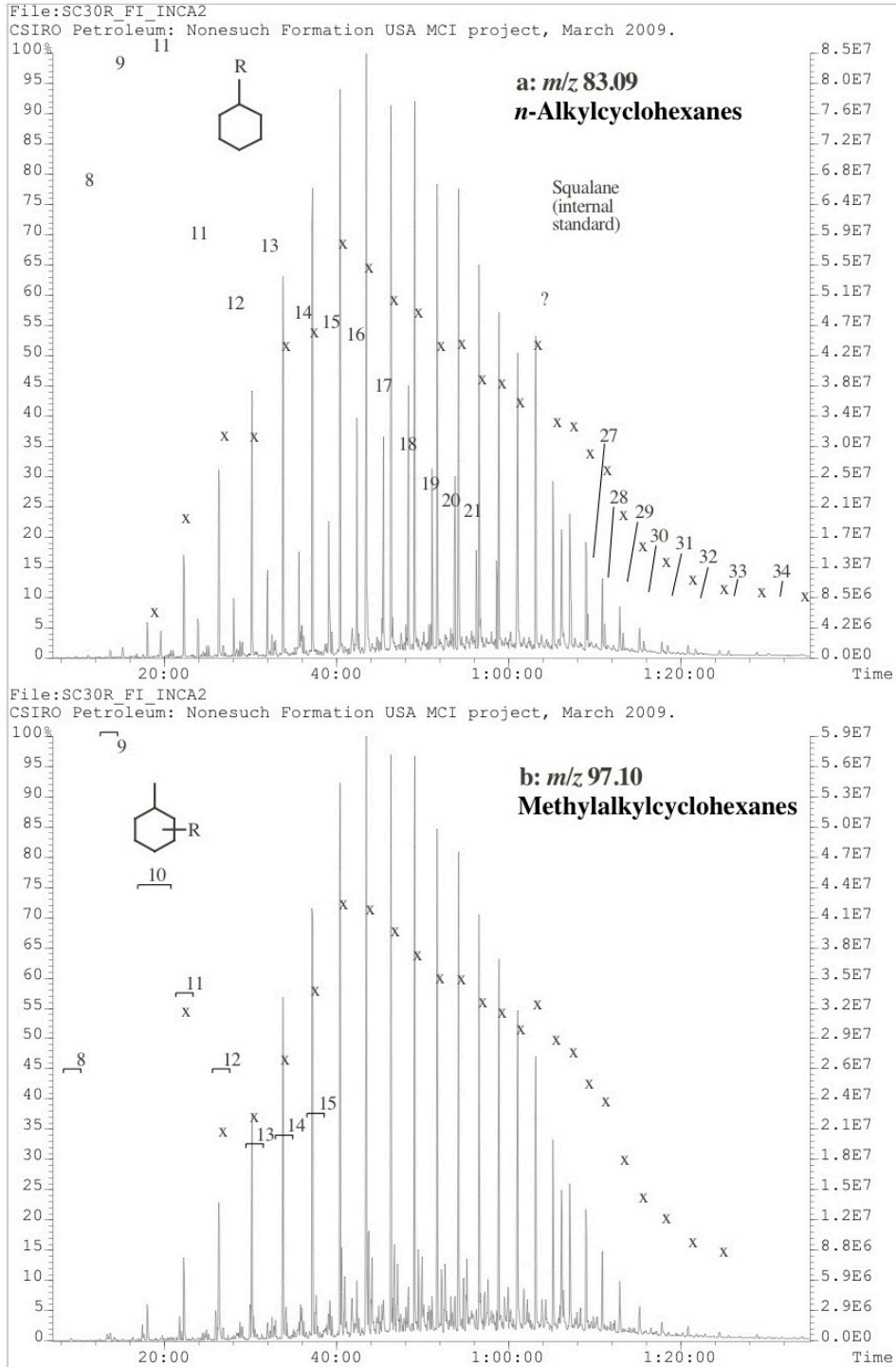


Figure B5: Partial m/z 83.09 and 97.10 mass chromatograms for the Well-30R, 2263 ft, Nonesuch Formation, Keweenaw Basin, USA MCI sample, showing the distribution of (a) *n*-alkylcyclohexanes and (b) methylalkylcyclohexanes. Numbers refer to *n*-alkylcyclohexane and methylalkylcyclohexane chain length. Peaks marked with "x" are due to *n*-alkane interference.

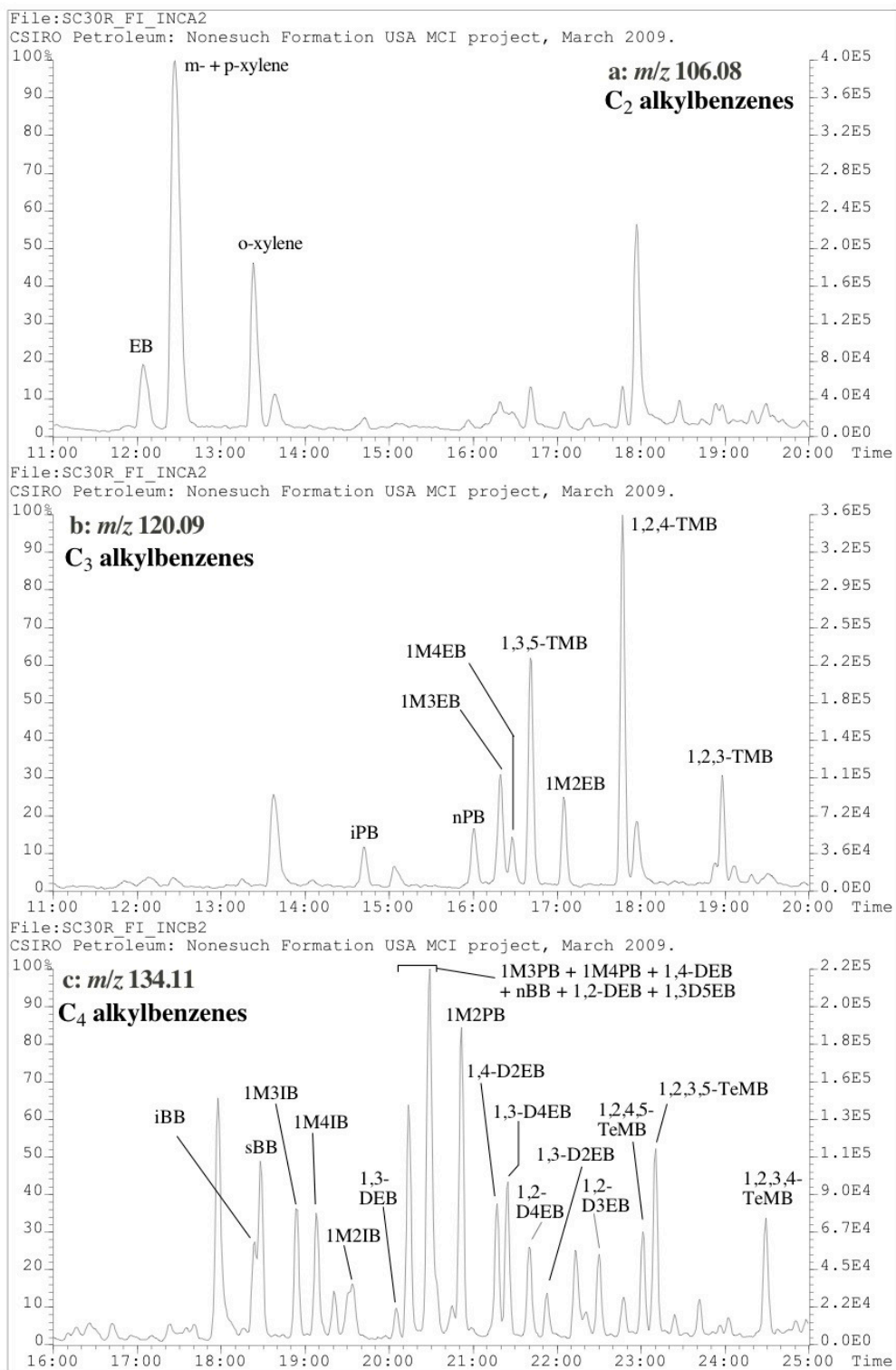


Figure B23: Partial m/z 106.08, 120.09 and 134.11 mass chromatograms for the Well-30R, 2263 ft, Nonesuch Formation, Keweenaw Basin, USA MCI sample, showing the distribution of (a) C_2 alkylbenzenes, (b) C_3 alkylbenzenes and (c) C_4 alkylbenzenes respectively. Peak abbreviations are listed in Table A4.

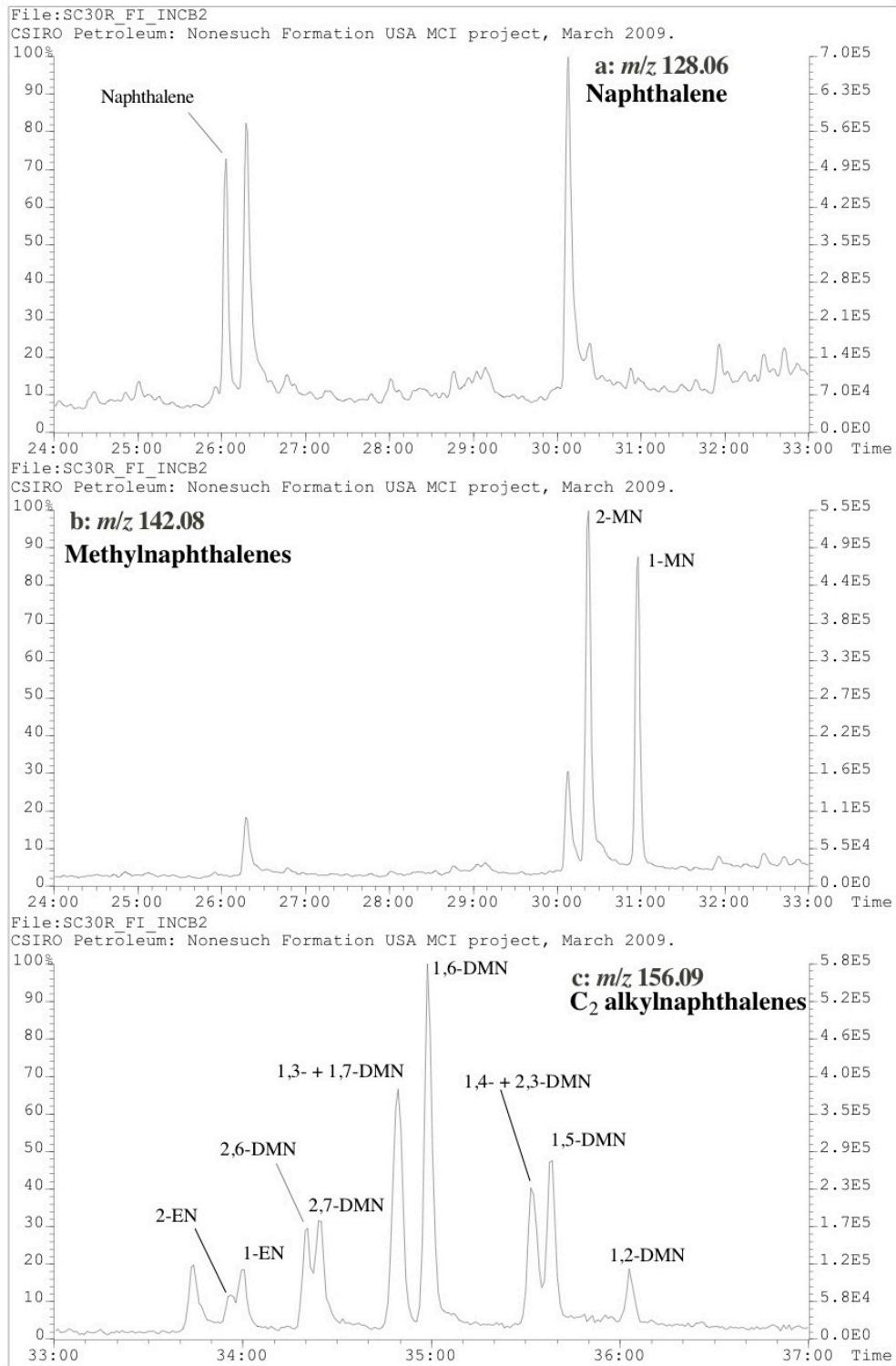


Figure B25: Partial m/z 128.06, 142.08 and 156.09 mass chromatograms for the Well-30R, 2263 ft, Nonesuch Formation, Keweenaw Basin, USA MCI sample, showing the distribution of (a) naphthalene, (b) methylnaphthalenes and (c) ethylnaphthalenes and dimethylnaphthalenes respectively. Peak abbreviations are listed in Table A4.

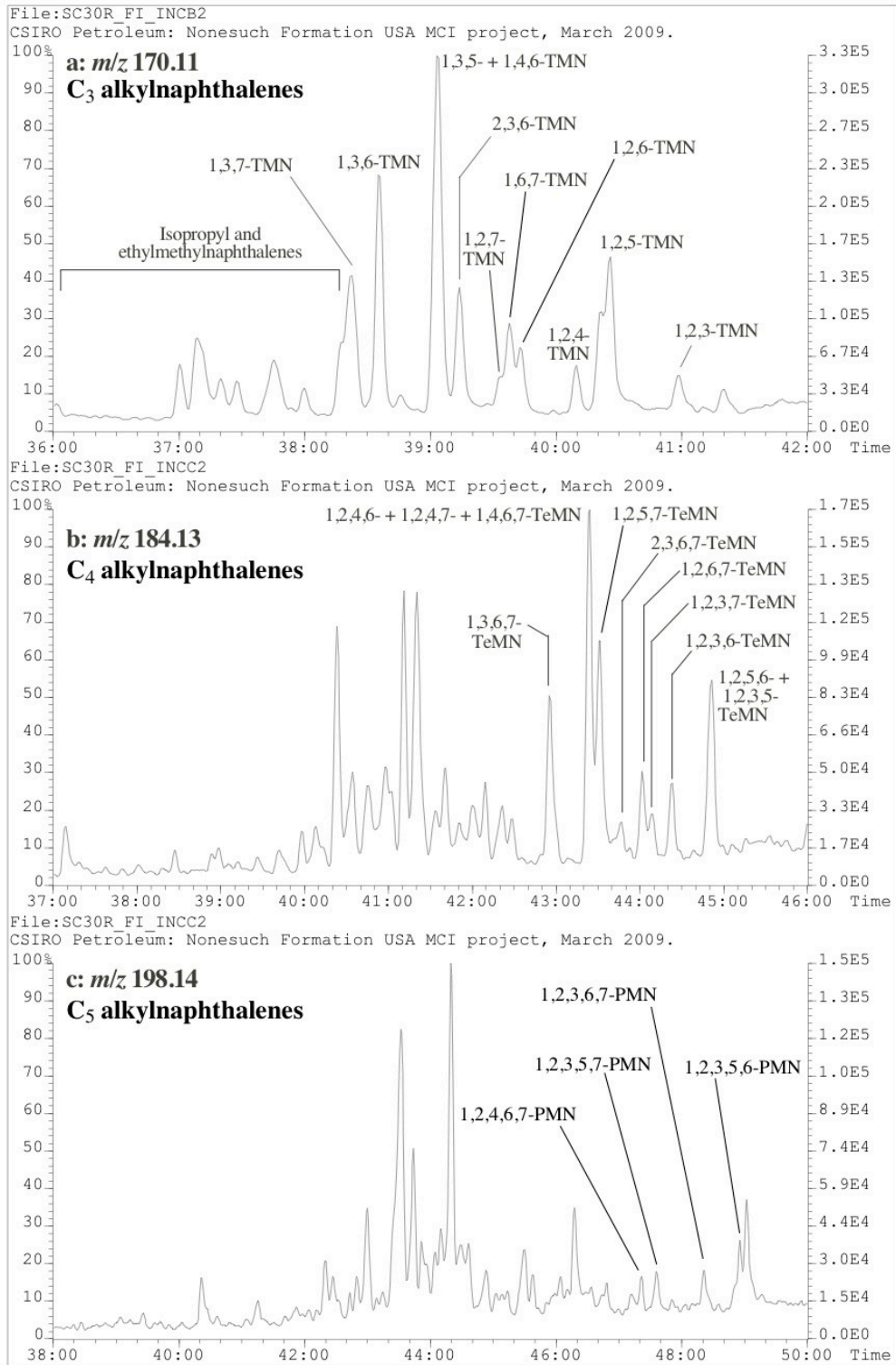


Figure B27: Partial m/z 170.11, 184.13 and 198.14 mass chromatograms for the Well-30R, 2263 ft, Nonesuch Formation, Keweenaw Basin, USA MCI sample, showing the distribution of (a) trimethylnaphthalenes, (b) tetramethylnaphthalenes and (c) pentamethylnaphthalenes respectively. Peak abbreviations are listed in Table A4.

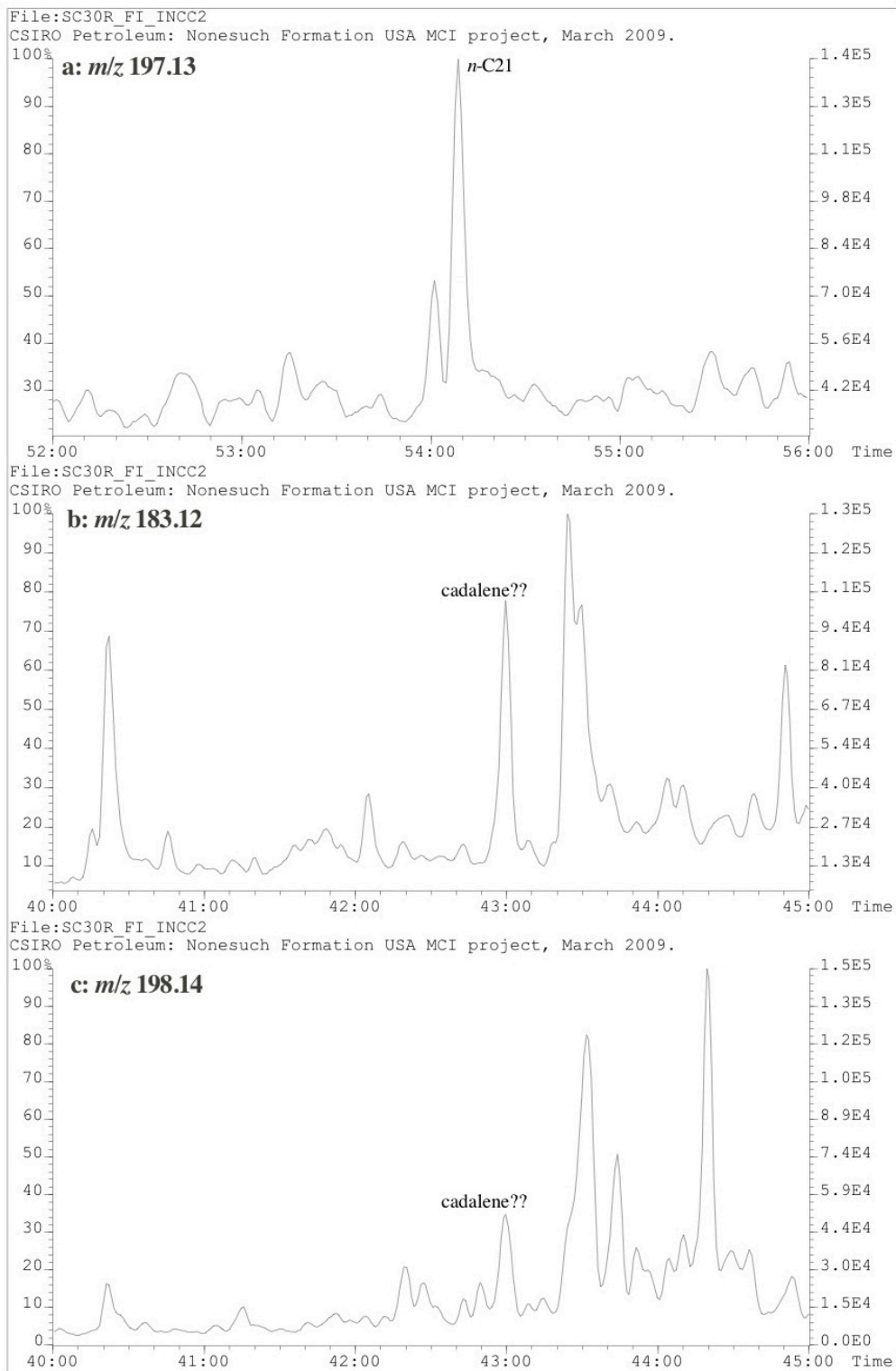


Figure B29: Partial m/z 197.13, 183.12 and 198.14 mass chromatograms for the Well-30R, 2263 ft, Nonesuch Formation, Keweenaw Basin, USA MCI sample, showing the distribution of (a) *iso*-hexylmethylnaphthalene, and (b) and (c) *cadalene*. n -C_{xx} = *n*-alkane interference.

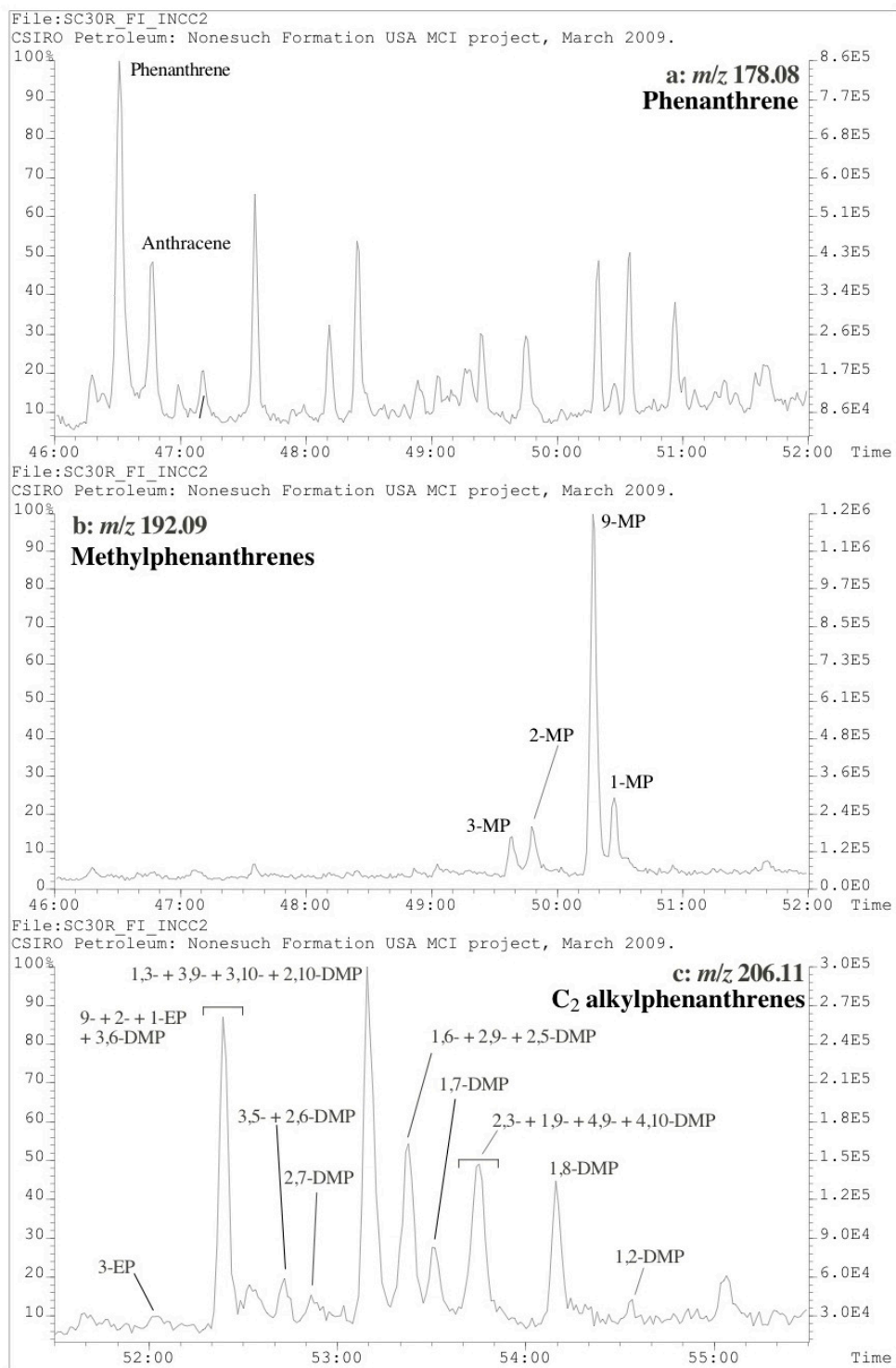


Figure B31: Partial m/z 178.08, 192.09 and 206.11 mass chromatograms for the Well-30R, 2263 ft, Nonesuch Formation, Keweenaw Basin, USA MCI sample, showing the distribution of (a) phenanthrene, (b) methylphenanthrenes and (c) ethylphenanthrenes and dimethylphenanthrenes respectively. Peak abbreviations are listed in Table A4.

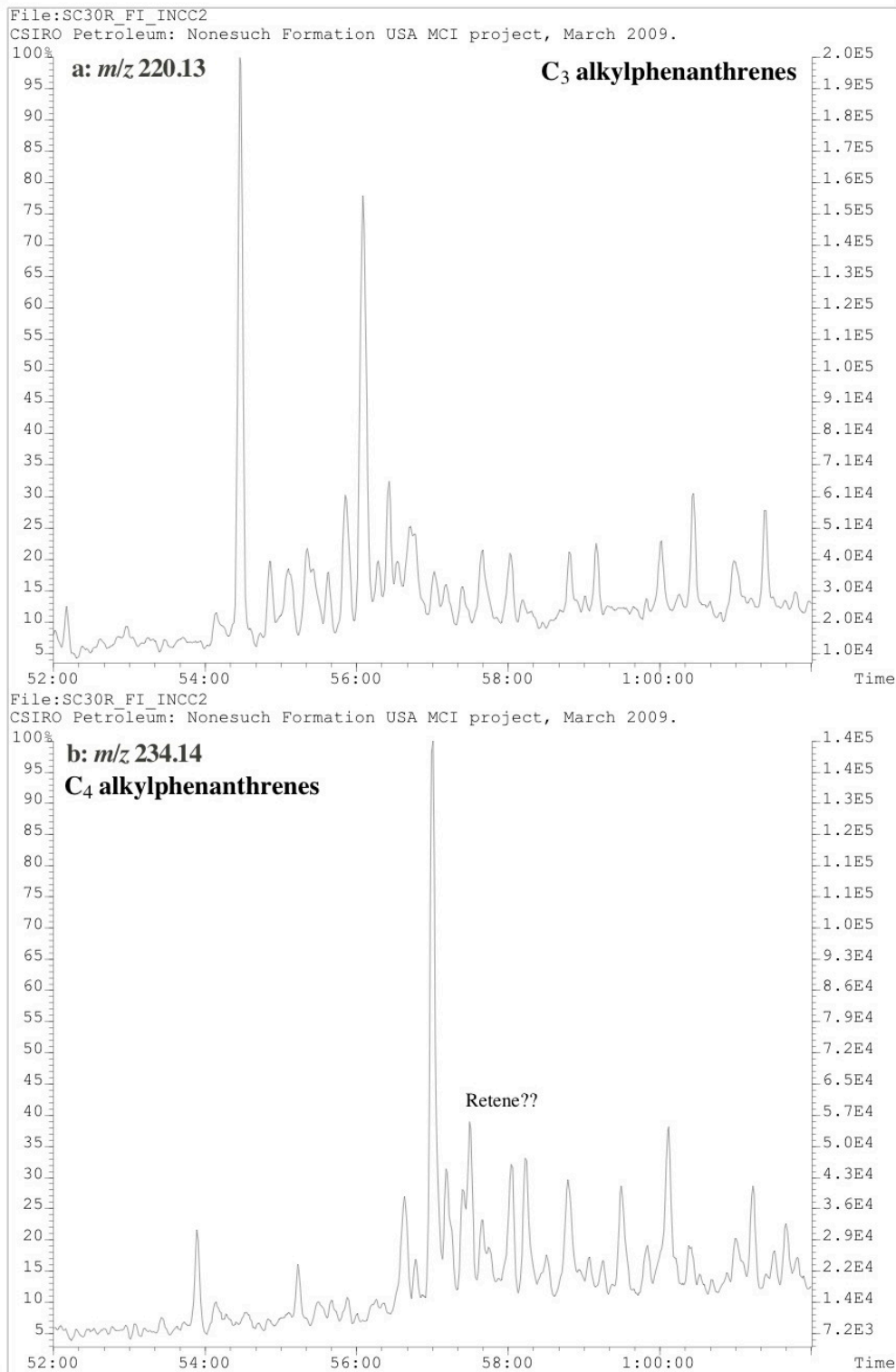


Figure B33: Partial m/z 220.13 and 234.14 mass chromatograms for the Well-30R, 2263 ft, Nonesuch Formation, Keweenaw Basin, USA MCI sample, showing the distribution of (a) trimethylphenanthrenes and (b) retene and tetramethylphenanthrenes. Peak abbreviations are listed in Table A4.

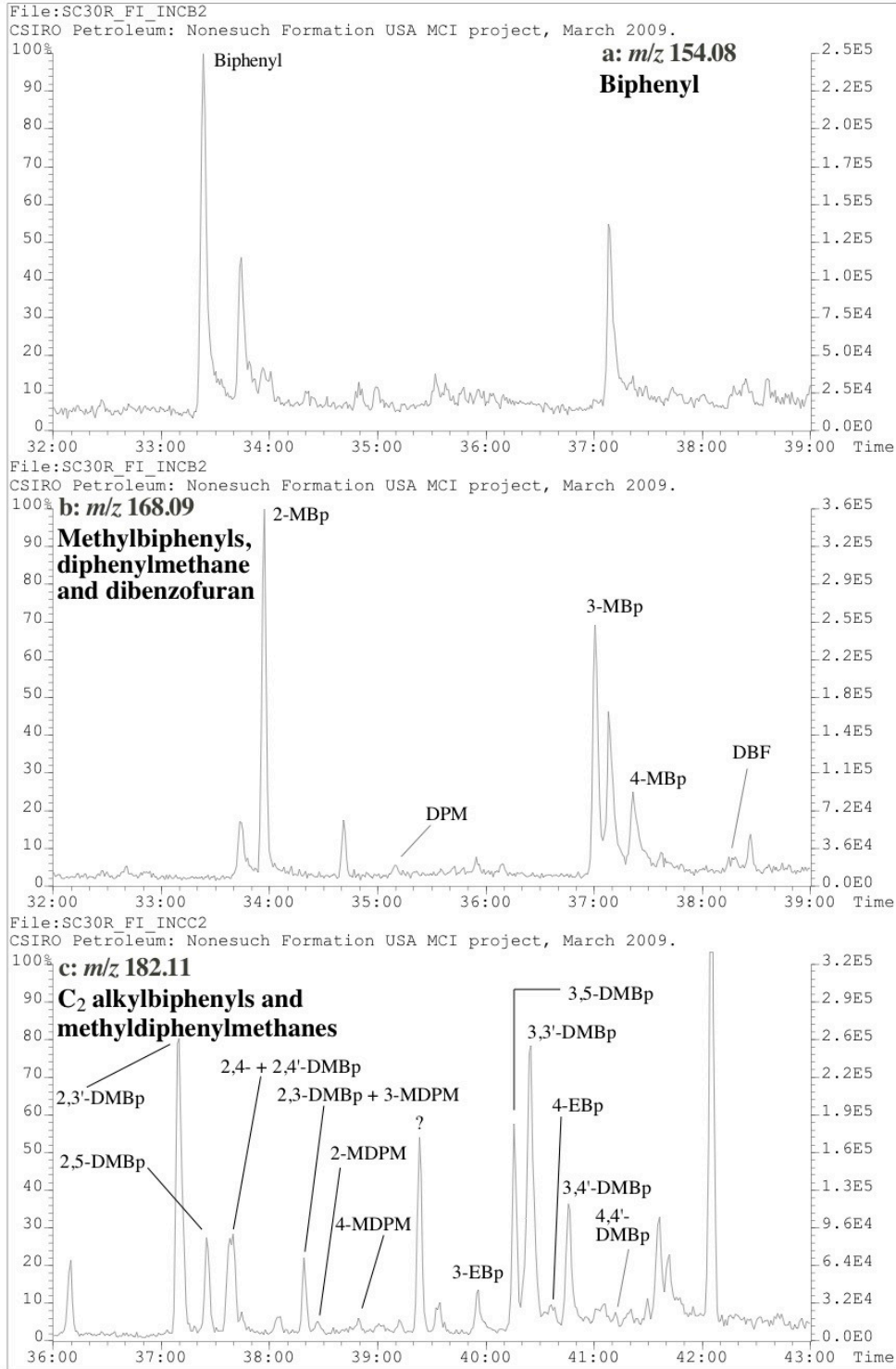


Figure B35: Partial m/z 154.08, 168.09 and 182.07 mass chromatograms for the Well-30R, 2263 ft, Nonesuch Formation, Keweenaw Basin, USA MCI sample, showing the distribution of (a) biphenyl, (b) methylbiphenyls, diphenylmethane and dibenzofuran, and (c) dimethylbiphenyls, ethylbiphenyls and methyldiphenylmethanes respectively. Peak abbreviations are listed in Table A4.

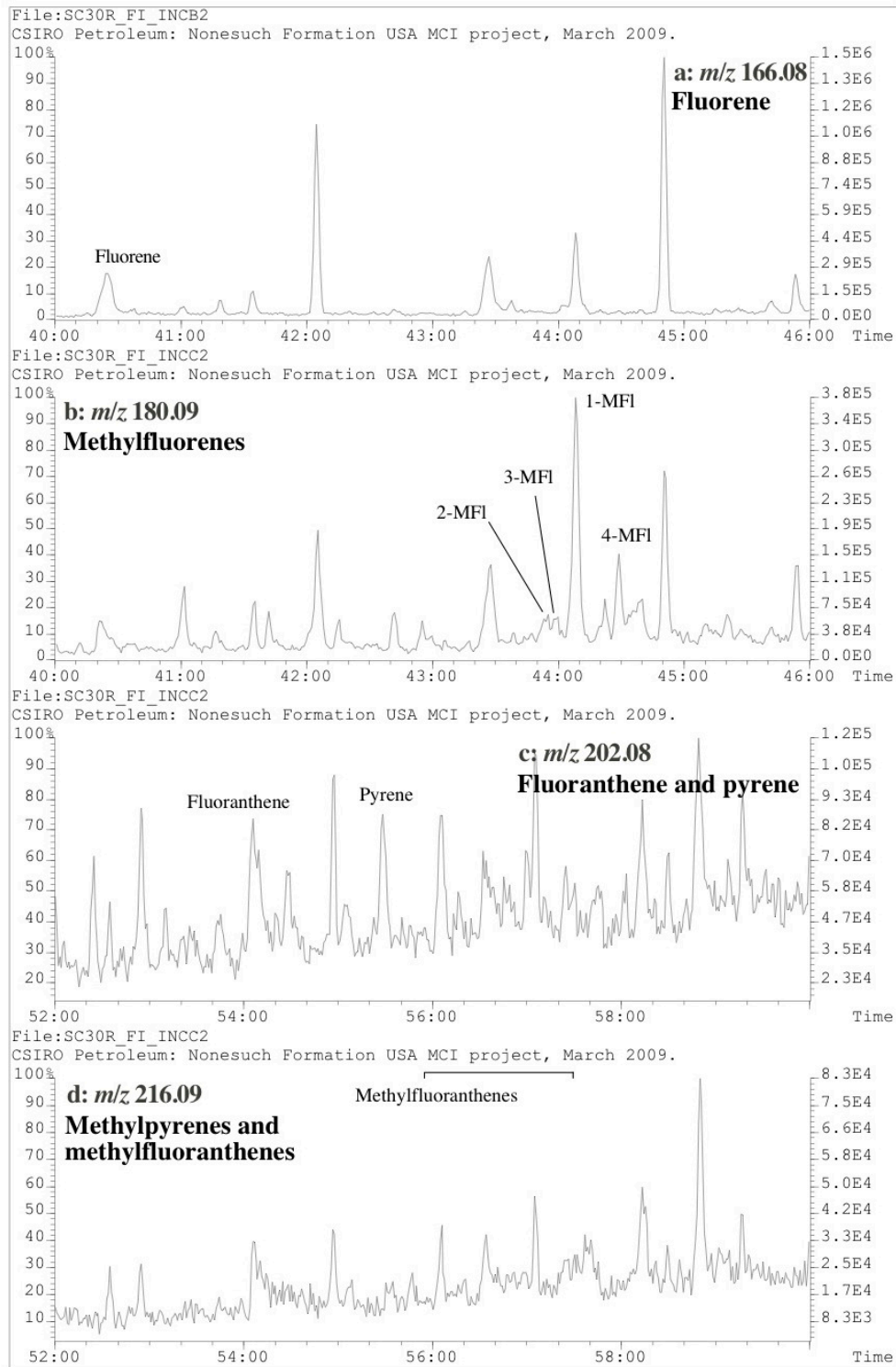


Figure B37: Partial m/z 166.08, 180.09, 202.08 and 216.09 mass chromatograms for the Well-30R, 2263 ft, Nonesuch Formation, Keweenaw Basin, USA MCI sample, showing the distribution of (a) fluorene, (b) methylfluorenes, (c) fluoranthene and pyrene, and (d) methylfluoranthenes and methylpyrenes respectively. Peak abbreviations are listed in Table A4.

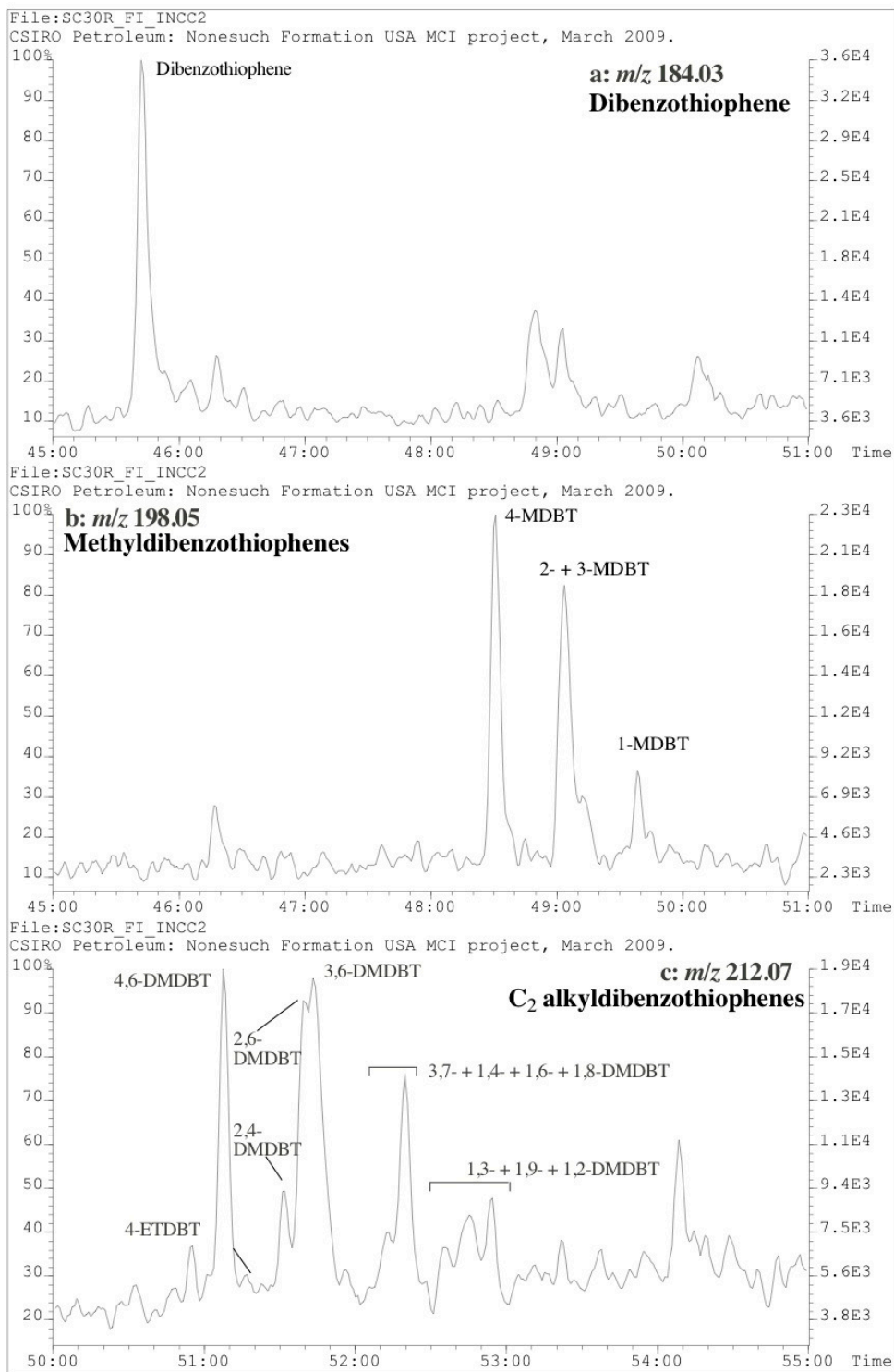


Figure B39: Partial m/z 184.03, 198.05 and 212.07 mass chromatograms for the Well-30R, 2263 ft, Nonesuch Formation, Keweenaw Basin, USA MCI sample, showing the distribution of (a) dibenzothiophene, (b) methylthiophenes and (c) dimethylthiophenes and ethylthiophenes respectively. Peak abbreviations are listed in Table A4.